IN VIVO MECHANICAL AND PHYSIOLOGICAL CHARACTERISATION OF LOWER LIMB SOFT TISSUE BY A LOCAL INDENTATION TECHNIQUE

WOO SIANG SI, MATTHEW

(B.Eng.(Hons.), NUS)

A THESIS SUBMITTED

FOR THE DEGREE OF MASTER OF SCIENCE (BIOENGINEERING)

GRADUATE PROGRAMME IN BIOENGINEERING

NATIONAL UNIVERSITY OF SINGAPORE

2006

Acknowledgements

The author wishes to express sincere appreciation and gratitude to the following people:

1. A/Prof. Toh Siew Lok, A/Prof. James Goh Cho Hong and A/Prof. Peter Lee Vee Sin for their counsel and guidance.
2. Andy Yew Khye Soon for his selfless help and invaluable advice in every area, without which it would have been a real struggle to complete this project. For that I am immensely grateful.
3. Lim Chin Ghim for always being so obliging and eager to lend a helping hand, especially the many hours spent at the AML manufacturing RMM braces for me to perform indentation tests.
4. Ooi Chun Keat for his earnest assistance during the time that he was around.
5. Mark Chung for being so willing to troubleshoot the indentor software on numerous occasions, even after the 3-month support period.
6. Grace Lee for graciously allowing us to use the Gait Lab, and for being so accommodating to us while we were there.
7. Hazlan Bin Sanusi for gladly providing us the tools and imparting to us his expertise in taking plaster casts.
8. All others who have contributed in one way or other to the successful completion of this project.

Finally, all praise and glory to God for bringing me through to the completion of this Masters course.

Table of Contents

ABSTRACT

Computer-Aided Design/Manufacturing (CAD/CAM) has been used in prosthetics applications over the last two decades to simplify the socket rectification process and improve reproducibility. Recently, Finite Element Analysis (FEA) techniques have also been introduced to improve the quality of socket fit by predicting the pressure distribution at the stump-socket interface due to loading. In order to create accurate finite element models, relevant properties of the bulk soft tissue need to be known and fed into the model. This can be achieved by performing *in vivo* indentation tests on the bulk soft tissue of the residual limb.

Through indentation, two important physiological properties of the soft tissue such as tissue modulus and the discomfort/pain threshold were obtained. Tissue modulus was calculated using Hayes' equation and based on the indentation force-displacement data. Discomfort/pain threshold was obtained through feedback from the patient.

Comprehensive grids of tissue modulus and discomfort/pain threshold values of the lower limbs of 2 unilateral trans-tibial amputees and 3 normal volunteers were produced in this study. It was found that on average, regions with bony prominences had the highest tissue modulus, followed by tendon, and then soft tissue. Highest pain threshold was noticed in regions with tendon, followed by bony prominences, and then soft tissue. These biomechanical properties can be fed into the Finite Element stump model and used to predict pressure distribution and discomfort/pain levels when donning the prosthetic socket.

FEA software (ABAQUS 6.4) was used to simulate the indentation of soft tissue. Axisymmetric models with hyperelastic material were created to represent the geometric and biomechanical properties of the residual limb at each indentation location. A comparison between several types of hyperelastic strain energy models was carried out.

A method of determining the physiological properties of soft tissues using an integrated indentation and pain feedback system has been established. Consequently a map of tissue modulus and discomfort/pain threshold tolerance for the entire residual limb was generated. This would enable correlation of stump-socket interface pressure to physiological response, giving a practical application to the FEA-predicted pressures.

List of Tables

List of Figures

Chapter 1: INTRODUCTION

1.1 Background

1.1.1 Lower Limb Prosthetic Sockets

The purpose of a lower-limb prosthetic socket is to integrate the prosthesis as a functional extension of the residual limb by providing coupling between the stump and the prosthesis. The entire load from the residual limb is transferred to the prosthesis through the stump's soft tissues in contact with the prosthetic socket, liner and socks. The main factor in determining comfort of the prosthesis and its effectiveness in restoring the amputee's mobility is the fit of the prosthetic socket.

Basic principles of socket design range from transferring almost all the load to specific load bearing regions or distributing the load uniformly over the entire stump. Regardless of the design principle, designers need to investigate the load transfer pattern at the stump-socket interface so as to understand the biomechanical principles that determine the quality of socket fit.

Load transfer at the stump-socket interface is made complicated by the compliance of the stump's soft tissues when subjected to external forces. The skin and underlying soft tissues are not physiologically suited to undergo high compressive pressures, shear stresses, abrasive motions, and other physical irritations present at the stump-socket interface.

Designing the socket to distribute the load appropriately is thus a critical process in lower-limb prosthetic socket design as improper load distribution may cause damage and pain to the skin and soft tissues. Socket design includes modifications to account for variations in the stump shape among amputees and variations in pressure tolerances among soft tissues at different regions of the stump.

Traditionally, prosthetists rely on their skill and experience to design and fabricate the prosthetic socket. To achieve a satisfactory socket, a trial and error approach has to be adopted until a successful fit is obtained. As a result, conventional socket designs are largely subjective and the quality of fit is dependent on the prosthetist.

1.1.2 Use of CAD/CAM and FEA

Over the last two decades, Computer-Aided Design and Computer-Aided Manufacturing (CAD/CAM) technologies have been employed in prosthetic socket design [1-4]. However, such software was only a tool and the exact socket design still depended on the experience of the prosthetists and their subjective assessment of the patient's residual limb shape and soft tissue properties. The quantitative biomechanical properties of soft tissues were still not being considered.

This was until the introduction of Finite Element Analysis (FEA) to study the stresses generated at the stump-socket interface due to loading. FEA is a computational technique originally developed for full-field analysis of structural stress/strain in engineering mechanics. Its ability to determine the state of stress and strain in a particular field makes it ideal for parametric analyses in the design process. It has since been used commonly in the area of orthopaedics biomechanics [5].

The FEA software alone cannot assess the quality of fit of a socket as biomechanical properties of the residual limb soft tissues such as modulus, Poisson's ratio and tissue thickness are required as inputs for residual limb finite element models. Once these biomechanical properties are available, FEA can then provide information on the interaction at the stump-socket interface, as well as the stresses within the soft tissues.

Finite element methods, based on information of limb tissue properties, can be integrated into CAD/CAM techniques to optimise and improve prosthetic socket design. Assessment of the socket design can be done by evaluating the FEA results before the socket is actually manufactured. The design can then be modified until satisfactory results are achieved. Two main advantages in the use of FEA in prosthetic socket design are that firstly, FEA increase our understanding of the biomechanical interactions taking place at the stump-socket interface. Secondly and probably more importantly, is the speed with which FEA can parametrically analyse complex situations.

The main challenge in prosthetic socket design thus remains to be able to attain a physiologically suitable pressure distribution at the stump-socket interface. Achieving such an ideal pressure distribution pattern depends mainly on being able to obtain accurate information on the geometry, biomechanical properties, and stress tolerance levels of the residual limb. In order to design a good socket fit with optimal mechanical load distributions, it is critical to understand how the residual limb tissues respond to the external loads and other physical phenomena at the interface.

1.1.3 Biomechanical Properties Assessment

Biomechanical and geometric properties of the residual limb tissues have been recognised as important inputs to FE modelling of the prosthetic socket [6-10]. The challenge is not of obtaining the mechanical properties of prosthetic components or bone, but the *in vivo* mechanical properties of the soft tissues.

Soft tissues are non-homogeneous, comprising of skin, fat, muscles, embedded blood vessels, tendons and ligaments. They are of irregular geometry and have complex material properties such as anisotropicity, viscoelasticity and time dependency which vary from location to location in the musculoskeletal system depending on the composition of soft tissue at each region.

Load transfer in human tissues, e.g. tendons, ligaments, muscles and skin usually takes place along their longitudinal axis or plane of surface in the case of skin. However, at interfaces where some weight of the body is supported, such as the buttock tissues when sitting down, the plantar tissues of the foot when standing or walking, or the residual limb tissues when using a prosthetic socket, significant loads are transmitted via the soft tissues to the underlying bone structure, normal to the skin surface. Thus, biomechanical assessment of soft tissues normal to the body surface is important in the design of body support interfaces.

A common way to assess the biomechanical characteristics of residual limb tissue in a clinical setting is palpation, in which the prosthetist feels the shape and firmness of a stump with his hands. This produces a subjective assessment and requires substantial

clinical experience. In addition, the subjective nature of palpation makes it difficult to collect quantitative data.

A quantitative biomechanical assessment method is needed, and among the various mechanical testing methods that have been utilized, indentation testing is probably the most popular. An indentation test very much resembles the situation of palpation but it is able to quantitatively determine the *in vivo* mechanical behavior of skin and soft subcutaneous tissues when subjected to compressive loading. Indentation testing is thus an effective and relatively simple way to gather biomechanical properties of soft tissue which can be used in conjunction with CAD-FEA prosthetic design systems.

1.2 Project Objective

The objective of this project was to determine the *in vivo* biomechanical properties of lower limb soft tissues, namely tissue modulus and discomfort/pain threshold, using an indentation and pain feedback system. These soft tissue properties would be used in a CAD-FEA lower limb prosthetic design system.

1.3 Thesis Overview

The next chapter contains a review of the literature relevant to this project, including areas such as prosthetic socket designs, computational modeling, assessment of biomechanical properties and tissue responses under mechanical loading. The methodology used in this study will be explained in chapter 3. Indentation and finite element simulation results will be presented in chapter 4, followed by a discussion of these results.

Chapter 2: LITERATURE REVIEW

2.1 Prosthetic Socket Designs

The prosthetic socket, being a human-device interface, should be designed so as to achieve optimal load transmission, stability, and effective control of motion. Some early designs of the prosthetic socket such as the "plugfit," were designed as a simple conical shape with very little biomechanical rationale involved. Over the years, it became obvious that biomechanical understanding of the interaction between the prosthetic socket and the residual limb is crucial to improving the socket design. With an understanding of the residual limb anatomy and the biomechanical principles involved, more reasonable designs soon came about.

2.1.1 Trans-Tibial Prosthetic Sockets

Trans-tibial prosthetic sockets are for lower-limb amputees who have their leg amputated below the knee, i.e. across the tibia. By considering the weight-bearing characteristics of interface designs, trans-tibial sockets can be classified into three categories [11]:

The first category is Specific-Area Weight Bearing, also known as Patellar Tendon Bearing (PTB), which was developed following World War II [12]. This design (Fig. 2.1) transfers the weight-bearing stress solely to specific anatomical areas like the patella tendon, popliteal fossa, and the medial tibia flair as such areas are more pressure-tolerant. Relief is given to the more pressure-sensitive areas such as bony prominences.

The PTB socket is still practicable for, and preferred by many patients, especially those with shorter or bony residual limbs, or those requiring additional knee stability. This socket may not be suitable for patients with residual limb scar tissue, and those who experience chronic skin breakdown. A Pelite or foam liner is often used instead of a silicone or gel liner to provide the best fit.

Figure 2.1. Patellar Tendon Bearing (PTB) design

By the 1980s, the second and third categories, namely Total Surface Bearing (TSB) and Hydrostatic Weight Bearing (HST), were introduced. The TSB design (Fig. 2.2) distributes the weight-bearing forces as uniformly as possible over the entire residual limb surface. The aim is to uniformly maintain a minimum amount of skin pressure. This usually involves a gel sleeve to help redistribute the pressure in high-pressure areas in the residual limb.

It is a primary option for patients with residual limb inconsistencies and can be used for all residual limb lengths. Drawbacks include potential hygiene issues for some

wearers and the cost of replacement liners, particularly for “high maintenance” patients.

Figure 2.2. Total Surface Bearing (TSB) design

The HST design applies fluid mechanics principles and a compression chamber (Fig. 2.3) to produce a uniform fit. This socket can be considered a specific version of the TSB design, incorporating a gel liner and cast in a compression environment to achieve uniform pressure distribution across the residual limb surface. Examples include the silicone suction socket [13], ICEROSS [14] and PCast system [15,16].

The design encourages tissue elongation within the liner by increasing padding at the distal residual limb. The advantages of this relatively new design include less potential for skin breakdown, a comfortable fit due to nearly equal force distribution across the residual limb, and the security of distal suspension. It has been shown to be a good choice for some patients with pronounced bony prominences in their residual limb. Conversely, HST sockets are not appropriate for long residual limbs, patients

prone to perspiration, and those who because of either advanced age or medical limitations are unable to stand up to the rigors of donning a distal suspension prosthesis.

Figure 2.3. Össur ICECAST compression casting bladder

2.2 Computational Modelling

2.2.1 CAD/CAM

The technology in this area is getting relatively mature as more and more commercial CAD socket design systems are available. A method for defining and comparing manual socket modifications quantitatively was developed by Lemaire *et al*. [17] and integrated into a CAD software package. The numerical comparison procedure comprised: (a) Digitizing premodification and post-modification models of a prosthetic socket, (b) Aligning the two shapes to a common axis, and (c) Generating a color coded 3D image. The differences between sockets were used to outline

individual modifications. Modification outlines from a series of patients were averaged to determine a prosthetist's general modification style.

Sidles *et al*. [18] used different colors to represent the modifications done on a 3D image of a prosthetic socket, which also indicate the distribution of pressure build-ups and relieves. Borchers *et al*. [19] used different colors to represent the shape differences between a foot and a shoe.

2.2.2 FE Modelling

Finite Element Analysis was first introduced to the field of prosthetic socket design during the late 1980s when Krouskop *et al*. [3] created an FE model of the socket shape for above-knee (AK) amputees; whereas Steege *et al*. [8,20-23] established the first below-knee (BK) stump-socket FE model and discussed if interfacial pressures could be predicted by this method.

Since then, several FE models [24–39] have been developed, as reviewed by Zhang *et al*. [40], Silver-Thorn *et al*. [41], and Zachariah and Sanders [42]. According to Zhang *et al*. [40], the development of these models can be phased into three generations. The first generation involves linear static analysis established under assumptions of linear material properties, linear geometry with infinitesimal deformation and linear boundary condition without considering any friction or slip at the interface. Models in this generation require relatively little computational time.

The second generation can be referred to as nonlinear analysis as they involve of consideration nonlinear material properties, nonlinear geometry and nonlinear

boundary conditions including friction/slip contact boundary. Such nonlinear FE analyses normally require an iterative process to solve. While relatively more computational time is required, more accurate solutions can be obtained by such nonlinear analyses.

The third generation would involve dynamic models. Analyses of this type not only consider variable external loads, but also material inertial effects and time-dependent material properties.

In almost all of the previous FE models, two obstacles to be overcome were (a) accurate modelling of the residual limb soft tissues and (b) the effects of donning procedures with friction/slip interfacial conditions. Residual limb tissues, being biological soft tissues, have complex mechanical properties and are able to undergo large deformation. The lack of an accurate description of such properties has hindered the development of an accurate computational model.

Existing data on soft tissue properties were mainly collected through indentation testing [43–50]. The material constants were extracted by curve-fitting the indentation force-deformation data with the use of FE technique [25] or using relevant mathematical model, usually with the assumption of linear elasticity, isotropy, and material homogeneity. The mathematical model most commonly used is the one derived by Hayes *et al*. [51]. This model will be discussed in greater detail in the section below. The effects of friction between the indentor and the soft tissue surface, as well as the effects of large deformation on the calculated Young's modulus were studied by Zhang *et al*. [52]. The Mooney-Rivlin material model has been used by

Steege and Childress [21] to model residual limb tissues with nonlinear elastic properties.

As mentioned, the accurate simulation of the donning process, with consideration of friction/slip interfacial conditions remains an obstacle to be overcome. The difficulty lies with the simulation of large displacements that take place during this donning procedure. Most socket rectifications are simulated by changing the displacement boundary conditions at the nodes along the outer surface of the socket or liner [3,25,29,30,32,34,39]. These changes in displacement boundary conditions are then applied to deform the residual limb soft tissue or liner to conform to the rectified socket shape. However, this does not accurately represent the donning process as the friction/slip that takes place is neglected.

Zhang *et al*. [28,29,39] used elements at the interface to simulate the friction/slip boundary conditions between the skin and liner. These were four-node elements that connected the skin and liner through corresponding nodes. However, they still could not fully simulate the donning process due to the large sliding motion between the liner and socket. Zachariah and Sanders [27] used an automated contact method to simulate the friction/slip interface whilst Finney [53] simulated the donning process by sliding the deformable residual limb into a rigid socket shell, using a simple idealized geometry.

2.3 Biomechanical Properties Assessment Methods

2.3.1 Indentation

i. Indentation Systems

Indentation testing is a long-established and the most popular method for determining the *in vivo* biomechanical properties of soft tissues. An indentation apparatus was first developed by Schade [54] to study the changes of creep properties of skin and subcutaneous limb tissues in oedematous conditions. Subsequent studies using various indentation apparatus reported that the biomechanical properties of limb soft tissues depended on factors like subjects, test sites, states of muscular contraction, age, gender and pathological conditions [55–63]. The testing sites used in these studies were usually on lower limbs and forearms. Since the late 1980s, several indentation apparatus have been developed for biomechanical assessment of residual limb soft tissues [8,9,21,43,45,47,48,50,64–71].

Whenever indentation tests are used in the assessment of *in vivo* biomechanical properties of soft tissues, the following issues have to be considered: (a) how to fasten and align the indentor, (b) how to drive the motion of the indentor, (c) how to determine the indentation depth, (d) how to determine the tissue thickness and (e) how to interpret the indentation data.

Various kinds of mechanical alignment devices have been used to fasten the indentor and provide an anchorage for the indentor to be driven toward the tissue surface [43,54,55,58–61]. A common fastening method is to secure the indentation apparatus

to the prosthetic socket or a similar shell. The indentation would then be done through specific ports in the socket or shell [8,9,66,68,70,72]. These indentors could either be driven manually [8,64,67] or by microprocessor-controlled stepping motors [9,43]. Pathak *et al*. [70] and Silver-Thorn [71] reported using portable, motor-driven indentation apparatus which still needed to be attached to a frame or shell during testing.

In most cases, the depth of indentation is equated with the displacement of the indentor. When the indentor is driven manually, this displacement was usually determined using a Linear Variable Differential Transformer. When the indentor is driven by a motor, this displacement can be calculated from the rotational motion of the step motor, which can also be used to control the rate of indentation. The applied load during the indentation test is recorded using force sensors or load cells.

A number of hand-held indentors have been reported in the literature [47,48,62,63,69]. The indentors were driven either manually [48,50,62] or pneumatically [47,63] onto the skin surface. Horikawa *et al*. [62] used a laser distance sensor to determine the indentation depth. This laser sensor used a point on the skin surface some distance away from the indentor as a reference point for displacement measurement. However, an inaccuracy in measurement could arise if the reference point was too close to the indentor and was affected by the movement of the indentor. Ferguson-Pell *et al*. [63] used a pneumatic indentation apparatus with a variable compressive force adjusted using a close-loop control.

Vannah *et al*. [47] used a pencil-like indentation probe with a pneumatically driven piston that could indent the tissue at a frequency of 10 times per second. The indentor tip contained an electromagnetic digitizing element, which recorded the position and orientation of the indentor. The pneumatic pressure was measured at the inlet of the hose connector. One particular use of this indentor could be to make a scan around the limb and map the behaviour of the limb tissues under compression.

A common shortcoming in the indentation apparatus mentioned so far is that they are unable to simultaneously determine the thickness of the soft tissues being indented. Zheng and Mak [48,49,69], though, developed an ultrasound palpation system that was able to do this. Their system had a pen-sized hand-held indentation probe and an ultrasound transducer at the tip of the probe which served as the indentor. The thickness and deformation of the soft tissue layer could be determined from the ultrasound echo signal. A load cell was connected in series with the ultrasound transducer to determine the tissue's reaction forces. The probe was manually-driven, with the indentation rate calculated from the indentation response. This ultrasound system has been used for the assessment of residual limb soft tissues [50], plantar foot tissues [72] and neck fibrotic tissues [73]. It has also been used to determine the properties of different tissue sub-layers [48,74].

However, ultrasound indentation systems are known to produce noisy signals. Also, the fact that the indentation probe is hand-held makes it difficult to ensure repeatability in the positioning and alignment of the probe. Maintaining a constant indentation rate by hand is almost impossible.

ii. Indentation Rate

The effect of indentation rate on the extraction of the effective tissue modulus from indentation test data is a common concern. Some investigators measured the instantaneous and equilibrium modulus just after the ramp indentation phase and after a long enough force-relaxation time [43]. That study showed that the instantaneous modulus was slightly larger than the equilibrium modulus for the residual limb tissues. There have been studies on the effects of indentation rate on load-indentation response. For Reynolds' study, the loading rates were 0.3, 0.8, and 1.3 mm/s [67]; for Torres-Moreno's study the rates were 9.9, 14.2, and 19.8 mm/s [9]; and for Silver-Thorn's study the rates were 1, 5, and 10 mm/s [71,139]. In these studies, the limb tissues were confined within sockets or other type of shells and the interaction between the limb tissues and the socket or shell was not analyzed. Hence, it was not known whether all the rate-dependent responses observed in these studies were caused by tissue viscoelasticity or not.

It was shown in these studies that such rate sensitivities also depended on variations among test subjects and sites. Krouskop *et al*. [75] reported that the extracted modulus of soft tissues was rate insensitive. They used three indentation rates ranging from approximately 0.2 to 10 mm/s in their *in vitro* study on normal and abnormal excised breast and prostate tissues. The corresponding variation in stiffness was noted to be within 10 %. Zheng *et al*. [50] found that the extracted Young's modulus was roughly rate independent by conducting *in vivo* tests on forearms with 5 manually controlled indentation rates ranging from 0.75 to 7.5 mm/s. Silver-Thorn [71] found that testing at a higher indentation rate might not result in a larger slope of the load-indentation response. In general, relatively small rate dependence was observed in these studies.

iii. Alignment of Indentor

The alignment of the indentor is another important issue when carrying out indentation tests. A FEA study showed that during indentation, the stress distribution in the tissue directly under the indentor was influenced significantly by the alignment of the indentor. However, the total resultant force transient of the indentation response was only slightly affected for a misalignment of up to 8^{o}, when the Poisson's ratio is assumed to be from 0.3 to 0.45 [76].

Tissue responses to indentation could be significantly influenced by the alignment of the indentor at sites where the tissue thickness is equal to or less than the diameter of the indentor. It was observed that when the indentor was misaligned up to 12.5^{o}, the effect on the indentation response decreased as the tissue thickness increased and became almost negligible when the thickness was more than 2 times the indentor diameter [69]. Similar results were observed in an *in vivo* experiment [50].

iv. Confinement of Tissue

Some investigators measured the limb soft tissue properties with the limb placed in a socket or in other types of structures that confined the tissues [8,9,21,25,45,64-67,68,70,71]. In some studies, the indentation apparatus was attached to the socket and the indentation test was performed through a port in the socket. In other studies, investigators tested the limb tissues in a free state [43,47,49,50,69]. When the tissues were confined, the load-indentation response was affected by the boundary/interface conditions. Torres-Moreno [9] showed that the interaction between the socket and the residual limb tissue would affect the indentation response when the test was conducted through a port on the socket. Therefore, for the extracted material

properties to be an accurate representation, the conditions at the stump-socket interface should be taken into account.

2.3.2 Vibration Method

Vibration methods have also been used to measure biomechanical properties of soft tissue. Krouskop *et al*. [77] developed an ultrasound measurement apparatus with a vibration device that vibrated the limb tissue at 10 Hz. The response of the internal tissue to this vibration was measured using an ultrasound Doppler technique. The Young's modulus of the tissue was then calculated from the tissue's response to vibration and the tissue density. This method was able to measure the biomechanical properties of tissues at different depths.

Another vibration method by Lindahl *et al*. [78] made use of a piezoelectric vibrator functioning in ultrasound frequency. This vibrator was put in contact with the skin surface and the resultant change in the vibrator's resonant frequency, due to the tissue acoustic impedance, was measured and used to calculate the tissue modulus. Since the biomechanical properties measured were those of the tissues in the superficial layer, this method was mainly used for the biomechanical assessment of skin.

2.4 Tissue Responses under Mechanical Loading

Soft tissues have wide-ranging and complicated responses to external forces. They include tissue deformation, interstitial fluid flow, ischemia, reactive hyperemia, sweat, pain, skin temperature and skin colouration, among others. Forces encountered under normal physiological conditions will usually not impair tissue functions. However, when an abnormally large force or a smaller but sustained and repetitive force is exerted on the tissue, it may damage the tissue's functions and/or internal structure. As with all mechanical structures, forces exerted on the surface of the skin will be transmitted to the underlying tissues, producing stresses and strains. These stresses and strains affect the functions and various biophysical processes in the cells of the tissue.

For example, a very large and sudden force may cause a tear in the skin; whereas a sustained compressive force applied to the skin may cause the underlying blood vessels and lymphatic ducts to be partially or fully occluded. Oxygen and other nutrients necessary for the tissue's metabolic activity can no longer be sufficiently delivered by the blood vessels, and metabolic waste products would accumulate as the lymphatic system would be unable to remove them quickly enough. Over time, the ability of cells to function would be impaired and could eventually fail [81]. This is why tissue breakdown occurs not only at the skin surface but is often found also in underlying tissues [80,81].

A repetitive force may damage tissues by an accumulation of its effect. Even if a force is not large enough to cause damage to the tissues directly and immediately, repeated exertion over time could start an inflammation reaction, and even result in tissue

necrosis. The tissue may also adapt by altering its composition and structure when the load is applied over a certain duration [134].

Besides the magnitude of the force, other characteristics such as its direction, distribution, duration and loading rate should also be considered. Forces applied to the skin surface can be resolved into a normal component perpendicular to the skin surface and a shear component tangential to the skin surface. Some researchers suggested that tissue deformation or distortion, rather than the pressure alone, are important factors when studying tissue damage by external loads [84,85]. When the pressures are evenly distributed over a large area, damage to the tissue is apparently less than when they are concentrated over a localised area [86].

There seems to exist an inverse relationship between the intensity and duration of the external loads required to cause ulceration [80,87-89]. A number of researchers have attempted to give a theoretical explanation for this inverse relationship [90-93]. Mak *et al*. [92,93] put forward the physics of interstitial fluid flows induced by a given epidermal pressure to account for the corresponding endurance time. Landsman *et al*. [94] hypothesised that a higher strain rate of tissue deformation may cause a higher pressure buildup in the tissues and a higher elevation of intracellular calcium concentration, potentially leading to more damage to the involved tissues.

Residual limb soft tissues can be said to be in a very harsh environment when in a prosthetic socket. Firstly, pressures and shear forces are continually and repetitively exerted on the residual limb tissues by the walls of the tightly-fitted socket. Secondly, as the skin rubs against the edge of the socket or its inner surface, it might cause

deformation and irritation of the skin. In extreme cases, there will be abrasion of the skin, accompanied by generation of heat. Thirdly, a tightly-fitted socket prevents circulation of air into, and perspiration out of the socket, thereby increasing the temperature and humidity inside the socket. Fourthly, the tissues may be sensitive to, or have allergic reactions to the materials used to make the socket or liner [95,96].

In view of this, restoration of mobility to the amputee is not the only consideration when designing a prosthetic socket. Equally, if not more important, is whether the residual limb soft tissues will break down or have adverse reactions to the daily use of the socket [97].

2.4.1 Tissue Modulus

Early indentation tests were commonly carried in a loading-creep-unloading sequence and the tissue responses were characterised empirically [55]. In 1972, Hayes *et al*. [51] derived a rigorous elasticity solution to the problem of an infinitesimal indentation by a frictionless, rigid, axisymmetric indentor on a thin elastic layer bonded to a rigid foundation. Solution of partial differential equations following from boundary conditions led to the expression of Young's modulus:

$$E = \frac{\left(1 - \nu^2\right)}{2ak} \cdot \frac{P}{\omega} \qquad \text{-----} \quad (1)$$

where P is the load exerted, ω is the depth of the indentation, v is the Poisson's ratio of the tissue layer, a is the radius of the indentor tip and k is the scaling factor. The boundary conditions used and the solution of partial differential equations have been described in more detail in Appendix 6.

Hayes et al. formulated their elastic contact problem by considering the equilibrium of an infinite elastic layer resting on an immovable rigid half-space, which in our case can be represented by the lower limb's soft tissue assumed to adhere to the underlying bone surface. The soft tissue deformed under the action of a rigid axisymmetric indentor pressed normal to the skin surface by an axial force. Shear tractions between indentor and skin surface were also assumed to be negligible. Hence the boundary conditions used in the solution by Hayes et al. are very similar to the experimental conditions reported in this thesis.

The scaling factor k provides a theoretical correction for the finite thickness of the elastic layer and depends purely on both the aspect ratio a/h (h being the tissue thickness) and Poisson's ratio.

From equation (1) above,

$$k = P(1- \nu^2)/(2aE\omega) \qquad \text{-----} \qquad (2)$$

k is a dimensionless factor obtained by Hayes *et al*. [51] through numerical methods from the above equation at given values of the parameters a/h and ν. Tables of values of k over a range of a/h and ν were provided by Hayes *et al*. [51] for both plane-ended and spherical-ended indentors, and have been included in Appendix 6. Values of k used in this thesis were extracted from the paper by Hayes *et al*. [51] and have been included in Appendix 4.

A closed form solution of the factor k was proposed by Sakamoto *et al*. [98] and the results agreed well with those obtained by Hayes *et al*. [51]. For a plane-ended

indentor, as the aspect ratio a/h tends towards zero, k tends towards 1. For a spherical-ended indentor, as the aspect ratio a/h tends towards zero, k tends towards 0.675.

Other than Hayes' solution, computational methods involving the use of FEA were developed to extract the tissue modulus from the indentation tests [8,45,64,67]. Reynolds [67] modelled an indentation of an assumed infinite tissue layer with idealized material properties and used it to estimate the Young's modulus by matching its predictions with the experimental load-indentation curves. Steege *et al*. [8] and Silver-Thorn [64] developed another method to estimate tissue modulus from indentation test data by using the stump-socket FE model that was initially established for the study of the interaction between the socket and the residual limb. The testing sites were identified on the FE model and a unit-normal compressive load was applied. The soft tissue was assigned an initial E value and an analysis was carried out. By comparing the FE analysis results with the experimental indentation depths, an estimation of Young's modulus was obtained. In a similar FE approach, Vannah and Childress [45] used a strain energy function to represent the tissue properties and extract them from indentation test data.

The effective Young's modulus of lower limb soft tissues reported so far were 60 kPa [8], 53–141 kPa [44,77], 50–145 kPa [25], 27–106 kPa [9], 21–194 kPa [43], 10.4–89.2 kPa [49] and 60–175 kPa [50]. Results from these studies showed that several factors like age, testing site, body posture, muscular contraction, biological condition, and gender significantly affected the effective Young's modulus of lower-limb soft tissues. Only tissue properties of specific sites were investigated in most studies due to the difficulties of imaging the entire residual limb.

2.4.2 Nonlinearity

Soft tissues commonly give a nonlinear biomechanical response when subjected to loading [99]. It has been reported that the load-indentation responses of limb soft tissues could be represented by second-order polynomials when the tissues were unconfined [49,50], and by third-order polynomials when confined by a prosthetic socket [64,71]. Torres-Moreno [9] measured the modulus at different indentation depths to demonstrate the nonlinear dependence of the soft tissue properties. Zheng and Mak [69,100] derived an initial modulus and a nonlinear factor using an incremental method. The effective modulus could be calculated in an incremental manner with the tissue thickness adjusted in each step. They also managed to extract the nonlinear properties of limb soft tissues using a quasilinear viscoelastic indentation model [48,69]. Vannah and Childress [45] used a strain energy function to extract their nonlinear material parameters of soft tissues. Recently, Tönük and Silver-Thorn [139] estimated the nonlinear elastic material properties of lower-extremity residual limb soft tissues through indentation. They used MRI and CT scans to obtain average values of soft tissue thickness.

However, the usefulness of the derived polynomial coefficients for nonlinearity responses was limited because these indentation responses depended on the biomechanical properties of the soft tissues, as well as the tissue thickness and the boundary/interface condition at each location. The extracted biomechanical properties also depended on the amount of preloading and the total load applied during indentation.

2.4.3 Large Deformation Effects

In addition to the material nonlinearity, large deformation effects of indentation on a soft tissue layer should also be taken into consideration. In the mathematical solution proposed by Hayes *et al*. [51], infinitesimal deformation was assumed. This assumed condition was not always satisfied in the indentation tests. To address this issue, Zhang *et al*. [52] conducted a large deformation finite element analysis of Hayes' elastic layer problem. It was shown that the scaling factor k in Hayes' solution increased slightly with the depth of indentation. Thus, the nonlinearity of the indentation responses is partially caused by this large deformation effect. Using Hayes' solution for an infinitesimal elastic layer to calculate the tissue modulus for a large indentation depth may produce an erroneous result, especially for large aspect ratios a/h [50,52].

2.4.4 Poisson's Ratio

One material parameter normally assumed in any analysis is the Poisson's ratio. According to Hayes' solution, the value of Poisson's ratio chosen would cause affect the tissue modulus obtained, especially for aspect ratios a/h greater than one [50]. In most of the indentation tests on skin and subcutaneous tissues so far, researchers assumed the Poisson's ratio to be a constant ranging from 0.45 to 0.5 to simulate the nearly incompressible behavior of the tissue as a whole [8,9,43,45,50,62,64,67].

Although this assumption was consistent with the interpretation of the instantaneous or short-time indentation results using the modern biphasic theories [101,102], the assumption of the same Poisson's ratio for different indentation sites, different states

of muscular activity, subjects of different ages and for both normal and residual limb tissues was rather bold. The Poisson's ratio should ideally be measured *in vivo* along with the tissue modulus. However, methods for measuring the Poisson's ratio of soft tissues *in vivo* are lacking and require further investigation.

2.4.5 Viscoelasticity

Viscoelasticity of soft tissues can be observed in load-indentation responses such as hysteresis and rate dependence. Most of the investigators selected the loading phase for the extraction of material properties to avoid complications due to hysteresis.

Coletti *et al*. [103] modelled the phenomenon using a Kelvin-type standard linear solid model to address the indentation creep behaviour of articular cartilage. Silver-Thorn [71] used a similar one-dimensional model to extract the viscoelastic parameters of limb soft tissues from the load-indentation response. Parsons and Black [104] extended Hayes' solution to a generalized Kelvin-type viscoelastic solid. A continuous relaxation spectrum was derived from the experimental data with the use of some approximations. Mow *et al*. [102] obtained a mathematical solution for the indentation creep and stress-relaxation behaviour of articular cartilage using a biphasic model. Spilker *et al*. [105] and Suh and Spilker [106] reported further biphasic analysis of the indentation of articular cartilage using finite element analysis.

Fung [99] proposed a quasi-linear viscoelastic theory to describe the load-deformation relationship of biological soft tissues. His theory suggested that the load response of a tissue to an applied deformation history was expressed in terms of a convolution integral of a reduced relaxation function and a nonlinear elastic function. Zheng and

Mak [107] applied this solution form to the indentation solution. The quasi-linear viscoelastic indentation model was used to study the nonlinear and time-dependent behaviour of the limb soft tissues. Linear and nonlinear moduli and the associated time constants for the limb soft tissues were extracted from the cyclic load-indentation response using a curve-fitting procedure.

2.4.6 Pain

A sensation of pain or discomfort is the immediate physiological response when the body is subjected to large external loads. Usually, the degree of pain experienced is directly proportional to the magnitude of the load exerted. The normal pain sensory function of a human body can warn of excessive loads applied to the skin surface, prompting the person to take action to prevent further application of the load and thus prevent subsequent tissue. Neuropathy can lead to the loss of this important function and may result in tissue damage such as the formation of pressure sores in patients with diabetes or spinal cord injuries.

Pain thresholds in response to loads vary between different anatomical locations and between different people. Studies have been done by Fischer [108] to quantify the body's ability to withstand external loading based on the pressure threshold, i.e. the minimum pressure to induce pain or discomfort, and the pressure tolerance, i.e. the maximum pressure a person can tolerate without excessive effort. Wu *et al*. [109] also conducted an assessment for socket fitness by obtaining the pain-pressure threshold and tolerance for a below-knee amputee and combining this information with finite element analysis. For residual limbs, the tolerant and sensitive areas have been identified qualitatively [12]. Studies have been reported on the load-tolerance levels

of the distal ends of residual limbs [110,111]. Lee *et al*. [112] investigated the regional differences in pain threshold and tolerance of the trans-tibial residual limb due to 2 different indentor materials, using an indentor with a manually-controlled load rate of about 4 N/s.

2.4.7 Microvascular Responses

It is the general belief that ischemia is linked to the formation of pressure sores by depriving an area of necessary nutrients. Changes in local skin blood supply under various external loading conditions have been studied for a number of years. A series of reports have described the effects of external loads on skin blood flow using radionuclide clearance [113-115], photoplethysmography [116,117], transcutaneous oxygen tension [118-120], and laser Doppler flowmetry [121-128]. The results of these studies seemed to indicate that blood supply was affected by epidermal loading, and the rate and amount of blood supply decreased when epidermal loads increased.

Investigations have been done to study the effects of shear forces in conjunction with normal forces [116,125-127,129]. It was found that cutaneous blood flow was reduced with the increased application of either the normal force or the shear force. The resultant force is a critical parameter in assessing the combined effect of these multi-axial loads [126]. Tam *et al*. [127] compared the reactive hyperemia in skin induced by the application of a normal force and that due to the application of both normal and shear forces. It was found that the addition of shear force increased the tissue recovery time from the effects of hyperemia.

2.4.8 Lymphatic Supply and Metabolites

The lymphatic system consists of a complex network of vessels, and allows the drainage of excess fluid, protein, and metabolic wastes from the tissue of origin into the circulatory system. External loads may interfere with the ability of this system to function. Husain [86] found that with tissue oedema, poor lymphatic function was associated with the formation of pressure sores. Krouskop *et al*. [130] suggested that the smooth muscle of the lymphatics was sensitive to anoxia, and thus the impairment of the lymphatic function combined with changes in the microvascular system could compromise tissue viability through the accumulation of metabolic wastes.

The levels of metabolites in sweat may be used as indicators of the tissue viability status [131,132]. Studies showed that epidermal loads could change the amounts and composition of sweat [133]. It was found that there was a significant increase in sweat lactate during loading and a decrease in sweat volume during ischemia.

2.4.9 Skin Abrasion

The human skin is subjected to many physical abuses, the most common of which is frictional rubbing [134]. Frictional injuries can produce a variety of skin lesions such as calluses, corns, thickening, abrasions, and blisters [135]. Repetitive rubbing produces heat, which may cause uncomfortable and detrimental consequences [96]. Naylor [134] mentioned two kinds of skin reactions to repeated rubbing. One involved the thickening of the skin if the abrasive force is small but rubbing is frequently repeated. The other involved the formation of blisters if the abrasive force is large enough. Akers [135] observed that blisters apparently do not often form on thin skin, but on tough and thick skin.

Experiments have been conducted to study skin lesions under repetitive pressure with and without the involvement of frictional force [135-137]. Results indicated that the addition of friction would accelerate skin damage. Sanders [138] measured the thermal response of skin to cyclic pressure alone and to cyclic pressure with shear. The results from three normal subjects indicated that the thermal recovery time was higher for the combined pressure and shear compared to the values for pressure alone. The apparent additional damage due to shear found in this study was consistent with other skin perfusion studies [127].

2.4.11 Shear, Friction and Slippage

Coupling between the residual limb and the prosthetic socket is an important factor in socket fit. It is affected by the relative slippage between the skin and the socket, as well as the deformation of the residual limb tissues. Socket shape can change the pressure distribution and the perceptible tightness of fit. Usually, a loose fit allows slippage but compromises in stability, while a tight fit offers more stability but increases the interface pressures. Excessive slippage at the socket interface should be avoided in socket fitting. However, absence of slippage may cause other problems such as discomfort due to the increase in interface temperature and perspiration inside the socket [140].

Another important factor affecting slippage is the friction between the skin and the socket surface. Shear forces are applied to the skin surface because of friction. Studies conducted on friction within the prosthetic socket include (a) investigation of the coefficient of friction of skin with various interface materials [141–143], (b)

measurements of shear stresses [145-148,175,179] and slip at the interface [101,144], and (c) the contribution of frictional shear to the load transfer.

Frictional properties of human skin under various skin conditions have been investigated [142,149–152]. Sanders *et al.* [142] measured the *in vivo* coefficient of friction of human skin with eight interface materials, using a biaxial force-controlled load applicator. Measurements were conducted on shaved and cleaned skin of the lower limb. The coefficients of friction were found to range from 0.48 to 0.89. Zhang and Mak [143] also measured the *in vivo* coefficient of friction of human skin but with five materials, namely aluminum, nylon, silicone, cotton sock and Pelite. Measurements were conducted on untreated skin over six anatomical sites. The average coefficient of friction was found to be 0.46. Among the five materials studied, silicone gave the highest value of 0.61 and nylon gave the lowest value of 0.37.

Measurements of shear stresses acting on the skin were first reported by Appoldt *et al*. [145]. They developed a beam deflection strain-gauge transducer that could measure the normal force and shear force in one direction. Sanders *et al*. [146–148,177,178] developed triaxial transducers to measure interface stresses on trans-tibial sockets. Two-directional shear was measured by mounting metal-foil strain gauges on an aluminum beam. These transducers have been used assess the shear stress magnitude [146], the transient shape of the stress waveform during walking [178], and the effects of alignment on these interface stresses [147,148].

Williams *et al*. [167] developed a small triaxial transducer that could measure normal force and shear force in two orthogonal directions. The normal force was sensed by

diaphragm deflection strain gauges. Biaxial shear forces were sensed by magneto resistors fixed at the center of the disk, which could slide on a cruciform to resolve the shear force into two orthogonal directions. Zhang *et al*. [175] further used these transducers to measure the stresses applied on the skin surface at eight locations of five trans-tibial sockets. A maximum shear stress of 61 kPa was found at the medial tibia area with PTB sockets during walking.

Appoldt *et al*. [144] reported on the measurements of slippage between skin and prosthetic sockets. They developed a slip gauge consisting of a pen whose inking tip was in light contact with the skin while being rigidly held to the wall of a trans-femoral socket. Marks made on the skin by the pen were used to assess the slip magnitude and direction. The results indicated that in a well-fitted total-contact suction socket the relative slip was less than 6 mm.

There are two main effects of friction between the residual limb and the prosthetic socket. Firstly, friction produces a shear action on the skin which leads to tissue distortion. This may affect tissue functions and can be harmful. On the other hand, friction at the skin surface can assist in supporting the ambulant load and in suspending of the prosthesis during the swing phase. Zhang *et al*. [175] developed an idealized cone-shaped model and a finite element model using the real limb geometry to predict the effects of friction on the load transfer. Their results showed that the smaller the friction, the smaller the shear stresses, but the larger the normal stresses required to support the same load.

Hence, reduction of interface friction may not always alleviate residual limb tissue problems. An adequate coefficient of friction could be desirable to support loads and to prevent undesirable slippage. However, a surface with large friction could experience high local stresses and tissue distortion when donning the socket, as well as during ambulation. A suitable amount of friction would be needed to balance between effective prosthetic control and minimization of interfacial risks [175].

2.5 Pressure Measurements

The pressure distribution at the stump-socket interface is a vital consideration for the purpose of determining quality of fit in socket design and testing. Studies on pressure distribution as well as methods of pressure measurement in prosthetic sockets have been conducted for about 50 years. Information on pressure distributions have been used to understand the mechanics of socket load transfer, to assess the socket design, or to validate the computational modelling.

Interfacial pressure measurements require the use suitable transducers, their correct placement at the prosthetic interface, as well as the related data acquisition and interpretation approach. An ideal system should be able to continually gather data on both normal and shear interfacial stresses without significant interfering with the original interface conditions. A range of transducers have been developed for socket pressure measurements. They can be classified, based on their operation principle, as fluid-filled sensors [153–155], pneumatic sensors [156–158], diaphragm deflection strain gauge [159–167], cantilever/beam strain gauge [168–170], and printed circuit sheet sensors [171–176], as reviewed by Sanders [177] and Silver-Thorn *et al*. [41].

Transducers at the stump-socket interface can be either inserted between the skin and the liner/socket, or placed within or through the socket and/or liner. Only sensors such as the diaphragm deflection strain-gauge sensors [160,161,163,164], the fluid-filled transducers [153], the pneumatic transducers [156,158], and the printed circuit sheet sensors [171–176], are thin enough to be inserted between the skin and socket. However, since many of these sensors have a finite thickness, minimal interference from their protrusion into the socket volume is unavoidable [167,168].

The diameter of each sensing element is another important factor to consider. Only the average pressure over an area can be measured with a sensing element that is too large, whereas edge effects may be significant in a sensing element that is too small, especially for a stiff sensor. Positioning the transducers within or through the socket such that the sensing surface is flush with the skin would make the transducer thickness less critical. For such mounting, recesses would need to be made on the experimental sockets to contain the transducers [167,168,178–180].

The techniques mentioned above were able to measure pressures at discrete focal sites because of the size of the sensing cells. Sensor mats with an array of pressure cells made it possible to measure the pressure distribution. However, a piece of material inserted at the interface may change the original conditions. Systems such as the Rincoe Socket Fitting System, Tekscan F-Socket Pressure Measurement System, and Novel Pliance 16P System have been commercially designed to measure *in situ* socket pressures.

Houston *et al*. [172] reported a specially designed Tekscan P-Scan transducer with 1,360 pressure cells. Rincoe force sensors were embedded in a polyvenilidyne fluoride strip with a thickness of 0.36 mm [182]. This system had a total of 60 cells arranged on 6 separate strips, each comprising 10 sensors. Shem *et al*. [183] reported on the use of this system. The sensor pad of the Novel Pliance 16P System had 434 matrix capacitance sensors with 1 mm thickness. The system allowed up to 16 sensor pads to be used simultaneously. There were advantages and disadvantages with each system. The performances in terms of accuracy, hysteresis, signal drift and response to curvature, of the above three systems have been compared by Polliack *et al*. [181,182].

There was a wide variation of pressures at socket interfaces reported among sites, individuals, and clinical conditions. For the PTB socket, the maximum peak pressure reportedly reached about 400 kPa [82], the highest among all the measurements reported. However, the measurements conducted in the last 10 years showed that the maximum interface pressure for PTB sockets during walking was usually below 220 kPa [171,178,179]. Such a wide range of pressure measurements among various studies may have resulted from (a) the diversity of the prostheses and fitting techniques used, (b) the difference in residual limb size, soft tissues thickness, and gait style, (c) the different positions studied, and (d) the different characteristics and limitations associated with each specific measurement and mounting method.

In the next chapter, the methodology employed in this project will be presented.

Chapter 3: METHODOLOGY

3.1 Soft Tissue Indentation

3.1.1 Experimental Set-up / System Components

Soft tissue properties of 2 unilateral trans-tibial amputees and 3 normal volunteers were investigated in this study. The properties investigated were tissue modulus, discomfort threshold - defined as the minimum discomfort-inducing pressure, and pain threshold - defined as the pressure at which the discomfort turns into acute pain.

Information on the subjects is shown in Table 3.1 below. Both of the amputees underwent amputation due to their diabetic condition which led to vascular disease. The nature, objective and procedure of the study were explained in detail to all subjects and their informed consent was obtained before any tests began. A sample of the "Patient Informed Consent Form" used has been included in Appendix 1. The study was conducted in accordance with the ethical guidelines of the National University of Singapore Institutional Review Board (NUS-IRB) and the National Healthcare Group Domain Specific Review Board (NHG-DRSB).

Table 3.1. Basic information on the five subjects

Subject	Sex	Age	Mass (kg)	Height (m)	Status	Test leg	Stump length (cm)	No. of years since amputation
1	F	20	50	1.65	Normal	Left	N.A.	N.A.
2	M	30	65	1.74	Normal	Right	N.A.	N.A.
3	M	27	63	1.82	Normal	Right	N.A.	N.A.
4	M	56	73	1.72	Amputee	Left	12	4
5	M	57	78	1.70	Amputee	Left	12.5	12

In order to obtain a systematic and comprehensive map of the limb tissue properties, a grid system was used. Starting with the patellar tendon, indentation was performed at 8 equidistant points around the limb circumference in the horizontal plane and repeated every 4 cm in the distal direction as far as the residual limb extended (Fig. 3.1). For the normal volunteers, the limb to be tested was chosen at random and points were taken up till 12 cm from the patellar tendon in the distal direction.

The grid system was numbered such that position 1,1 began with the patellar tendon. Positions 1,2 to 1,8 would then follow in an anticlockwise direction when looking from the proximal view. Row 1 comprised of the indentation points on the horizontal plane containing the patellar tendon (Fig. 3.2). Rows 2, 3 and 4 would each be 4 cm below the row preceding it. Positions 2,1, 3,1 and 4,1 coincided with the tibial edge as far as possible. Numbering of subsequent positions for each row followed the same anticlockwise direction as Row 1.

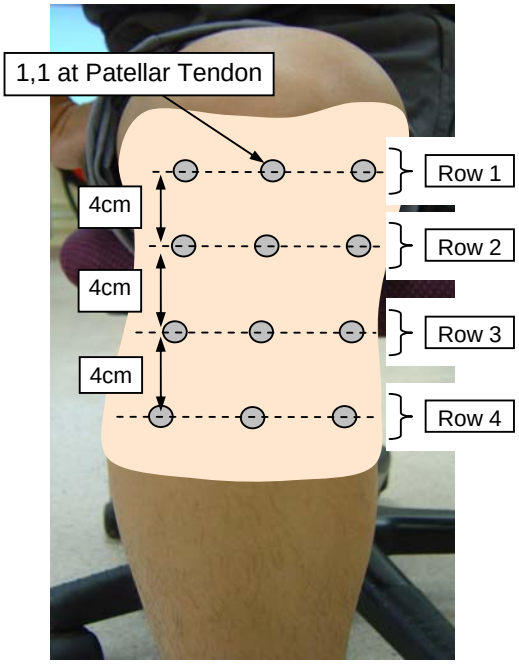

Figure 3.1. Positioning of indentation points relative to limb

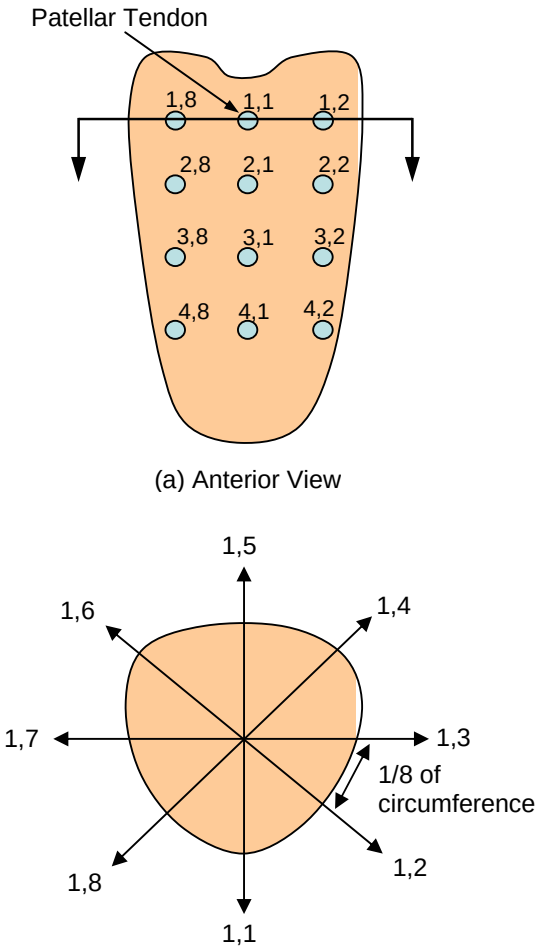

Figure 3.2. Anterior and transverse views of indentation grid system, respectively

Subjects first had a plaster cast of their test leg made by a prosthetist, from which a positive mould was obtained. The surface geometry of this positive mould was captured using CAPOD's prosthetic workstation (Össur Systems, Sweden), as shown in Fig. 3.3. A socket was then manufactured using a Rapid Manufacturing Machine (RMM) according to the geometry of the scanned image, as shown in Fig. 3.4. This method of prosthetic socket fabrication has been reported by Ng *et al*. [184].

Figure 3.3. Positive mould of residual limb in CAPOD's prosthetic workstation

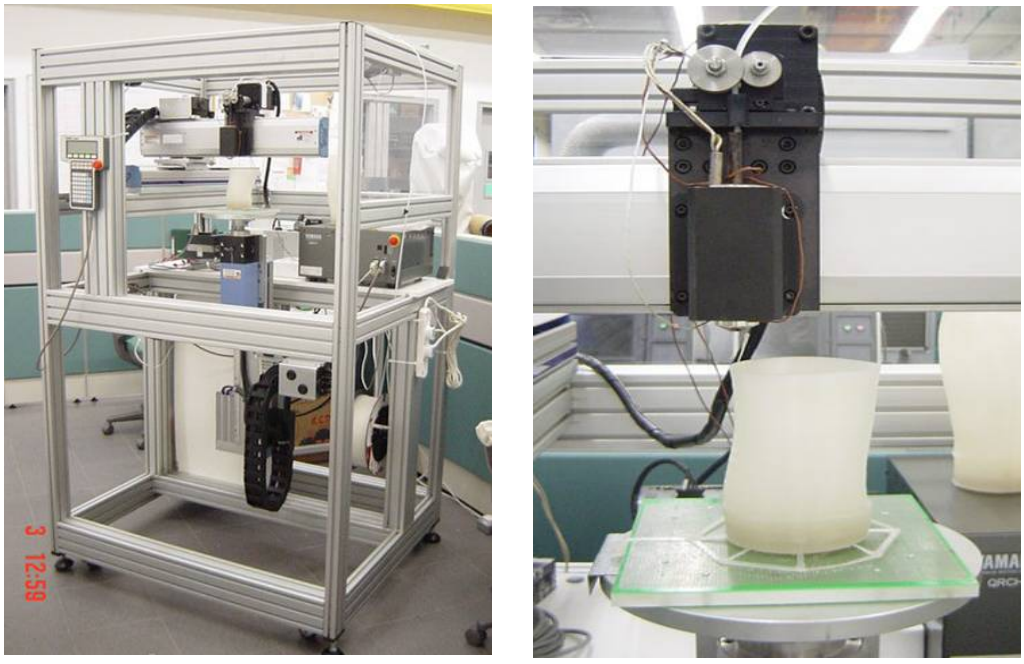

(a) Entire RMM system (b) Close-up of socket fabrication component

Figure 3.4. Rapid Manufacturing Machine used in socket fabrication

For the indentation test, normal subjects wore a RMM brace which extended from the patella to the mid calf area. They were asked to sit with both feet resting flat on the floor and knees bent at approximately 90^{o} (Fig. 3.5). Amputees wore a RMM socket with a flat base. They were asked to sit with both their knees bent at approximately 90^{o} and the foot of their good leg resting flat on the floor. The base of their socket rested on a platform that was adjustable in height (Fig. 3.6). The indentor was then secured in position on the exterior of RMM braces/sockets by screwing it into holes drilled and tapped through the brace/socket wall.

Figure 3.5. Leg position of normal subject during indentation test

Figure 3.6. Leg position of amputee during indentation test

The indentation system used for indentation tests comprised of an indentor and a pain feedback device. A schematic diagram showing the entire indentation system with its various components is shown in Fig. 3.7.

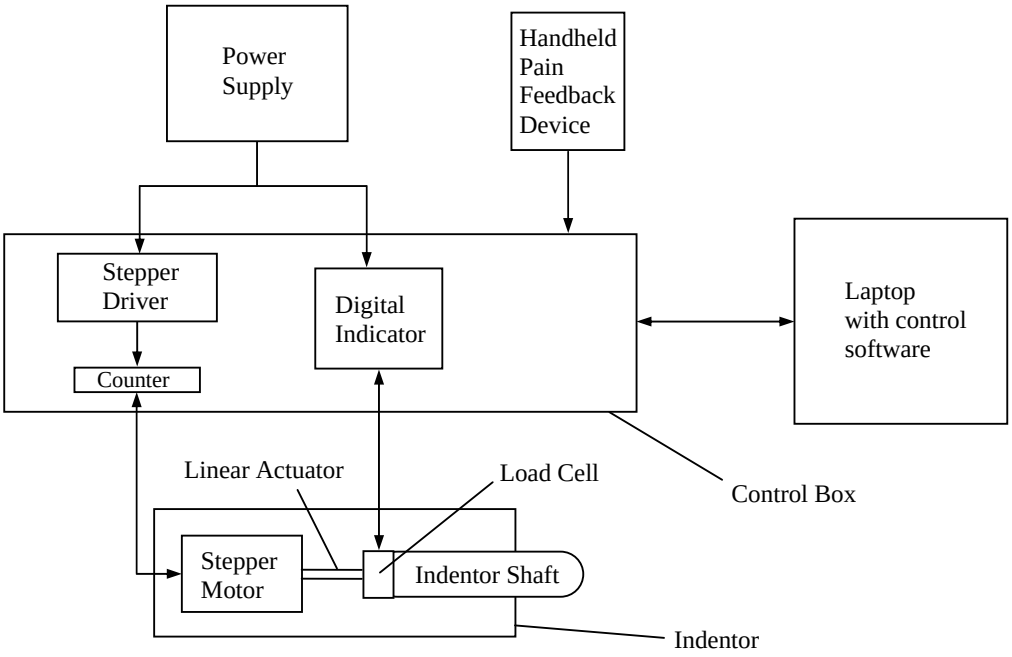

Figure 3.7. Schematic diagram of the indentation system

Indentation was performed using a cylindrical indentor with a hemispherical-ended stainless steel tip of 5 mm diameter (Fig. 3.8). The indentor shaft was driven by a linear actuator and stepper motor (Mycom 5 Phase Stepper Motor). A load cell (Futek L1610) in contact with the upper end of the indentor tip recorded the magnitude of reaction force exerted by the soft tissue. The load cell resolution was 0.001N and the stepper motor had a linear resolution of 0.1 mm. Technical drawings of the indentor have been included in Appendix 2.

Figure 3.8. Indentor

Subjects were given a handheld feedback device to indicate the onset of discomfort, i.e. when they just started to feel discomfort, and the onset of pain, i.e. when the discomfort turned into acute pain. There were several buttons on this handheld device (Fig. 3.9). Button “1” was pressed to indicate discomfort and button “2” was pressed to indicate pain. Buttons “3” to “5” were unused in this study but could be used to define pain in smaller intervals (e.g. from a scale of 1-5) in future studies. An emergency “stop” button was included to cancel the indentation process and retract the indentor shaft to its original position in case the pain became unbearable. The “pause” button was used to pause the indentation process in case the subject did not feel ready yet.

When either button “1” or “2” was pressed, this pain feedback device linked the point of indication to the corresponding force magnitude and depth of indentation as measured by the indentor. All this information was instantaneously recorded in the data log by the control software. The graph in Fig. 3.10 illustrates the various points in time when the subject indicated either “discomfort” or “pain”.

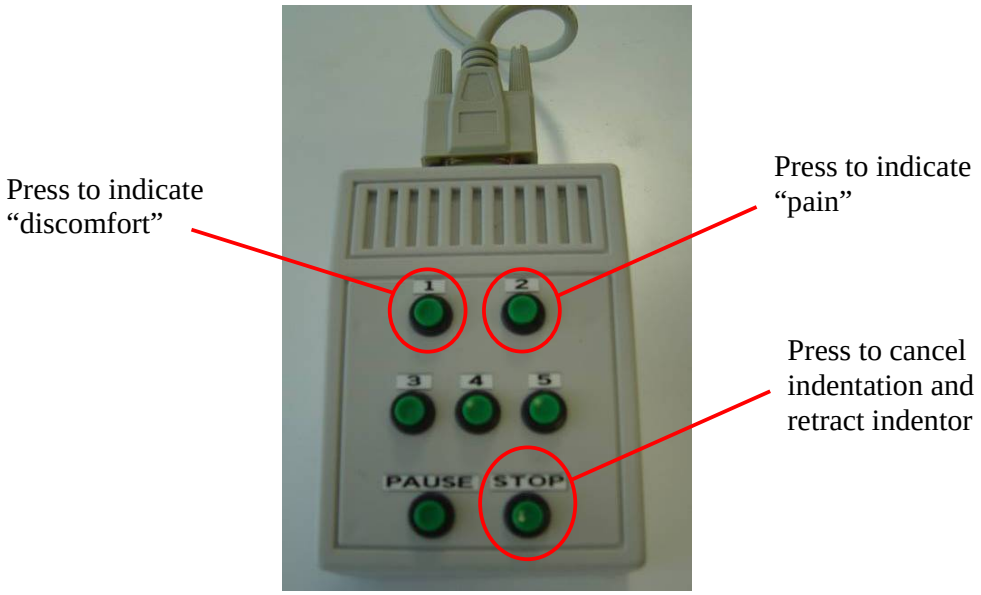

Figure 3.9. Pain feedback device

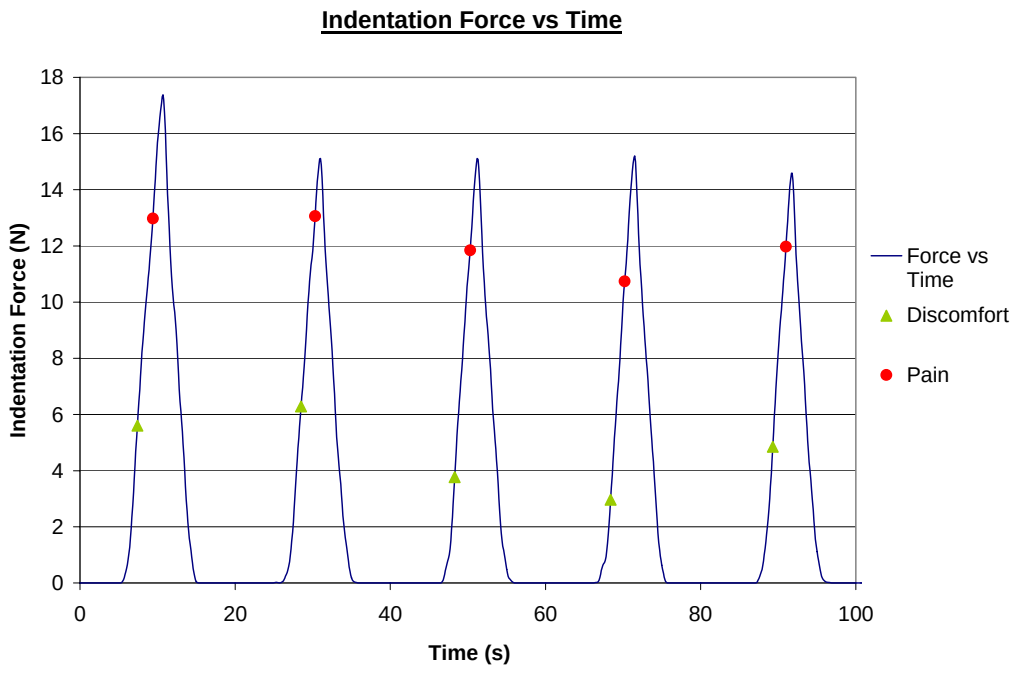

Figure 3.10. Graph illustrating time markers when “discomfort” and “pain” were indicated by subject

The indentation force-displacement response of the soft tissue was obtained from the magnitude of reaction forces recorded by the indentor's load cell and the control of linear motion by the stepper driver. Tissue modulus was calculated using equation (1) derived by Hayes *et al*. [51] as shown earlier on page 21.

The gradient of the force-displacement graph, i.e. P/w, was taken at the onset of discomfort. Only the loading cycles were considered. Discomfort and pain threshold levels were calculated by dividing the force magnitude at the point of indication by the hemispherical contact area of the indentor tip.

Large deformation effects may produce erroneous results when using Hayes' equation. However, in this study, the experimentally-derived tissue modulus calculated using Hayes' equation is only a first-guess value to be validated by finite element analysis. When the indentation forces predicted by the finite element analysis agree with the experimental indentation forces, the tissue modulus value of that finite element model would then be taken as the accurate value.

Five cycles of indentation were performed for each site; the first cycle was to precondition the soft tissue and its results were not considered. The indentation depth for each location was a maximum of 24 mm, or as soon as the subject indicated the onset of pain. Cutoff force was set at 40 N as a safety feature [70]. Indentation was automatically terminated whenever the force exceeded this amount. The rate of indentation for all subjects was 1 mm/s, which was similar to earlier studies [67,71,139].

3.1.2 Calibration of Indentor

Three different tests were carried out to calibrate this indentation system before it was used to perform indentation experiments on test subjects. These tests were (a) Static Loading Test, (b) Static Displacement Test and (c) Cyclic Loading/Unloading Test. Data and graphs for all three tests have been included in Appendix 3.

Static Loading Test

The static loading test was to verify the accuracy of the indentor's load cell in measuring forces. A jig was constructed such that when the indentor shaft was extended and held in position, it supported the entire weight of the platform (Fig. 3.11). The platform was constrained such that it could only move freely in the vertical direction. Known masses were placed on the platform from 0-1000 g in increments of 50 g. The load recorded by the indentor load cell was then compared with the actual weight of the masses it was supporting. The weight of the platform was taken into account.

This test was repeated three times, and each time, the force measured by the load cell was plotted against the actual weight of the masses. The R-squared values obtained for the three tests were 0.9999, 0.9997 and 0.9998, showing that there was good agreement between the force indicated by the load cell and the actual load it was measuring.

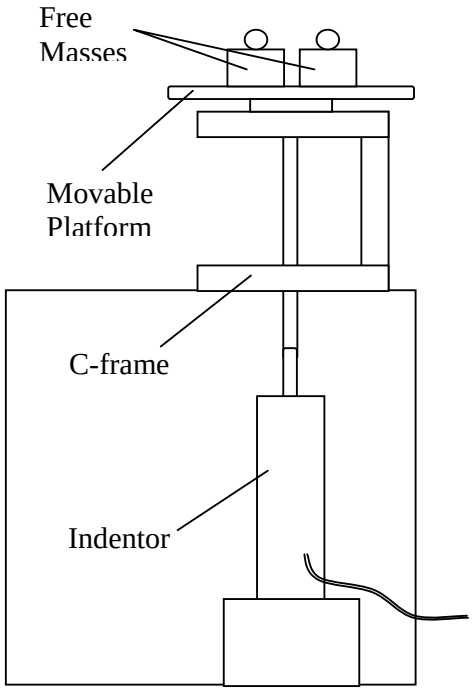

(a) Schematic diagram

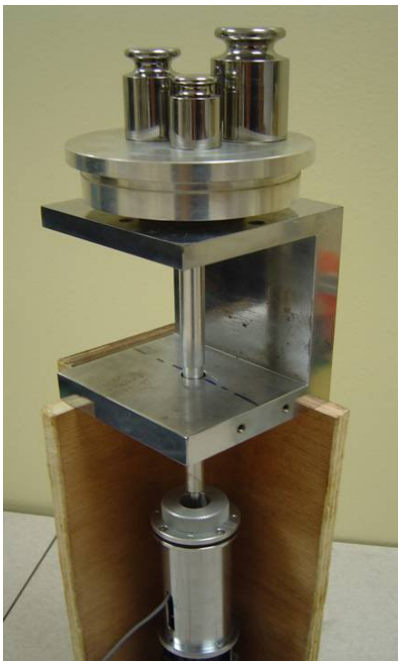

(b) Photograph

Figure 3.11. Schematic diagram and photograph of the static loading test jig, respectively

Static Displacement Test

The static loading test was to verify the accuracy of the indentor's stepper driver in controlling and measuring indentation depth. The same jig as the static loading test was used, except that instead of free masses, a dial gauge was placed at the top of the platform (Fig. 3.12). The purpose of the dial gauge was to measure the vertical distance that the platform moved. During the test, the indentor shaft was extended to a maximum of 20 mm, pausing every 5 mm to take readings off the dial gauge.

This test was done two times for each indentation speed of 0.5 mm/s, 1.0 mm/s and 1.5 mm/s. For each test, the indentation distance indicated by the indentor's stepper driver was plotted against the displacement measured by the dial gauge. The average

R-squared values obtained for tests at each indentation speed were 0.9999, 0.99965 and 0.9998, respectively. This showed that the stepper driver was able to control and measure indentation depth accurately.

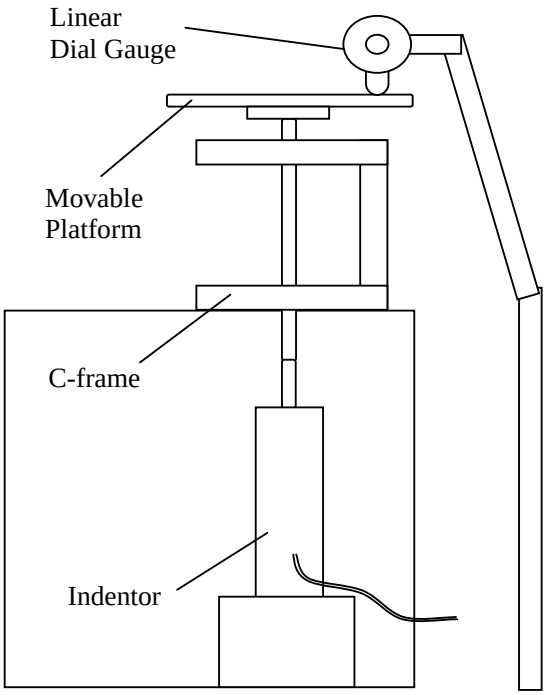

(a) Schematic diagram

(b) Photograph

Figure 3.12. Schematic diagram and photograph of the static displacement test jig, respectively

Cyclic Loading/Unloading Test

The cyclic loading/unloading test was to verify the repeatability of the indentor in measuring load-displacement response over both the loading and unloading cycles. A jig was constructed such that the indentor compressed a spring that was held inside a hollow cylindrical acrylic casing (Fig. 3.13). The spring was not in contact with the sides of the casing so as to reduce friction, and the distance compressed was only 5 mm to prevent the spring from buckling.

This test was done for three loading/unloading cycles. The gradients of the force-displacement graphs for the loading cycles were 0.9033 N/mm, 0.8781 N/mm and 0.9085 N/mm, giving a maximum deviation of 3.5%. The gradients of the force-displacement graphs for the unloading cycles were 0.8861 N/mm, 0.9183 N/mm and 0.8943 N/mm, giving a maximum deviation of 3.6%. These results showed that the indentor was able to determine load-displacement responses consistently over repeated indentation cycles.

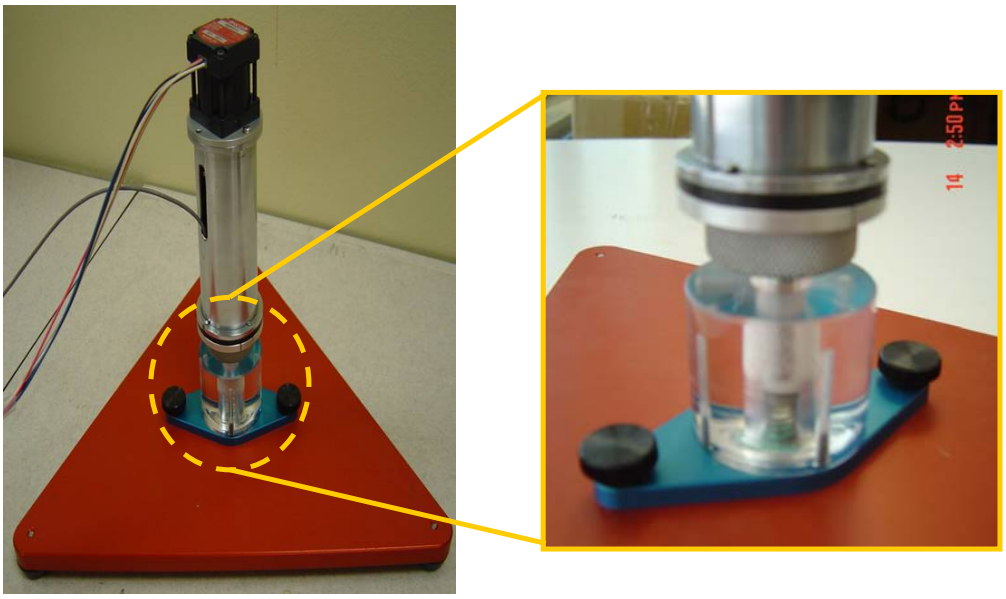

Figure 3.13. Cyclic loading/unloading test jig

3.2 FE Modelling

Axisymmetric contact models of the indentor shaft and soft tissue were created using FEA software (ABAQUS 6.4). Axisymmetric models were used as they required less computational resources when solving as compared to a full 3-D model.

3.2.1 Boundary Conditions

Being an axisymmetric model, nodes at the left edge were fixed in displacement for the horizontal direction. Nodes at the bottom edge were fixed in displacement for the horizontal and vertical directions (Fig. 3.14). The assumption was that in the stump, the underlying soft tissue is bonded to the bone, which is a rigid surface. Another assumption was that the model was wide enough for effects of indentation at the outer edge to be negligible. Hence, nodes at the outer edge were not assigned any boundary conditions. A vertical displacement was applied at the top of the indentor to simulate indentation.

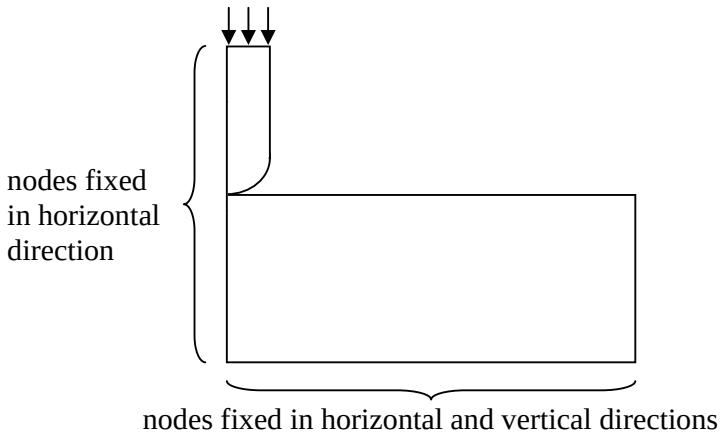

Figure 3.14. Schematic diagram of boundary conditions

3.2.2 Geometric Consideration

The cylindrical indentor shaft in the FE model had a length of 20 mm, a cross-sectional diameter of 5 mm and a hemispherical end with 2.5 mm radius curvature. Effects of finite tissue thickness were taken into account as each region of the stump had a different tissue thickness. Soft tissue thickness values at various anatomical regions around the lower limb were derived from the study by Tönük and Silver-Thorn [139], and their corresponding indentation sites are shown in Table 3.2.

Table 3.2. Lower limb soft tissue thickness values

Data obtained from Tönük and Silver-Thorn [139]		Corresponding indentation sites based on the grid system	
Stump Region	Avg. Soft Tissue Thickness (mm)	Left Leg	Right Leg
Distal Popliteal	52.09	3,4	3,4
		3,5	3,5
		3,6	3,6
		4,4	4,4
		4,5	4,5
		4,6	4,6
Prox. Popliteal Area	37.78	1,4	1,4
		1,5	1,5
		1,6	1,6
		2,4	2,4
		2,5	2,5
		2,6	2,6
Dist. Medial Tibial Flare	24.76	3,8	3,2
		4,8	4,2
Prox. Medial Tibial Flare	13.54	1,8	1,2
		2,8	2,2
Dist. Lateral Tibial Flare	25.46	3,2	3,8
		4,2	4,8
Prox. Lateral Tibial Flare	16.58	1,2	1,8
		2,2	2,8
Fibular Head	16.23	1,3	1,7
		2,3	2,7
Fibular Shaft	32.06	3,3	3,7
		4,3	4,7
Patellar Tendon	9.99	1,1	1,1
Other regions not listed (interpolated data)	25.66	1,7	1,3
	16.23	2,1	2,1
	25.66	2,7	2,3
	16.23	3,1	3,1
	38.43	3,7	3,3
	16.23	4,1	4,1
	38.43	4,7	4,3

Tönük and Silver-Thorn [139] estimated the soft tissue thickness values of each of their seven transtibial amputees based on magnetic resonance images or computer tomography scans of their residual limbs. No additional information regarding the seven individuals was provided in their paper. The values used in Table 3.2 above were average values of the seven individuals' data, which were presented as separate values in their paper.

Although these values may not be accurate for the subjects in this study, it was used because it was the only set of soft tissue thickness data available in the literature for the relevant anatomical sites of the lower limb. In particular, the measured indentation depth was greater than the value used for the tissue thickness at the patellar tendon (location 1,1) for Subjects 1 to 4.

The patellar tendon is actually a thin piece of tendon with a cavity between it and the knee joint behind. That was probably why the indentor was able to indent a depth larger than the tissue thickness by stretching the tendon and pressing it into the cavity behind.

This lack of accuracy has been acknowledged in point (e) under the section "Limitations of Study" on page 76. A recommendation to address this issue has been provided in point (a) under the section "Future Work" on page 78.

3.2.3 Materials Consideration

The soft tissue was modelled with hyperelastic material using CAX4R elements, which had 4-node bilinear and reduced integration properties. Different stress-strain values were fed into models for each indentation site. These stress-strain values were based on the indentation force-displacement data gathered from each site. The soft tissue was assumed to be isotropic and incompressible, with a Poisson's Ratio of 0.49. This was consistent with earlier studies [8,9,43,45,50,62,64,67]. The indentor shaft was modelled as a rigid body because the Young's modulus of stainless steel (210 GPa) was much higher than that of the soft tissue. Contact elements were defined for elements at the topmost edge of the soft tissue and the rigid indentor. An axisymmetric model is shown below (Fig. 3.15).

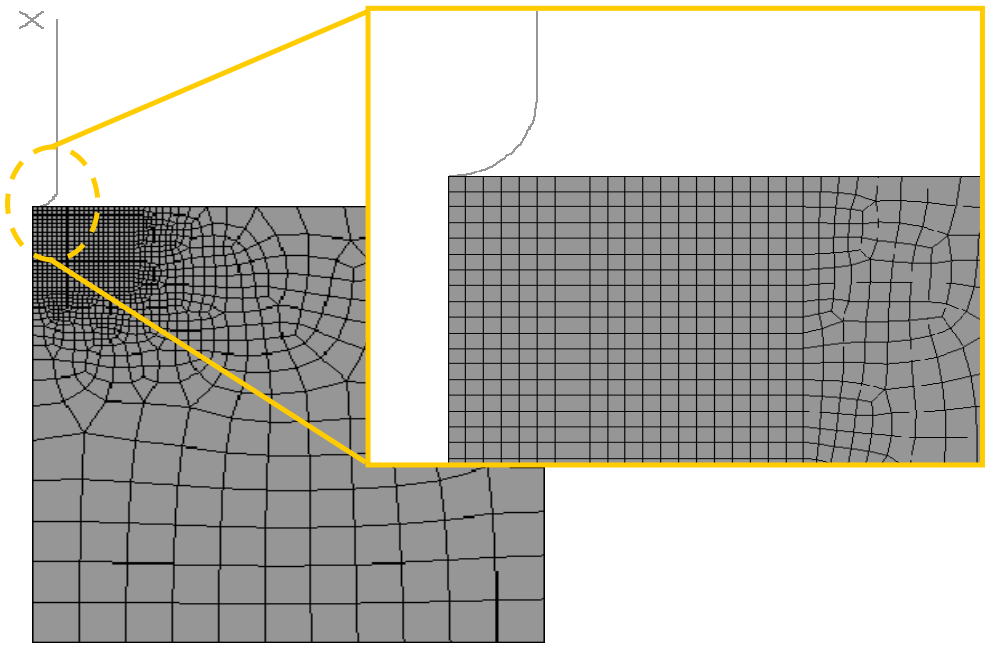

Figure 3.15. Axisymmetric finite element indentation model

3.2.4 Validation

Finite Element simulations of the indentation were carried out according to the depth of indentation performed at each indentation location. The reaction forces obtained from the simulation were validated against those obtained during actual experiments. A comparison was carried out between several types of hyperelastic models, namely Arruda Boyce, Marlow, Mooney-Rivlin, Neo Hookean, Ogden, Reduced Polynomial and Yeoh, to determine which strain energy model gave the closest approximation to the experimental data.

The forms of each of the strain energy models used by ABAQUS 6.4 to perform the finite element analyses have been included in Appendix 7. The parameters required for each form were calculated by the software based on uniaxial stress-strain values obtained from experimental results and fed into the software. These stress-strain values have been included in Appendix 5.

Chapter 4: RESULTS and DISCUSSION

4.1 Indentation Results

The experimentally obtained tissue modulus and discomfort/pain threshold values of each subject will be presented in this chapter. The graphs below are organised according to the indentation grid system introduced in Chapter 3 (Figs. 3.1 and 3.2 on pages 37 and 38). Values of tissue modulus and discomfort/pain thresholds, as well as values of variables used to calculate them, have been included in Appendix 4.

Results for Subject 1 are shown below in Fig. 4.1.

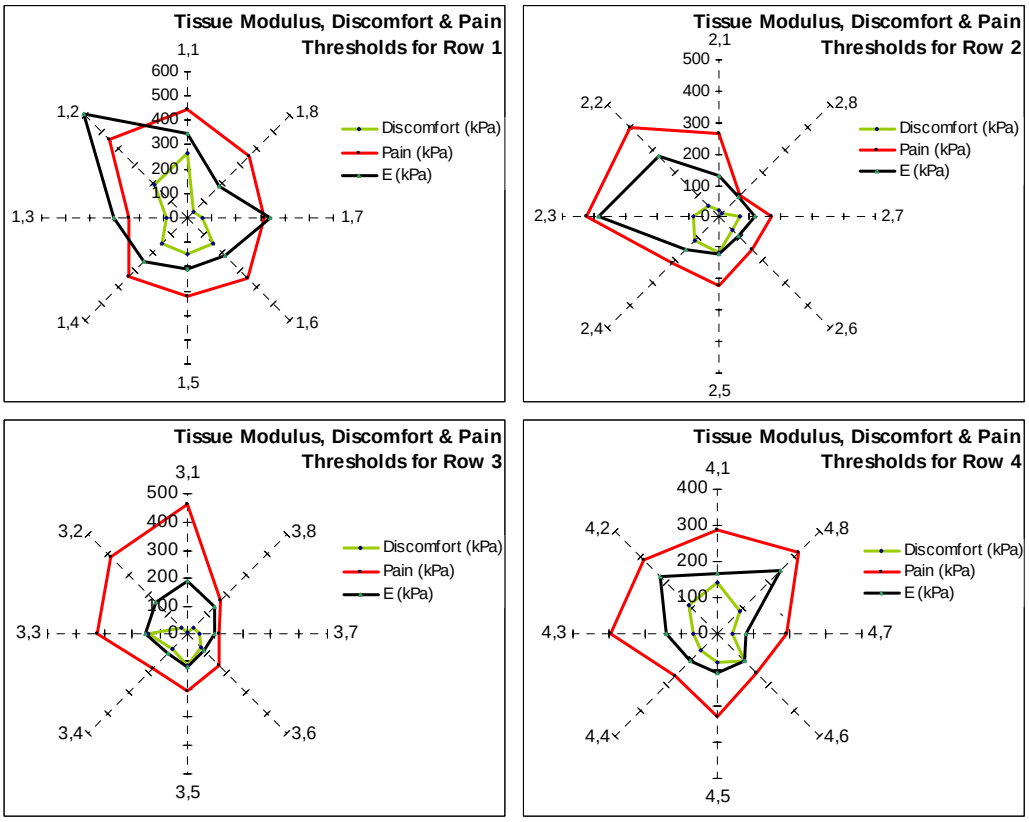

Figure 4.1. Tissue Modulus, Discomfort and Pain Threshold of various locations for Subject 1

In Row 1, the highest tissue modulus (595 kPa) was at location 1,2 while the lowest (175 kPa) was at location 1,8. The highest Discomfort Threshold (266 kPa) was at location 1,1 while the lowest (38 kPa) was at location 1,8. The highest Pain Threshold (450 kPa) was at location 1,2 while the lowest (241 kPa) was at location 1,3.

In Row 2, the highest tissue modulus (386 kPa) was at location 2,3 while the lowest (90 kPa) was at location 2,8. The highest Discomfort Threshold (114 kPa) was at location 2,5 while the lowest (14 kPa) was at location 2,8. The highest Pain Threshold (423 kPa) was at location 2,3 while the lowest (97 kPa) was at location 2,8.

In Row 3, the highest tissue modulus (188 kPa) was at location 3,1 while the lowest (82 kPa) was at location 3,6. The highest Discomfort Threshold (141 kPa) was at location 3,3 while the lowest (6 kPa) was at location 3,1. The highest Pain Threshold (462 kPa) was at location 3,1 while the lowest (113 kPa) was at location 3,7.

In Row 4, the highest tissue modulus (245 kPa) was at location 4,8 while the lowest (78 kPa) was at location 4,7. The highest Discomfort Threshold (142 kPa) was at location 4,1 while the lowest (42 kPa) was at location 4,7. The highest Pain Threshold (321 kPa) was at location 4,8 while the lowest (155 kPa) was at location 4,6.

For the entire limb, the highest tissue modulus (595 kPa) was at location 1,2 while the lowest (78 kPa) was at location 4,7. The highest Discomfort Threshold (266 kPa) was at location 1,1 while the lowest (6 kPa) was at location 3,1. The highest Pain Threshold (462 kPa) was at location 3,1 while the lowest (97 kPa) was at location 2,8.

Results for Subject 2 are shown below in Fig. 4.2.

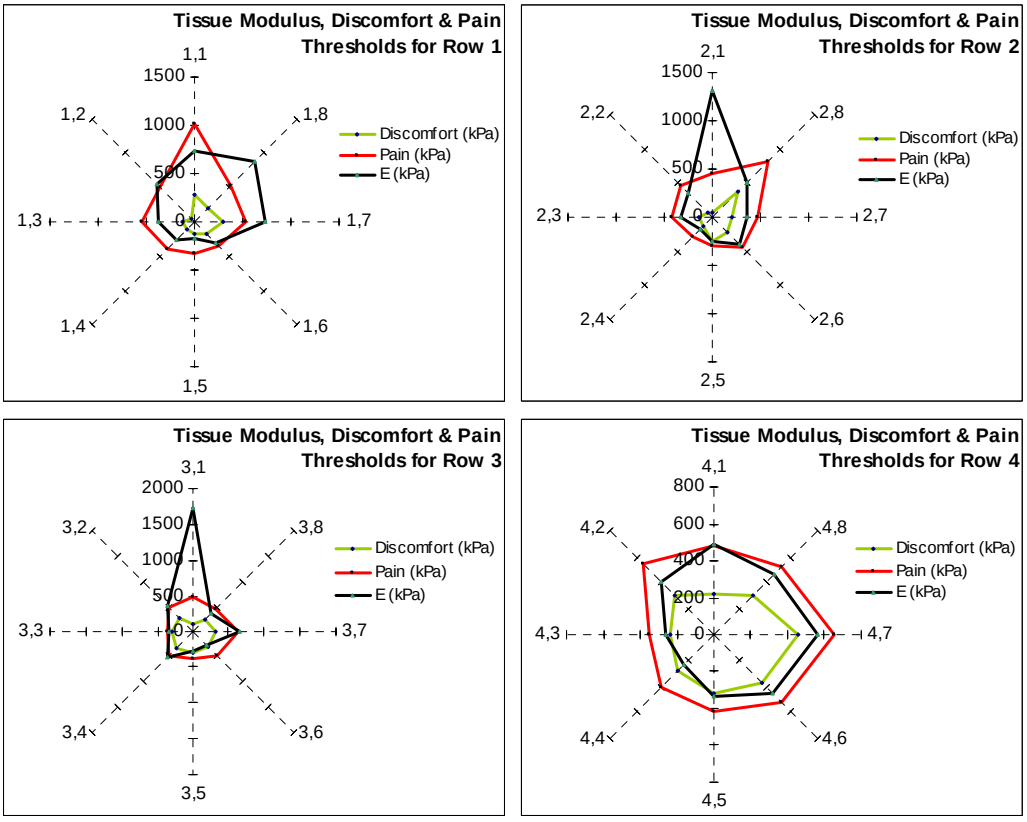

Figure 4.2. Tissue Modulus, Discomfort and Pain Threshold of various locations for Subject 2

In Row 1, the highest tissue modulus (861 kPa) was at location 1,8 while the lowest (163 kPa) was at location 1,5. The highest Discomfort Threshold (301 kPa) was at location 1,7 while the lowest (46 kPa) was at location 1,2. The highest Pain Threshold (1005 kPa) was at location 1,1 while the lowest (330 kPa) was at location 1,5.

In Row 2, the highest tissue modulus (1320 kPa) was at location 2,1 while the lowest (178 kPa) was at location 2,4. The highest Discomfort Threshold (382 kPa) was at location 2,8 while the lowest (48 kPa) was at location 2,1. The highest Pain Threshold (827 kPa) was at location 2,8 while the lowest (276 kPa) was at location 2,4.

In Row 3, the highest tissue modulus (1719 kPa) was at location 3,1 while the lowest (267 kPa) was at location 3,5. The highest Discomfort Threshold (315 kPa) was at location 3,7 while the lowest (285 kPa) was at location 3,5. The highest Pain Threshold (634 kPa) was at location 3,7 while the lowest (348 kPa) was at location 3,3.

In Row 4, the highest tissue modulus (564 kPa) was at location 4,7 while the lowest (227 kPa) was at location 4,4. The highest Discomfort Threshold (454 kPa) was at location 4,7 while the lowest (217 kPa) was at location 4,1. The highest Pain Threshold (654 kPa) was at location 4,7 while the lowest (353 kPa) was at location 4,3.

For the entire limb, the highest tissue modulus (1719 kPa) was at location 3,1 while the lowest (163 kPa) was at location 1,5. The highest Discomfort Threshold (454 kPa) was at location 4,7 while the lowest (46 kPa) was at location 1,2. The highest Pain Threshold (1005 kPa) was at location 1,1 while the lowest (276 kPa) was at location 2,4.

Results for Subject 3 are shown below in Fig. 4.3.

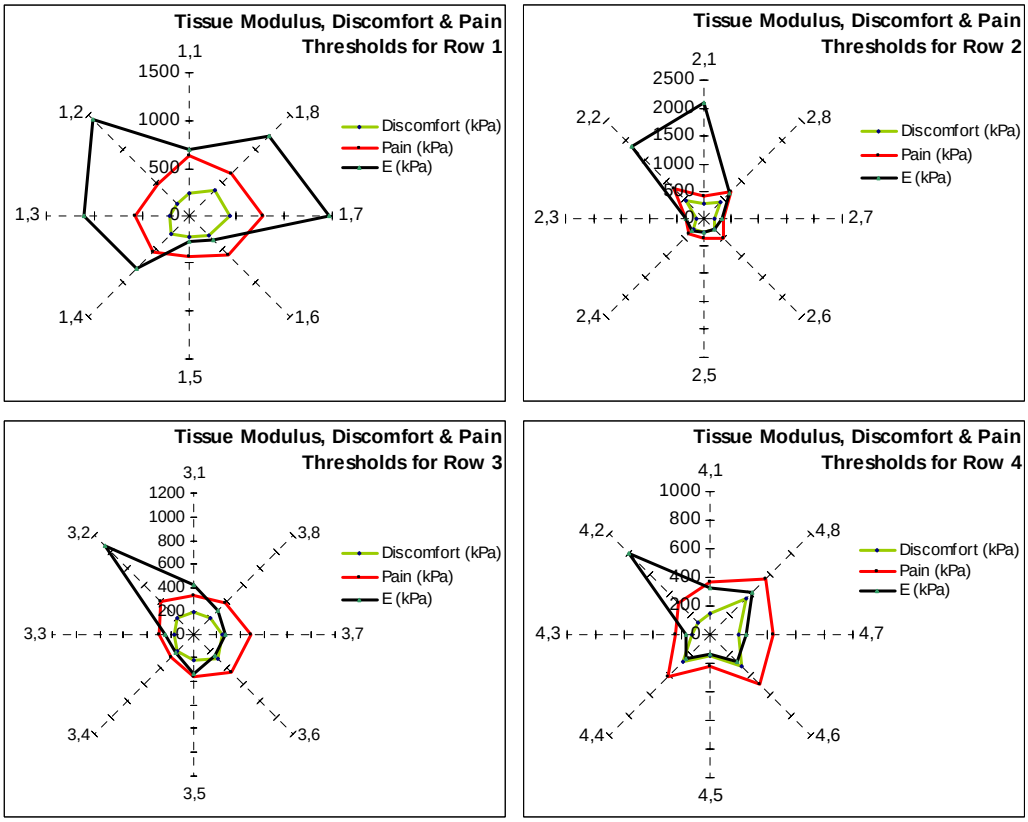

Figure 4.3. Tissue Modulus, Discomfort and Pain Threshold of various locations for Subject 3

In Row 1, the highest tissue modulus (1463 kPa) was at location 1,7 while the lowest (263 kPa) was at location 1,5. The highest Discomfort Threshold (432 kPa) was at location 1,7 while the lowest (177 kPa) was at location 1,2. The highest Pain Threshold (767 kPa) was at location 1,7 while the lowest (430 kPa) was at location 1,5.

In Row 2, the highest tissue modulus (2103 kPa) was at location 2,1 while the lowest (250 kPa) was at location 2,5. The highest Discomfort Threshold (456 kPa) was at

location 2,2 while the lowest (48 kPa) was at location 2,1. The highest Pain Threshold (771 kPa) was at location 2,2 while the lowest (317 kPa) was at location 2,3.

In Row 3, the highest tissue modulus (1066 kPa) was at location 3,2 while the lowest (218 kPa) was at location 3,4. The highest Discomfort Threshold (276 kPa) was at location 3,6 while the lowest (161 kPa) was at location 3,3. The highest Pain Threshold (480 kPa) was at location 3,7 while the lowest (273 kPa) was at location 3,4.

In Row 4, the highest tissue modulus (810 kPa) was at location 4,2 while the lowest (134 kPa) was at location 4,5. The highest Discomfort Threshold (359 kPa) was at location 4,8 while the lowest (120 kPa) was at location 4,2. The highest Pain Threshold (555 kPa) was at location 4,8 while the lowest (219 kPa) was at location 4,5.

For the entire limb, the highest tissue modulus (2103 kPa) was at location 2,1 while the lowest (134 kPa) was at location 4,5. The highest Discomfort Threshold (456 kPa) was at location 2,2 while the lowest (120 kPa) was at location 4,2. The highest Pain Threshold (771 kPa) was at location 2,2 while the lowest (219 kPa) was at location 4,5.

Results for Subject 4 are shown below in Fig. 4.4.

Indentation results for Row 4 of Subject 4 are not available as the amputee's stump was not long enough for indentation to be performed there. Also, Subject 4 was not able to experience acute pain due to a complication of his diabetic condition which had led to peripheral neuropathy. Hence, results for pain threshold levels are not available. Indentation was not performed at locations 1,4, 1,5 and 1,6 as that part of the socket was trimmed off to allow the subject to bend his knee.

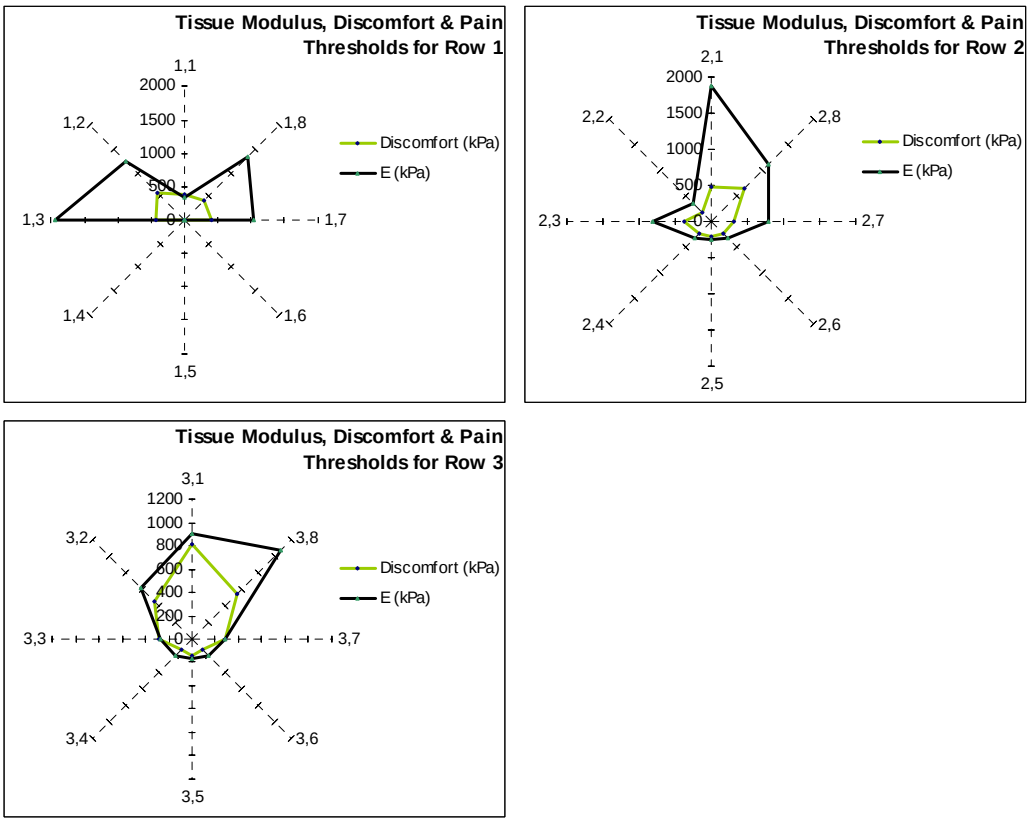

Figure 4.4. Tissue Modulus, Discomfort and Pain Threshold of various locations for Subject 4

In Row 1, the highest tissue modulus (1943 kPa) was at location 1,3 while the lowest (340 kPa) was at location 1,1. The highest Discomfort Threshold (561 kPa) was at location 1,2 while the lowest (380 kPa) was at location 1,1.

In Row 2, the highest tissue modulus (1879 kPa) was at location 2,1 while the lowest (246 kPa) was at location 2,5. The highest Discomfort Threshold (655 kPa) was at location 2,8 while the lowest (165 kPa) was at location 2,2.

In Row 3, the highest tissue modulus (1065 kPa) was at location 3,8 while the lowest (171 kPa) was at location 3,5. The highest Discomfort Threshold (809 kPa) was at location 3,1 while the lowest (133 kPa) was at location 3,4.

For the entire limb, the highest tissue modulus (1943 kPa) was at location 1,3 while the lowest (171 kPa) was at location 3,5. The highest Discomfort Threshold (809 kPa) was at location 3,1 while the lowest (133 kPa) was at location 3,4.

Results for Subject 5 are shown below in Fig. 4.5.

Indentation results for Row 4 of Subject 5 are not available as the amputee's stump was not long enough for indentation to be performed there. Also, Subject 5 was not able to experience acute pain due to a complication of his diabetic condition which had led to peripheral neuropathy. Hence, results for pain threshold levels are not available.

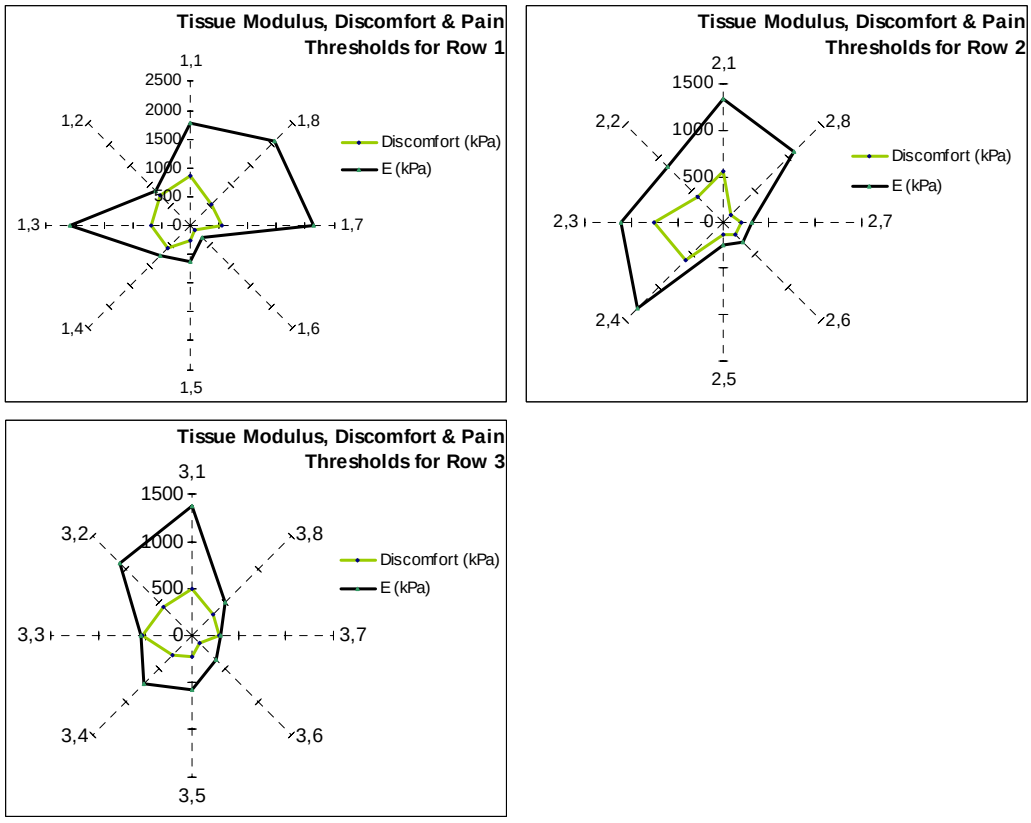

Figure 4.5. Tissue Modulus, Discomfort and Pain Threshold of various locations for Subject 5

In Row 1, the highest tissue modulus (2139 kPa) was at location 1,7 while the lowest (321 kPa) was at location 1,6. The highest Discomfort Threshold (853 kPa) was at location 1,1 while the lowest (117 kPa) was at location 1,6.

In Row 2, the highest tissue modulus (1345 kPa) was at location 2,1 while the lowest (241 kPa) was at location 2,5. The highest Discomfort Threshold (744 kPa) was at location 2,3 while the lowest (118 kPa) was at location 2,8.

In Row 3, the highest tissue modulus (1373 kPa) was at location 3,1 while the lowest (305 kPa) was at location 3,7. The highest Discomfort Threshold (523 kPa) was at location 3,3 while the lowest (117 kPa) was at location 3,6.

For the entire limb, the highest tissue modulus (2139 kPa) was at location 1,7 while the lowest (241 kPa) was at location 2,5. The highest Discomfort Threshold (853 kPa) was at location 1,1 while the lowest (117 kPa) was at location 1,6.

Table 4.1 shows their average tissue modulus and discomfort/pain threshold values classified according to tissue type. Table 4.2 shows their average discomfort and pain threshold values classified according to location.

Table 4.1. Average tissue modulus and discomfort/pain threshold values classified by tissue type

Subject	Type	Avg Discomfort Threshold (kPa)	Avg Pain Threshold (kPa)	Avg Tissue Modulus (kPa)
1 (normal)	bony	70.29	305.81	247.68
	soft	80.65	235.34	141.23
	tendon	186.43	374.85	269.93
2 (normal)	bony	185.10	511.55	622.55
	soft	269.04	441.98	346.76
	tendon	193.36	586.90	432.65
3 (normal)	bony	241.85	476.76	1032.96
	soft	243.40	409.59	286.79
	tendon	263.74	584.06	615.39
4 (amputee)	bony	499.05	-	1213.65
	soft	232.10	-	299.18
	tendon	380.48	-	339.57
5 (amputee)	bony	508.44	-	1377.40
	soft	309.34	-	616.68
	tendon	502.65	-	941.95

From the table above, regions with bony prominences were observed to have the highest tissue modulus, followed by tendon, then soft tissue, for 4 out of 5 subjects. Highest pain threshold was observed in regions with tendon, followed by bony prominences, then soft tissue, for all 3 normal subjects. Discomfort threshold levels were not consistent among the different tissue types for all subjects.

Table 4.2. Average discomfort and pain threshold values classified by location

Subject	Location	Avg Discomfort Threshold (kPa)	Avg Pain Threshold (kPa)
1 (normal)	Row 1	135.05	349.81
	Row 2	63.90	242.00
	Row 3	63.67	248.70
	Row 4	86.71	241.27
2 (normal)	Row 1	172.33	523.38
	Row 2	176.30	452.41
	Row 3	264.60	465.85
	Row 4	308.63	484.99
3 (normal)	Row 1	274.51	579.31
	Row 2	280.98	474.62
	Row 3	213.05	370.06
	Row 4	210.36	380.56
4 (amputee)	Row 1	438.88	-
	Row 2	338.16	-
	Row 3	349.03	-
5 (amputee)	Row 1	529.77	-
	Row 2	361.15	-
	Row 3	333.57	-

From the table above, regions in Row 1 were observed to have the highest average discomfort threshold for 3 out of 5 subjects. Regions in Row 1 also had the highest average pain threshold for all 3 normal subjects.

4.2 FE Validation

Finite element simulation of indentation was run using several hyperelastic strain energy models such as Arruda Boyce, Marlow, Mooney-Rivlin, Neo Hookean, Ogden, Reduced Polynomial and Yeoh. Experimental results of three indentation locations from Subject 3 were chosen for validation. These three indentation locations

represented each of the three tissue types, i.e. tendon (location 1,1), bony prominence (location 3,2) and soft tissue (location 3,5). Graphs comparing the predicted indentation reaction force with the experimental indentation reaction force are shown in Figs. 4.6 – 4.8. Numerical data of the FE simulation results have been included in Appendix 5.

Fig. 4.6 below shows a comparison of the predicted and experimental indentation force for the location 1,1, which was at the patellar tendon. Indentation here was simulated to a depth of 6 mm.

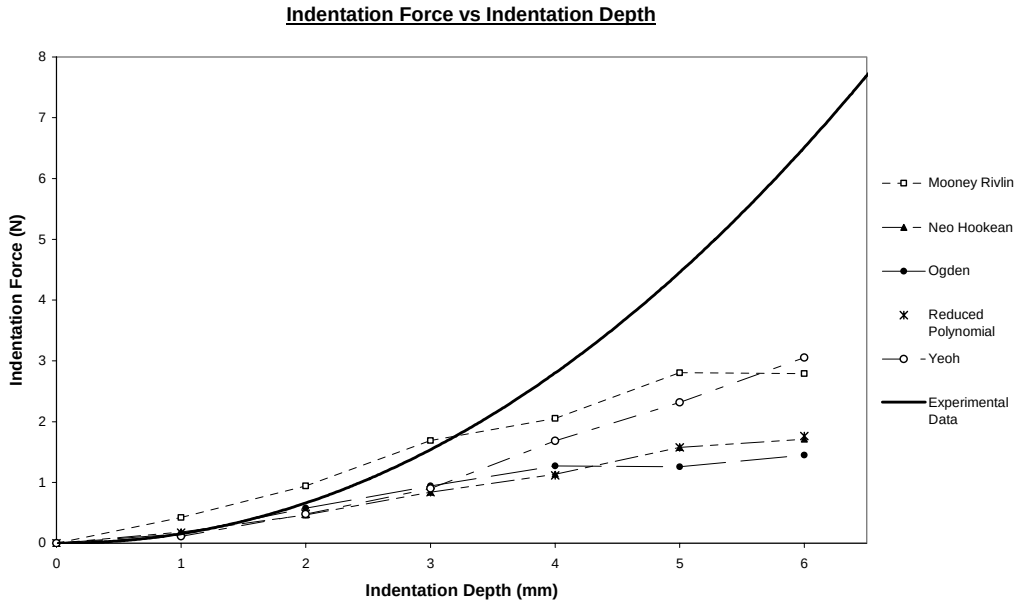

Figure 4.6. Graph of experimental and FE-predicted indentation reaction force against indentation depth for location 1,1 (patellar tendon)

Arruda Boyce and Marlow strain energy models produced errors when the simulation was run. From the graph above, it was observed that the reaction forces increased exponentially as the indentation depth increased. However, the rate of increase for the experimental values was much higher than those predicted by the FE simulations.

Of the 5 models, the Mooney-Rivlin and Yeoh models provided the closest approximates to the experimental values. At an indentation depth of 3.2 mm, the Mooney-Rivlin model predicted an indentation force almost equal to the experimental force.

Fig. 4.7 below shows a comparison of the predicted and experimental indentation force for the location 3,2, which was at the distal tibial edge. Indentation here was simulated to a depth of 4 mm.

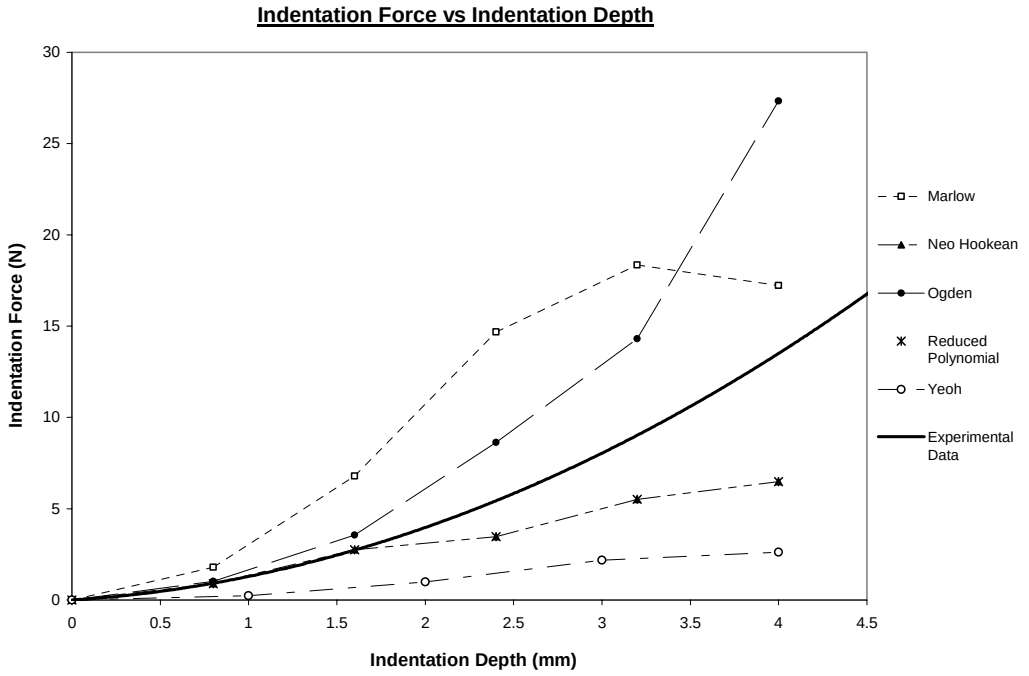

Figure 4.7. Graph of experimental and FE-predicted indentation reaction force against indentation depth for location 3,2 (distal tibial edge)

Arruda Boyce and Mooney-Rivlin strain energy models produced errors when the simulation was run. From the graph above, it was observed that even though all the predicted forces increased exponentially, 2 of the models predicted forces higher than

the experimental forces whereas 3 of the models predicted forces lower than the experimental forces.

Of the 5 models, the Neo Hookean and Reduced Polynomial models provided the closest approximates to the experimental values. They predicted an indentation force almost equal to the experimental force for indentation depths of up to 1.7 mm.

Fig. 4.8 below shows a comparison of the predicted and experimental indentation force for the location 3,5, which was at the distal popliteal region. Indentation here was simulated to a depth of 10 mm.

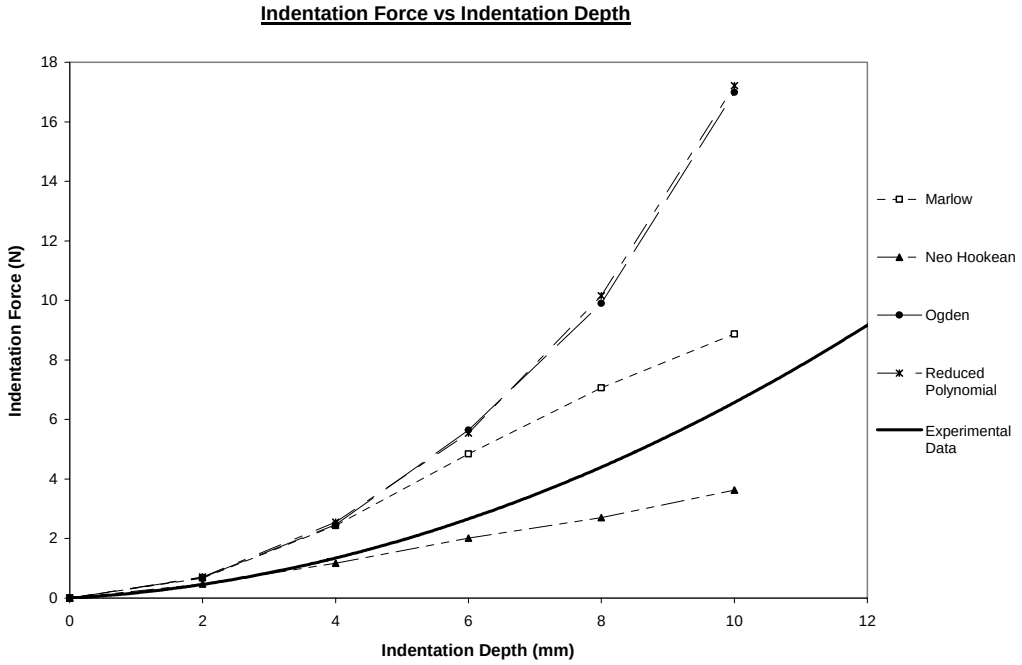

Figure 4.8. Graph of experimental and FE-predicted indentation reaction force against indentation depth for location 3,5 (distal popliteal region)

Arruda Boyce, Mooney-Rivlin and Yeoh strain energy models produced errors when the simulation was run. From the graph above, it was observed that all the predicted

forces increased exponentially, and all but one of the models predicted forces higher than the experimental forces.

Of the 4 models, the Neo Hookean model provided the closest approximate to the experimental values. It predicted an indentation force almost equal to the experimental force for indentation depths of up to 3 mm.

The errors encountered in running these finite element simulations were due to non-convergence issues. These errors persisted even after reducing the indentation increments to 10%. The errors were probably due to the material law. Current hyperelastic materials are based on rubber and foam, and to date are the closest approximate to soft tissue behaviour. However, even though rubber and soft tissue may be similar, rubber does not have some of the characteristics of soft tissue, e.g. viscoelasticity. Therefore a new material with a new set of constitutive equations is needed to accurately represent biological soft tissue.

The results of FE simulations for all 3 indentation locations showed that there was no particular hyperelastic strain energy model which was able to realistically predict the mechanical behaviour of soft tissue over a large depth of indentation. One likely reason was that viscoelastic properties of soft tissue were not considered in the hyperelastic FE models. Another possible reason was that the assumption of incompressibility, and hence a Poisson's ratio of 0.49, may not have been valid.

A lack of relevant data might also have contributed to the lack of accuracy in the FE predictions. Only data from the indentation test, which was essentially a uniaxial

compression test, was fed into the FE model. Data from other tests on soft tissue like the biaxial, planar (pure shear) and volumetric tests, would help to create more realistic and accurate FE models.

One further step to take would be to employ curve-fitting methods to match the FE-predicted curve with the experimental curve, based on the results of these initial simulations. This can be achieved by iteratively adjusting the hyperelastic constants of each FE model such that with every adjustment, the predicted values would be closer to the experimental values.

4.3 Discussion

4.3.1 Comparison of Tissue Properties between Tissue Types

Tissue Modulus

Regions with bony prominences were observed to have the highest tissue modulus, followed by tendon, and then soft tissue. This is probably due to the fact that at bony prominences, there is only a very thin layer of skin which did not undergo much compression. Therefore almost all of the indentation force was acting directly on the underlying rigid bone surface and this in turn produced a very high reaction force. Tendon is not as stiff as bone so even though regions with tendon are also covered by a very thin layer of skin, the modulus there is lower than that of bony prominences. For the regions with a thick layer of soft tissue, the soft tissue helped to cushion the indentation force, which resulted in a lower reaction force.

Discomfort and Pain Threshold

Highest pain threshold was noticed in regions with tendon, followed by bony prominences, and then soft tissue. This finding is similar to an earlier study by Lee *et al*. [112]. A possible explanation for this phenomenon could be due to pain receptors called nociceptors that are found in the epidermal and musculoskeletal tissue [185]. In particular, mechanical nociceptors are stimulated by excess pressure or mechanical deformation, resulting in a sensation of pain. The amputees experienced only discomfort and not acute pain due to a complication of their diabetic condition which led to peripheral neuropathy.

Soft tissue regions had the lowest pain threshold since they contained a larger number of nociceptors – in both the skin and underlying muscle tissues. Whereas for bony prominences and regions with tendon, the only nociceptors that contribute to pain sensation were those in the thin layer of skin. Regions with tendon had a higher pain threshold than bony prominences probably because the tendon could deform and the layer of skin tissue was not compressed by so much compared to that of a bony prominence.

4.3.2 Comparison of Tissue Properties between Amputees and Normal Subjects

Tissue Modulus

Average tissue modulus values of amputees were significantly higher than those of normal subjects. One reason for this could be due to the fact that after amputation, there was a gradual process of soft tissue shrinkage and muscular atrophy in their residual limbs. This caused their residual limbs to be generally more bony, which explains the higher tissue modulus obtained.

Another reason could be due to the fact that tissue modulus was calculated using the gradient of the indentation force-displacement graph taken at the discomfort threshold level. The amputees' sensitivity to discomfort in their residual limbs were somewhat numbed due to peripheral neuropathy, hence the tissue modulus was taken at a much larger depth of indentation compared to the normal subjects. Since the indentation force increased exponentially with indentation depth, the gradients used for amputees were much steeper, resulting in higher tissue modulus values.

Discomfort and Pain Threshold

Peripheral neuropathy due to the amputees' diabetic condition probably caused them to have higher average discomfort threshold levels when compared to the normal subjects. It is potentially dangerous for the amputees to be able to feel discomfort only when their residual limb soft tissues are subjected to excessive loads. This may lead to tissue damage such as pressure ulcers due to mechanical loading during the use of their prosthetic socket, without them realising it.

4.3.3 Comparison of Discomfort and Pain Threshold between Limb Locations

Tissue regions in Row 1 have the highest average discomfort threshold level for 2 out of 3 normal subjects and for both amputees, as well as the highest average pain threshold level for all 3 normal subjects. This was probably due to the fact that locations along Row 1 consisted mainly of regions with tendon and bony prominences, which as discussed earlier, are able to tolerate greater loads before feeling discomfort or pain.

The implication of these findings on the design of prosthetic sockets is that the loads should as much as possible be transferred to Row 1 regions of the stump, especially to the regions with tendon. This is typical of Patellar Tendon Bearing (PTB) sockets. This consideration is based purely on the basis of comfort, i.e. reducing the amount of discomfort or pain felt to as low as possible. However, it does not consider if avoiding sensations of discomfort or pain would necessarily prevent tissue damage due to sustained and/or repetitive mechanical loading.

4.3.4 Comparison of Tissue Properties between Subjects 2 and 3

Tissue properties of Subjects 2 and 3 have been chosen for comparison as both were normal male subjects at similar age. Both of them also used their right leg for the indentation test. The table below (Table 4.3) lists the indentation locations at which their maximum and minimum tissue modulus, discomfort threshold and pain threshold for each row was observed. The cells highlighted in yellow indicate where the maximum or minimum tissue property was observed at the same locations for both subjects, or with a difference of at most one position.

Table 4.3. Comparison of locations of maximum and minimum tissue properties between Subjects 2 and 3

			Subject 2	Subject 3
			Indentation Location	Indentation Location
Row 1	Tissue Modulus	Maximum	1,8	1,7
		Minimum	1,5	1,5
	Discomfort Threshold	Maximum	1,7	1,7
		Minimum	1,2	1,2
	Pain Threshold	Maximum	1,1	1,7
		Minimum	1,5	1,5
Row 2	Tissue Modulus	Maximum	2,1	2,1
		Minimum	2,4	2,5
	Discomfort Threshold	Maximum	2,8	2,2
		Minimum	2,1	2,3
	Pain Threshold	Maximum	2,8	2,2
		Minimum	2,4	2,3
Row 3	Tissue Modulus	Maximum	3,1	3,2
		Minimum	3,5	3,4
	Discomfort Threshold	Maximum	3,7	3,6
		Minimum	3,1	3,3
	Pain Threshold	Maximum	3,7	3,7
		Minimum	3,3	3,4
Row 4	Tissue Modulus	Maximum	4,7	4,2
		Minimum	4,4	4,5
	Discomfort Threshold	Maximum	4,7	4,8
		Minimum	4,1	4,2
	Pain Threshold	Maximum	4,7	4,8
		Minimum	4,3	4,5

It can be observed from the table above that most of the locations of maximum and minimum tissue modulus, discomfort threshold and pain threshold in each row coincide for both subjects. This suggests that tissue properties in the lower limb such as tissue modulus, discomfort threshold and pain threshold are strongly linked to the type and location of anatomical features. This is especially significant for discomfort and pain thresholds as they are supposedly subjective and depend on the subject's sensitivity towards discomfort/pain.

4.4 Limitations of Study

There are a few limitations in this study which could be improved upon in future studies.

(a) Due to the lack of suitable amputee subjects, as well as the limited time available, the sample size was not as large as desired. The relatively small sample size might affect the validity of the findings when applied to the general population.

(b) Subjects might have felt more discomfort and pain due to edge effects caused by the relatively small indentor tip. Although steps had been taken to reduce such edge effects by using a hemispherical tip instead of a flat-ended tip, the pain caused by a tip with a small cross-sectional area would probably be more acute than what is normally experienced when wearing a prosthetic socket.

(c) The *in vivo* indentation test only produced a uniaxial compression force normal to the surface of the skin. Shear and frictional forces which are normally present at the stump-socket interface, and which also cause discomfort and pain to the amputee, were not taken into consideration. If shear and frictional forces were considered, the discomfort and pain tolerance threshold levels would probably be lower.

(d) There may have been slippage of gears in the stepper motor as the indentation test was being performed. Even though this likelihood was very slim, it is possible that any slippage may have affected the accuracy in the indentation results.

(e) Soft tissue thickness values used in the axisymmetric FE models were generalised values obtained from an earlier study [139] and may not have been an accurate representation of the five subjects' limbs. Also, viscoelastic properties of soft tissue were not considered in the FE model. Accuracy of the FE simulation results may have been compromised as a consequence.

Chapter 5: CONCLUSION

The main objective of this project was to investigate the *in vivo* biomechanical properties of lower limb soft tissues, namely tissue modulus and discomfort/pain threshold, for use in a CAD-FEA lower limb prosthetic design system.

A method of determining two important biomechanical properties of lower limb soft tissues using an integrated indentation and pain feedback system has been established. Consequently, a systematic and comprehensive map of tissue modulus and discomfort/pain threshold levels for the entire residual limb was generated.

It was found that regions with bony prominences had the highest tissue modulus, followed by tendon, then soft tissue. Pain threshold, however, was the highest in regions with tendon, followed by bony prominences, then soft tissue. Amputees had higher tissue modulus and discomfort threshold levels than normal subjects. Limb regions along Row 1, i.e. in the same horizontal plane as the patellar tendon, had the highest discomfort and pain threshold levels.

Being able to extract these *in vivo* biomechanical properties would enable correlation of stump-socket interface pressure to physiological response. This would give a practical application to the FEA-predicted pressures and aid in the design process of prosthetic sockets using intelligent CAD-FEA systems.

5.1 Future Work

Possible work to be considered in the future:

(a) Incorporate a device into the indentor that can concurrently measure tissue thickness as the tissue is being indented. This would provide more accurate data on indentation depth as well as actual tissue thickness at any particular stump location. One option would be an ultrasound device.

(b) Employ an alternative system of motion control in the indentor instead of the stepper motor, where slippage is less likely to occur. One possibility would be a pneumatic system.

(c) Conduct a statistical study on the reliability of biomechanical tissue properties extracted from the test subjects if they are to be applied to the general population.

(d) Use of viscoelastic modelling in the finite element analysis so as to enable prediction of simulation results with better accuracy.

(e) Perform a computational study to obtain a map of hyperelastic constants for the entire stump. This can be achieved through an iterative, curve-fitting process that finds the best fit between the experimental and FE-predicted data.

REFERENCES

1. Dean D and Saunders CG. 1985. A software package for design and manufacture of prosthetic sockets for transtibial amputees. *IEEE Trans. Biomed. Eng.* 32:257–262.
2. Houston VL, Burges EM, Childress DS, Lehneis HR, Mason CP, Garbarini MA, LaBlance KP, Boone DA, Chan RB, Harlan JH and Brncick MD. 1992. Automated fabrication of mobility aids (AFMA): Below-knee CASD/CAM testing and evaluation program results. *J. Rehab. Dev. Res.* 29:78–124.
3. Krouskop TA, Muilenberg AL, Dougherty DR, and Winningham DJ. 1987. Computer-aided design of a prosthetic socket for an above-knee amputee. *J. Rehab. Res. Dev.* 24:31–38.
4. Saunders CG, Foort J, Bannon M, Dean D and Panych L. 1985. Computer-aided design of prosthetic sockets for below-knee amputees. *Prosthet. Orthot. Int.* 9:17–22.
5. Husain R and Chao EYS. 1983. A survey of finite element analysis in orthopaedics biomechanics: the first decade. *J Biomech*. 16:385–409.
6. Sanders JE. 1991. Ambulation with a prosthetic limb: Mechanical stress in amputated limb tissues. Ph.D. Dissertation, Univ. Washington, Seattle.
7. Silver-Thorn MB. 1991. Prediction and experimental verification of residual limb/prosthetic socket interface pressures for below-knee amputees. Ph.D. Dissertation, Northwestern Univ., Evanston, IL.
8. Steege JW, Schnur DS and Childress DS. 1987. Prediction of pressure at the below-knee socket interface by finite element analysis. Proc. Symp. Biomech. Normal Pathol. Gait. Boston, MA, AMSE, WAM. pp. 39–43.
9. Torres-Moreno R. 1991. Biomechanical analysis of the interaction between the above-knee residual limb and the prosthetic socket. Ph.D. Dissertation, Univ. Strathclyde, Glasgow, U.K..
10. Zhang M. 1999. Biomechanics of the Residual limb and prosthetic socket interface in below-knee amputees. Ph.D. Dissertation, Univ. London, England.
11. Kahle JT. 1999. Conventional and Hydrostatic Transtibial Interface Comparison. *J. Prosthet. Orthot.* 11:85-91.
12. Radcliff CW. and Foort J. 1961. The patellar-tendon-bearing below-knee prosthesis. Berkeley, CA: Biomechanics laboratory, University of California.
13. Fillauer CE, Pritham CH and Fillauer KD. 1989. Evaluation and development of the silicone suction socket (3S) for below-knee prostheses. *J. Prosthet. Orthot.* 1:92–103.
14. Kristinsson O. 1993. The ICEROSS concept: a discussion of a philosophy. Pressure and Shear Measurements. *Prosthet. Orthot. Int.* 17:49–55.
15. Murdoch G. 1965. The Dundee socket for below knee amputation. *Prosthet. Int*. 3:12–14.
16. Goh JCH, Lee PVS and Chong SY. 2003. Stump/socket pressure profiles of the pressure cast prosthetic socket. *Clin. Biomech*. 18:237-243
17. Lemaire ED and Jahnson F. 1996. A quantitative method for comparing and evaluating manual prosthetic socket modifications. *IEEE Trans. Rehabil. Eng.* 4:303–9.
18. Sidles JA, Boone DA, Harlan JS and Burgess EM. 1989. Rectification maps: a new method for describing residual limb and socket shapes. *J. Prosthet. Orthot.* 1:149–53.

19. Borchers RE, Boone DA, Joseph AW, Smith DG and Reiber GE. 1995. Numerical comparison of 3-D shapes: potential for application to the insensate foot. *J. Prosthet. Orthot.* 7:29–34.
20. Steege JW, Schnur DS, Vorhis RL and Rovick JS. 1987. Finite element analysis as a method of pressure prediction at the below-knee socket interface. Proceedings of RESNA 10th Annual Conference, California. pp. 814–6.
21. Steege JW and Childress DS. 1988. Finite element modelling of the below knee socket and limb: phase II, modelling and control issues in Biomechanical System Symposium. ASME WAM, BED. 11:121–9.
22. Steege JW and Childress DS. 1988. Finite element prediction of pressure at the below-knee socket interface. Report of ISPO Workshop on CAD/CAM in Prosthetics and Orthotics, Alexandria. Va: ISPO. pp. 71–82.
23. Steege JW, Silver-Thorn MB and Childress DS. 1992. Design of prosthetic socket using finite element analysis. Proceedings of 7th World Congress of ISPO, Chicago, IL. pp. 273.
24. Childress DS and Steege JW. 1987. Computer-aided analysis of below-knee socket pressure. *J. Rehabil. Res. Dev.* Progress Report. 2:22–4.
25. Reynolds DP and Lord M. 1992. Interface load analysis for computer-aided design of below-knee prosthetic sockets. *Med. Biol. Eng. Comput*. 30:419–26.
26. Sanders JE and Daly CH. 1993. Normal and shear stresses on a residual limb in a prosthetic socket during ambulation: comparison of finite element results with experimental measurements. *J. Rehabil. Res. Dev*. 30(2):191–204.
27. Zachariah SG and Sanders JE. 2000. Finite element estimates of interface stress in the transtibial prosthesis using gap elements are different from those using automated contact. *J. Biomech*. 33:895–9.
28. Zhang M and Roberts VC. 1993. Development of a nonlinear finite element model for analysis of stump/socket interface stresses in below knee amputee. In: Held KD, Brebbia CA, Ciskowski RD, Power H, editors. *Computational biomedicine*. Computational Mechanics Pub, Southampton. pp. 209–14.
29. Zhang M, Lord M, Turner-Smith AR and Roberts VC. 1995. Development of a nonlinear finite element modelling of the below-knee prosthetic socket interface. *Med. Eng. Phys*. 17(8):559–66.
30. Silver-Thorn MB and Childress DC. 1996. Parametric analysis using the finite element method to investigate prosthetic interface stresses for persons with trans-tibia amputation. *J. Rehabil. Res. Dev*. 33(3):227–38.
31. Quesada P. and Skinner H. B.. 1991. Analysis of a below-knee patellar tendon bearing prosthesis: a finite element study. *J. Rehabil. Res. Dev*. 3:1–12.
32. Brennan J. M. and Childress DS. 1991. Finite element and experimental investigation of above-knee amputee limb/prosthesis systems: a comparative study. *ASME Advances in Bioengineering*. 20:547–50.
33. Torres-Moreno R, Jones D, Solomonidis SE and Mackie H. 1999. Magnetic resonance imaging of residual soft tissues for computer-aided technology applications in prosthetics—a case study. *J. Prosthet. Orthot*. 11(1):6–11.
34. Torres-Moreno R, Solomonidis SE and Jones D. 1992. Three-dimensional finite element analysis of the above-knee residual limb. Proceedings of 7th World Congress ISPO. pp. 274.
35. Seguchi Y, Tanaka M, Nakagawa A and Kitayama I. 1989. Finite element analysis and load identification of above-knee prosthesis socket. Proceedings of 4th Int ANSYS Conf Exhib, Pittsburgh. pp. 12.31–12.44.

36. Krouskop TA, Dougherty DR and Vinson FS. 1987. A pulsed Doppler ultrasonic system for making noninvasive measurements of the mechanical properties of soft tissue. *J. Rehabil. Res. Dev*. 2:1–8.
37. Mak AFT, Yu YM, Hong LM and Chan C. 1992. Finite element models for analyses of stresses within above-knee stumps. Proceedings of 7th ISPO, Chicago. pp. 147.
38. Lee VSP, Solomonidis SE, Spence WD and Paul JP. 1994. A study of the biomechanics of the residual limb/prosthesis interface in transfemoral amputees. Proceedings of 8th Word Congress of ISPO, Melbourne, Australia. pp. 79.
39. Zhang M and Mak AFT. 1996. A finite element analysis of the load transfer between an above-knee residual limb and its prosthetic socket — Roles of interfacial friction and distal-end boundary conditions. *IEEE Trans. Rehabil. Eng*. 4(4):337–46.
40. Zhang M, Mak AFT and Roberts VC. 1998. Finite element modelling of a residual lower-limb in a prosthetic socket—a survey of the development in the first decade. *Med. Eng. Phys*. 20(5):360–73.
41. Silver-Thorn MB, Steege JW and Childress DS. 1996. A review of prosthetic interface stress investigations. *J. Rehabil. Res. Dev*. 33(3):253–66.
42. Zachariah SG and Sanders JE. 1996. Interface mechanics in lower-limb external prosthetics: a review of finite element models. *IEEE Trans. Rehabil. Eng*. 4(4):288–302.
43. Mak AFT, Liu GHW and Lee SY. 1994. Biomechanical assessment of below-knee residual limb tissue. *J. Rehabil. Res. Dev*. 31(3):188–98.
44. Malinauskas M, Krouskop TA and Barry PA. 1989. Noninvasive measurement of the stiffness of tissue in the above-knee amputation limb. *J. Rehabil. Res. Dev*. 3:45–52.
45. Vannah WM and Childress DS. 1996. Indentor tests and finite element modelling of bulk muscular tissue *in vivo*. *J. Rehabil. Res. Dev*. 33(3):239–52.
46. Vannah WM and Childress DS. 1993. Modelling the mechanics of narrowly contained soft tissues: the effects of specification of Poisson's ratio. *J. Rehabil. Res. Dev*. 30(2):205–9.
47. Vannah WM, Drvaric DM, Hastings JA, Stand JA and Harning DM. 1999. A method of residual limb stiffness distribution measurement. *J. Rehabil. Res. Dev*. 36(1):1–7.
48. Zheng YP and Mak AFT. 1996. An ultrasound indentation system for biomechanical properties assessment of soft tissues *in vivo*. *IEEE Trans. Biomed. Eng*. 43(9):912–8.
49. Zheng Y and Mak AFT. 1999. Effective elastic properties for lower limb soft tissues from manual indentation experiment. *IEEE Trans. Rehabil. Eng*. 7(3):257–67.
50. Zheng YP, Mak AFT and Lue BK. 1999. Objective assessment of limb tissue elasticity: development of a manual indentation procedure. *J. Rehabil. Res. Dev*. 36(2):71–85.
51. Hayes WC, Keer LM, Herrmann G and Mockros LF. 1972. A mathematical analysis for indentation tests of articular cartilage. *J. Biomech*. 5:541–51.
52. Zhang M, Zheng YP and Mak AFT. 1997. Estimating the effective Young's modulus of soft tissues from indentation tests. *Med. Eng. Phys*. 19(6):512–7.

53. Finney L. 2000. Simulation of donning a prosthetic socket using an idealized finite element model of the residual limb and prosthetic socket. Proceedings of 10th Int Conf Biomed Eng, Singapore. pp. 71.
54. Schade H. 1912. Untersuchungen zur organfunction des bindegewebes. Ztschr. f. Exper. Path. u. Therapis. 11:369–399.
55. Kirk E and Kvorning SA. 1949. Quantitative measurements of the elastic properties of the skin and subcutaneous tissue in young and old individuals. *J. Gerontol*. 4:273–84.
56. Kirk E and Chieffi M. 1962. Variations with age in elasticity of skin and subcutaneous tissue in human individuals. *J. Gerontol*. 17:373–80.
57. Lewis HE, Mayer J and Pandiscio AA. 1965. Recording skinfold calipers for the determination of subcutaneous edema. *J. Lab. Clin. Med*. 66(1):154–60.
58. Kydd WL, Daly CH and Nansen D. 1974. Variation in the response to mechanical stress of human soft tissues as related to age. *J. Prosthet. Dent*. 32(5):493–500.
59. Ziegert JC and Lewis JL. 1978. *In-vivo* mechanical properties of soft tissues covering bony prominences. *J. Biomech. Eng*. 100:194–201.
60. Dikstein S and Hartzshtark A. 1981. *In vivo* measurement of some elastic properties of human skin. In: R Marks, PA Payne, editors. *Bioengeering and skin*. Lancaster: MTP Press. pp. 45–53.
61. Bader DL and Bowker P. 1983. Mechanical characteristics of skin and underlying tissues *in vivo*. *Biomaterials.* 4:305–8.
62. Horikawa M, Ebihara S, Sakai F and Akiyama M. 1993. Noninvasive measurement method for hardness in muscular tissues. *Med. Biol. Eng. Comput*. 31:623–7.
63. Ferguson-Pell M, Hagisawa S and Masiello RD. 1994. A skin indentation system using a pneumatic bellows. *J. Rehabil. Res. Dev*. 31(1):15–9.
64. Silver-Thorn MB. 1991. Prediction and experimental verification of residual limb/prosthetic socket interface pressures for below knee amputees. PhD dissertation, Northwestern University, Illinois.
65. Silver-Thorn MB and Childress DS. 1992. Use of a generic, geometric finite element model of the below-knee residual limb and prosthetic socket to predict interface pressures. Proc 7th World Congress ISPO, Chicago. pp. 272.
66. Vannah WM and Childress DS. 1988. An investigation of the three-dimensional mechanical response of bulk muscular tissue: experimental methods and results. In: Spilker RL and Simon BR, editors. *Computational Methods in Bioengineering*. pp. 493–503.
67. Reynolds D. 1988. Shape design and interface load analysis for below knee prosthetic sockets. PhD dissertation, University of London.
68. Torres-Moreno R, Solomonidis SE and Jones D. 1992. Geometrical and mechanical characteristics of the above-knee residual limb. Proc 7th World Congress of ISPO, Chicago. pp. 149.
69. Zheng YP. 1997. Development of an ultrasound indentation system for biomechanical properties assessment of limb soft tissues *in vivo*. PhD dissertation, Hong Kong Polytechnic University.
70. Pathak AP, Silver-Thorn B, Thierfelder CA and Prieto TE. 1998. A rate-controlled indentor for *in vivo* analysis of residual limb tissues. *IEEE Trans. Rehabil. Eng*. 6:12–20.
71. Silver-Thorn MB. 1999. *In vivo* indentation of lower extremity limb soft tissues. *IEEE Trans. Rehabil. Eng*. 7:268–77.

72. Zheng YP, Choi YKC, Wong K, Chan S and Mak AFT. 2000a. Biomechanical assessment of plantar foot tissue in diabetic patients using an ultrasound indentation system. *Ultrasound Med. Biol.* 26:451–6.
73. Zheng YP, Leung SF and Mak AFT. 2000b. Assessment of neck tissue fibrosis using an ultrasound palpation system: a feasibility study. *Med. Biol. Eng. Comput.* 38:1–6.
74. Zheng YP, Mak AFT and Qin L. 1998. Load-indentation response of soft tissues with multi-layers. Proc 20th Ann Int Conf IEEE EMBS, Hong Kong. pp. 2270–2.
75. Krouskop TA, Wheeler TM, Kallel F, Garra BS and Hall T. Elastic moduli of breast and prostate tissues under compression. *Ultrasonic Imaging.* 20:260–74.
76. Huang DT and Mak AFT. 1994. A finite element analysis of indentation on a soft tissue layers—The effect of indentor misalignment and nonparallel tissue layer. Proc Int Conf Biomed Eng, Hong Kong. pp. 397–400.
77. Krouskop TA, Mulenberg AL, Doughtery DR and Winningham DJ. 1987. Computer-aided design of a prosthetic socket for an above knee amputee. *J. Rehabil. Res. Dev.* 24:31–8.
78. Lindahl OA, Omata S and Angquist KA. 1998. A tactile sensor for detection of physical properties of human skin *in vivo*. *J. Med. Eng. Tech*. 22:147–53.
79. Michel CC and Gillott H. 1990. Microvascular mechanisms in stasis and ischaemia. In: Bader DL, editor. *Pressure sores—clinical practice and scientific approach*. London: MacMillan Press. pp. 153–63.
80. Daniel RK, Priest DL and Wheatley DC. Etiologic factors in pressure sores: an experimental model. *Arch. Phys. Med. Rehabil*. 61:492–8.
81. Groth KE. 1942. Clinical observations and experimental studies on the origin of decubiti. *Acta. Chir. Scand. (Suppl)*. 76(1):1–209.
82. Mackenzie IC. 1974. The effects of frictional stimulation on mouse ear epidermis. *J. Inv. Dermatol*. 62:80–5.
83. Baker SR. 1991. Fundamentals of expanded tissue. *Head Neck*. 13:327–33.
84. Gillott H. 1985. Quantifying the fit of a hand orthosis. *Care. Brit. J. Rehabil. Tissue Viab*. 1(1):12–7.
85. Levine N. 1982. Friction blisters. *Physician and Sports medicine.* 10(3):84–92.
86. Husain T. 1953. An experimental study of some pressure effects on tissues with reference to the bed-sore problem. *J. Path. Bact*. 66:347–58.
87. Kosiak M. 1959. Etiology and pathology of ischemic ulcers. *Arch. Phys. Med. Rehabil.* 39:62–9.
88. Reswick JB and Rogers JE. 1976. Experience at Rancho Los Amigos Hospital with device and techniques to prevent pressure sores. In: Kenedi RM, Cowden JM, Scales JT, editors. *Bed sore biomechanics*. London: MacMillan Press. pp. 301–10.
89. Akbarzadeh MR. 1991. Behaviour for relieving pressure. In: Webster JG, editor. *Prevention of pressure sores, engineering and clinical aspects*. Bristol: IOP Pub Ltd. pp. 175–90.
90. Reddy NP, Cochran GVB and Krouskop TA. 1981. Interstitial fluid as a factor in decubitus ulcer formation. *J. Biomech*. 14(2):879–81.
91. Sacks AH. 1989. Theoretical prediction of a time-at pressure curve for avoiding pressure sores. *J. Rehabil. Res. Dev*. 26(3):27–34.
92. Mak AFT, Huang LD and Wang Q. 1994. A biphasic poroelastic analysis of the flow dependent subcutaneous tissue pressure and compaction due to

epidermal loading: issues in pressure sores. *Trans. ASME J. Biomech. Eng*. 116:421–9.
93. Zhang JD, Mak AFT and Huang LD. 1997. A large deformation biomechanical model for pressure ulcers. *Trans. ASME J. Biomech. Eng*. 119:406–8.
94. Landsman AS, Meaney DF, Cargill RS, Macarak EJ and Thibault LE. 1995. High strain rate tissue deformation. *J. Am. Podiatric Med. Assoc*. 85(10):519–27.
95. Levy SW. 1980. Skin problems of the leg amputee. *Prosthet. Orthot. Int*. 4:37–44.
96. Barnes G. 1956. Skin health and stump hygiene. *Artificial Limbs*. 3(1):4–19.
97. Sanders JE, Goldstein BS and Leotta DF. 1995. Skin response to mechanical stress: adaptation rather than breakdown—a review of the literature. *J. Rehabil. Res. Dev*. 32(3):214–26.
98. Sakamoto M, Li G, Hara T and Chao EYS. 1996. A new method for theoretical analysis of static indentation test, *J. Biomech*. 29:679–85.
99. Fung YC. 1980. Bio-viscoelastic solids. In: *Biomechanics: mechanical properties of living tissues*. New York: Springer-Verlag. pp. 196–260.
100. Zheng YP and Mak AFT. May 1996b. Determination of the *in-vivo* incremental modulus of soft tissues using an ultrasound indentation system. Abstract book of 2nd Medical Engineering Week of the World, Taiwan.
101. Mak AFT, Lai WM and Mow VC. 1987. Biphasic indentation of articular cartilage I: theoretical analysis. *J. Biomech*. 20:703–14.
102. Mow VC, Kuei SC, Lai WM and Armstrong CG. 1989. Biphasic creep and stress relaxation of articular cartilage in compression: theory and experiments. *J. Biomech. Eng*. 102:73–84.
103. Coletti JM, Akeson WH and Woo SLY. 1972. A comparison of the physical behavior of normal articular cartilage and arthroplasty surface. *J. Bone Joint Surg*. 54A:147–60.
104. Parsons JR and Black J. 1977. The viscoelastic shear behavior of normal rabbit articular cartilage. *J Biomech*. 10:21–9.
105. Spilker RL, Suh JK and Mow VC. 1992. A finite element analysis of the indentation stress-relaxation response of linear biphasic articular cartilage. J. Biomech. Eng. 114:191–201.
106. Suh JK and Spilker RL. 1994. Indentation analysis of biphasic articular cartilage: nonlinear phenomena under finite deformation. *J. Biomech. Eng*. 116:1–9.
107. Zheng Y and Mak AFT. 1999a. Extraction of quasilinear viscoelastic parameters for lower limb soft tissues from manual indentation experiment. *ASME T, J. Biomech. Eng*. 121:330–9.
108. Fischer AA. 1986. Pressure tolerance over muscles and bones in normal subjects. *Arch. Phys. Med. Rehabil*. 67:406–9.
109. Wu CL, Chang CH, Lin CC and Ho HJ. 2003. An evaluation protocol for below-knee socket selection – a finite element approach with pain-pressure tolerance. Summer Bioengineering Conference, Florida. pp. 873-4
110. Persson BM and Liedberg E. 1982. Measurement of maximum endweight-bearing in lower limb amputees. *Prosthet. Orthot. Int*. 6:147–51.
111. Katz K, Susak Z, Seliktar R and Najenson T. 1979. End-bearing characteristics of patellar-tendon-bearing prostheses—a preliminary report. *Bull. Prosth. Res*. BPR10–32:55–68.

112. Lee CW, Zhang M and Mak AF. 2005. Regional differences in pain threshold and tolerance of the transtibial residual limb: including the effects of age and interface material. *Arch. Phys. Med. Rehabil.* 86:641-9
113. Daly CH, Chimoskey JE, Holloway GA and Kennedy D. 1976. The effect of pressure loading on the blood flow rate in the human skin, In: Kenedi RM, Cowden JM, Scales JT, editors. Bed sore biomechanics. London: MacMillan Press. p. 69–77.
114. Larsen B, Holstein P and Lassen NA. On the pathogenesis of pressure sores, skin blood flow cessation by external pressure on the back. 1979. *Scand. J. Plas. Reconstr. Surg*. 13:347–50.
115. Romanus M, Stenqvist O, Svensjo E and Ehira T. 1983. Microvascular changes due to repeated local pressure-induced ischaemia: intravital microscope study on hamster cheek pouch. *Arch. Phys. Med. Rehabil*. 64:553–5.
116. Bennett L, Kavner D, Lee BK and Frieda A. 1979. Shear vs pressure as causative factors in skin blood flow occlusion. *Arch. Phys. Med. Rehabil*. 60:309–14.
117. Bennett L, Kavner D, Lee BY, Trainor FS and Lewis J. 1984. Skin stress and blood flow in sitting paraplegic patients. *Arch. Phys. Med. Rehabil*. 65:186–90.
118. Newson TP, Pearcy MJ and Rolfe P. 1981. Skin surface PO2 measurement and the effect of externally applied pressure. *Arch. Phys. Med. Rehabil.* 62:390–2.
119. Bader DL and Gant CA. 1988. Changes in transcutaneous oxygen tension as a result of prolonged pressers at the sacrum. *Clin. Phys. Physiol. Meas*. 9(1):33–40.
120. Sangeorzan BJ, Harrington RM, Wyss CR, Czerniecki JM and Matsen FA. 1989. Circulatory and mechanical response of skin to loading. *J. Orthop. Res*. 6(30):425–31.
121. Ek AC, Gustavsson G and Lewis DH. 1987. Skin blood flow in relation to external pressure and temperature in the supine position on a standard hospital mattress. *Scand. J. Rehabil. Med*. 19:121–6.
122. Sableman EE, Valainis E and Sacks AH. 1989. Skin capillary blood flow under very light pressure. Proc. Ann. Conf. Rehabil. Eng. Soc. N. Am. 12:256–7.
123. Sacks AH, O'Neill H and Perkash I. 1985. Skin blood flow changes and tissue deformations produced by cylinderal indentors. *J. Rehabil. Res. Dev*. 22(30):1–6.
124. Meijer JH, Schut GL, Ribbe MW, Groovaerts HG, Nieuwenhuys R, Reulen JPH and Schneider H. 1989. Method for the measurement of susceptibility to decubitus ulcer formation. *Med. Biol. Eng. Comput*. 27:502–6.
125. Zhang M and Roberts VC. 1993. The effect of shear forces externally applied to skin surface on underlying tissues. *J. Biomed. Eng*. 15(6):451–6.
126. Zhang M, Turner-Smith AR and Roberts VC. 1994. The reaction of skin and soft tissue to shear forces applied externally to the skin surface. *J. Eng. Med*. 208(4):217–22.
127. Tam EWC, Mak AFT, Evans JH and Chow YYN. 1998. Post occlusive hyperaemic of tissue under static and dynamic loading conditions. Proceedings of 20th Annual Int Conf IEEE/EMBS, Hong Kong. pp. 2294–6.

128. Herman EC, Knapp CF, Donofrio JC and Sacido R. 1999. Skin perfusion responses to surface pressure-induced ischemia: implication for the developing pressure ulcer. *J. Rehabil. Res. Dev*. 36(2):109–20.
129. Goossens RHM, Zegers R, Hoek van Dijke GA and Snijders CJ. 1994. Influence of shear on skin oxygen tension. *Clin. Physiol*. 14:111–8.
130. Krouskop TA, Reddy NP, Spencer WA and Secor JW. 1978. Mechanisms of decubitus ulcer formation—an hypothesis. *Med. Hypotheses*. 4(1):37–9.
131. Bader DL, Gigg SL and Polliack AA. 1994. The importance of pressure and time in determining soft tissue status. Proceedings 20th Word Congress of Biomechanics, Amsterdam, The Netherlands. pp. 11.
132. Ferguson-Pell M and Hagiswa S. 1988. Biochemical changes in sweat following prolonged ischemia. *J. Rehabil. Res. Dev*. 25(3):57–62.
133. Polliack A, Taylor R and Bader D. 1993. Analysis of sweat during soft tissue breakdown following pressure ischemia. *J. Rehabil. Res. Dev*. 30(2):250–9.
134. Naylor PFD. 1955. Experimental friction blisters. *Br. J. Dermatol*. 67:327–42.
135. Akers CWA. 1985. Measurements of friction injuries in man. *Am. J. Indus. Med*. 8:473–81.
136. Dinsdale SM. 1974. Decubitus ulcers: role of pressure and friction in causation. *Arch. Phys. Med. Rehabil*. 55:147–51.
137. Sanders JE, Garbini JL, Leschen JM, Allen MS and Jorgensen JE. 1997. A bidirectional load applicator for the investigation of skin response to mechanical stress. *IEEE Trans. Biomed. Eng*. 44(4):290–6.
138. Sanders JE. 2000. Thermal response of skin to cyclic pressure and pressure with shear: a technical note. *J. Rehabil. Res. Dev*. 37(5):511–5.
139. Tönük E and Silver-Thorn MB. 2003. Nonlinear material property estimation of lower extremity residual limb tissues. *IEEE Trans. Rehabil. Eng*. 11(1):43-53
140. Allende MF, Levy SW and Barnes GH. 1963. Epidermoid cysts in amputees. *Acta. Dermato-Venereologica*. 43:56–67.
141. Naylor PFD. 1955. The skin surface and friction. *Br. J. Derm*. 67:239–48.
142. Sanders JE, Greve JM, Mitchell SB and Zachariah SG. 1998. Material properties of commonly-used interface materials and their static coefficients of friction with skin and socks. *J. Rehabil. Res. Dev*. 35(2):161–76.
143. Zhang M and Mak AFT. 1999. *In vivo* friction properties of human skin. *Prosthet. Orthot. Int*. 23:135–41.
144. Appoldt FA, Bennett L and Contini R. 1968. The results of slip measurements in above-knee suction sockets. *Bull. Prosthet. Res*. Fall:106–12.
145. Appoldt FA, Bennett L and Contini R. 1970. Tangential pressure measurement in above-knee suction sockets. *Bull. Prosthet. Res*. Spring:70–86.
146. Sanders JE, Daly CH and Burgess EM. 1992. Interface shear stresses during ambulation with a below-knee prosthetic limb. *J. Rehabil. Res. Dev*. 29(4):1–8.
147. Sanders JE and Daly CH. 1999. Interface pressure and shear stresses: sagittal plane angular alignment effects in three transtibial amputee case studies. *Prosthet. Orthot. Int*. 23:21–9.
148. Sanders JE, Bell DM, Okumura RM and Dralle AJ. 1998. Effects of alignment changes on stance phase pressures and shear stresses on transtibial amputees: measurements from 13 transducer sites. *IEEE Trans. Rehabil. Eng*. 6(1):21–31.

149. Loden M. 1995. Biophysical properties of dry atopic and normal skin with special reference to effects of skin care products. *ACTA Dermato-Venereologica*. 192(Suppl):3–48.
150. Elsner P,Wilhelm D and Maibach HI. 1990. Frictional properties of human forearm and vulvar skin: influence of age and correlation with transepidermal water loss and capacitance. *Dermatological*. 181:88–91.
151. Comaish JS and Bottoms E. 1971. The skin and friction: deviations from amonoton's laws, and the effects of hydration and lubrication. *Br. J. Derm*. 84:37–43.
152. Cua AB,Wilhelm KP and Maibach HI. 1990. Frictional properties of human skin: relation to age, sex and anatomical region, stratum corneum hydration and transepidermal water loss. *Br. J. Derm*. 123:473–9.
153. Van Pijkeren TV, Naeff M and Kwee HH. 1980. A new method for measurement of normal pressure between amputation residual limb and socket. *Bull. Prosthet. Res*. 17(1):31–4.
154. Naeff M and Van Pijkeren TV. 1980. Dynamic pressure measurements at the interface between residual limb and socket—the relationship between pressure distribution, comfort, and brim shape. *Bull. Prosthet. Res*. 10-33:35–50.
155. Isherwood PA. 1978. Simultaneous PTB socket pressures and force plate values. BRADU Report, London: Biomechanical Res and Dev Unit. pp. 45–9.
156. Mueller SJ and Hettinger T. 1954. Measuring the pressure distribution in the socket of the prostheses. *Orthpadie-Technik Heft.* 9:222–5.
157. Lebiedowsky N and Kostewicz J. 1977. Determination of the order of pressure exerted by static forces on the skin of the lower limb stump with the prosthesis. *Chir Narz, Ruchu Orop polska.* 42:615–24.
158. Kroupskop TA, Brown J, Goode B and Winningham D. 1987. Interface pressures in above-knee sockets. *Arch. Phys. Med. Rehabil*. 68:713–4.
159. Sonck WA, Cockrell JL and Koepke GH. 1970. Effect of linear material on interface pressures in below-knee prostheses. *Arch. Phys. Med. Rehabil*. 51(11):666–9.
160. Rae JW and Cockrell JL. 1971. Interface pressure and stress distribution in prosthetic fitting. *Bull. Prosth. Res*. 10–16:64–111.
161. Pearson JR, Holmgren G, March L and Oberg K. 1973. Pressure in critical regions of the below-knee patellar-tendon-bearing prosthesis. *Bull. Prosth. Res*. 10–19:52–76.
162. Pearson JR, Holmgren G, March L and Oberg K. 1974. Pressure variation in the below-knee patellar tendon bearing suction socket. *J. Biomech*. 7:487–96.
163. Burgess EM and Moor AJ. 1977. A study of interface pressure in the below knee prosthesis (Physiological suspension: an interim report). *Bull. Prosthet. Res*. Fall:58–70.
164. Winaski D and Pearson JR. 1987. Least-squares matrix correlations between stump stresses and prosthesis loads for below-knee amputees. *J. Biomech. Eng*. 109:238–46.
165. Leavitt LA, Petersson CR, Canzoneri J, Pza R, Muilenburg AL and Rhyne VT. 1970. Quantitative method to measure the relationship between prosthetic gait and the forces produced at the stump-socket interface. *Am. J. Phys. Med.* 49:192–203.
166. Leavitt LA, Zuniga EN, Calvert JC, Canzoneri J and Petersson CR. 1972. Gait analysis and the tissue-socket interface pressures in above knee amputees. *Southern Med. J*. 65:1197–207.

167. Williams RB, Porter D and Roberts VC, 1992. Triaxial force transducer for investigating stresses at the stump/socket interface. *Med. Biol. Eng. Comput*. 1:89–96.
168. Appoldt FA and Bennett L. 1967. A preliminary report on dynamic socket pressure. *Bull. Prosthet. Res*. Fall:20–55.
169. Appoldt FA, Bennett L and Contini R. 1969. Socket pressure as a function of pressure transducer protrusion. *Bull. Prosthet. Res.* Spring:236–49.
170. Sanders JE and Daly CH. 1993. Measurement of stresses in the three orthogonal directions at the residual limb-prosthetic socket interface. *IEEE Trans. Rehabil. Eng*. 1(2):79–85.
171. Engsberg JR, Springer MJN and Harder JA. 1992. Quantifying interface pressure in below-knee-amputee socket. *J. Assoc. Children's Prosthetic-Orthotic Clinics*. 27(3):81–8.
172. Houston VL, Mason CP, LaBlanc KP, Beatties AC, Garbarini MA and Lorenze EJ. 1994. Preliminary results with the DVA-Tekscan BK prosthetic socket/residual limb stress measurement system. Proceedings of 20th Annual Meeting American Academy of Orthotist and Prosthetist, Nashville, TN. pp. 8–9.
173. Covery P and Buis AWP. 1998. Conventional patellar-tendon-bearing (PTB) socket/stump interface dynamic pressure distribution recorded during the prosthetic stance phase of gait of a trans-tibial amputee. *Prosthet. Orthot. Int.* 22:193–8.
174. Covery P and Buis AWP. 1999. Socket/stump interface dynamic pressure distribution recorded during the prosthetic stance phase of gait of a trans-tibial amputee wearing a hydrocast socket. *Prosthet. Orthot. Int*. 23:107–12.
175. Zhang M, Turner-Smith AR, Tanner A and Roberts VC. 1996. Frictional action at residual limb/prosthetic socket interface. *Med. Eng. Phys*. 18(3):207–14.
176. Zhang M, Mak AFT and Chung AKI. 1998. Dynamic pressure maps over areas of AK prosthetic sockets. Proceedings of 9th Word Congress of ISPO, Amsterdam. pp. 709–11.
177. Sanders JE. 1995. Interface mechanics in external prosthetics: review of interface stress measurement techniques. *Med. Biol. Eng. Comput.* 33:509–16.
178. Sanders JE, Daly CH and Burgess EM. 1993. Clinical measurement of normal and shear stresses on a transtibial stump: characteristics of wave-form shapes during walking. *Prosthet. Orthot. Int.* 17:38–48.
179. Zhang M, Turner-Smith AR, Tanner A and Roberts VC. 1998. Clinical investigation of the pressure and shear stress on the transtibial stump with a prosthesis. *Med. Eng. Phys*. 20(3):188–98.
180. Lee VSP, Solomonidis SE and Spence WD. 1997. Stump-socket interface pressure as an aid to socket design in prostheses for transfemoral amputees—a preliminary study. *J. Eng. Med*. 211:167–80.
181. Polliack AA, Sieh RC, Craig DD, Landsberger S, McNeil DR and Ayyappa E. 2000. Scientific validation of two commercial pressure sensor systems for prosthetic socket fit. *Prosthet. Orthot. Int*. 24:63–73.
182. Polliack AA, Landsberger S, McNeil DR, Sieh RC, Craig DD and Ayyappa E. 1999. Socket measurement systems perform under pressure. *Biomechanics*. June:71–80.

183. Shem KL, Breahey JW and Werner PC. 1998. Pressures at the residual limb-socket interface in transtibial amputees with thigh lacer-side joints. *J. Prosthet. Orthot.* 10:51–5.
184. Ng P, Lee PSV and Goh JCH. 2002. Prosthetic sockets fabrication using rapid prototyping technology. *Rapid Prototyping Journal*. 8:53-59.
185. Kandel ER, Schwartz JH and Jessell TM. 2000. In: *Principles of Neural Science*, 4th ed. New York: McGraw-Hill. pp. 472-479.
186. Lebedev NN and Ufliand IA. 1958. Axisymmetric contact problem for an elastic layer. *PMM*. 22:442-450.

APPENDIX 1: Patient Informed Consent Form

Version: 1.2 Date: 21 Mar 2005

Protocol Title:
Mechanical Characterisation of Bulk Tissue for Intelligent CAD-FEA Prosthetics Application: Combining in-vivo Experiments and Finite Element Modelling
Principal Investigator & Contact Details:
James Goh Cho Hong Orthopaedic Diagnostic Centre, National University Hospital, 5 Lower Kent Ridge Road, Singapore 119074 Email: dosgohj@nus.edu.sg Tel: 67724423

I voluntarily consent to take part in this research study.

I have fully discussed and understood the purpose and procedures of this study.

This study has been explained to me in _____(language)

on _____ (date) by _____(name of translator).

I have been given enough time to ask any questions that I have about the study, and all my questions have been answered to the best of my doctor's ability.

I agree / do not agree [circle selected option] to the use of the data for future studies.

I agree / do not agree [circle selected option] to the use of my blood/tissue samples for future studies.

I agree / do not agree [circle selected option] to be selected to undergo MRI of my residual stump.

_____	_____	_____
Name of Patient	Signature	Date
_____	_____	_____
Name of Witness	Signature	Date

Investigator Statement

I, the undersigned, certify to the best of my knowledge that the patient signing this informed consent form had the study fully explained and clearly understands the nature, risks and benefits of his/her participation in the study.

_____	_____	_____
Name of Investigator	Signature	Date

APPENDIX 2: Technical Drawings of the Indentor

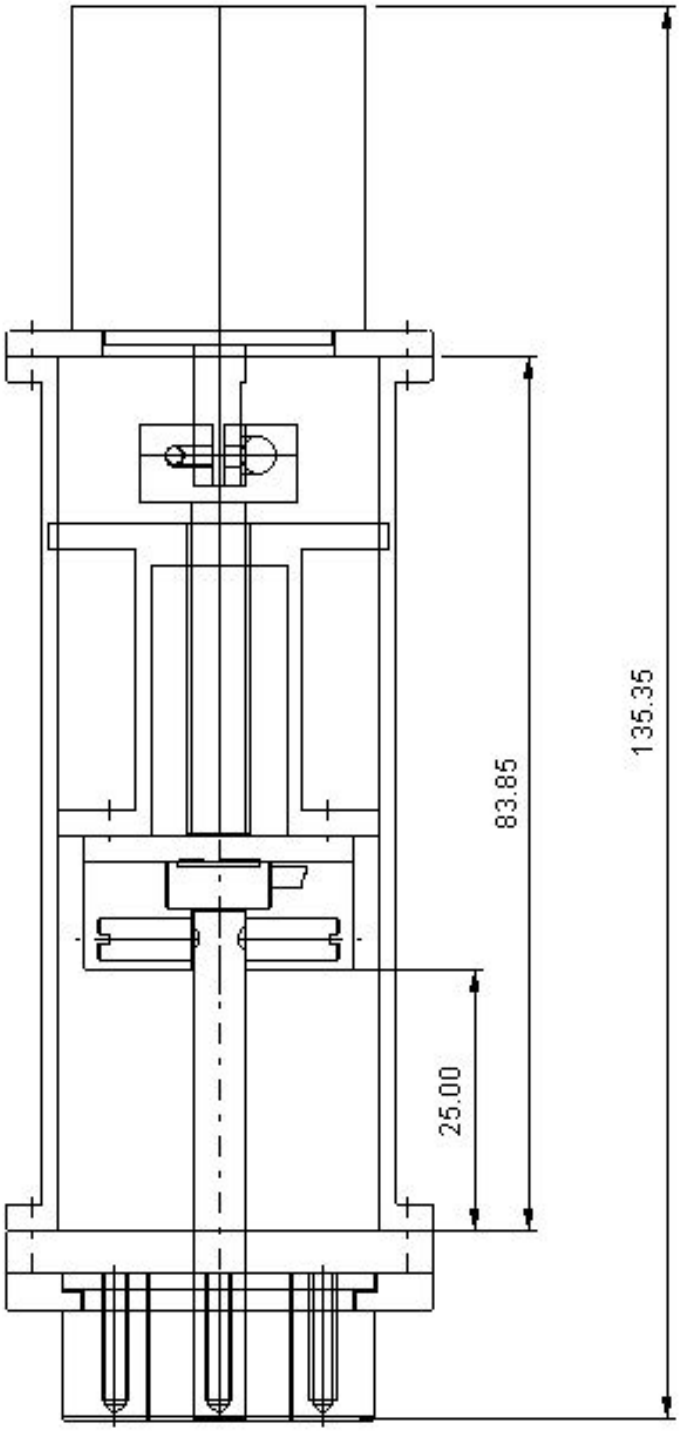

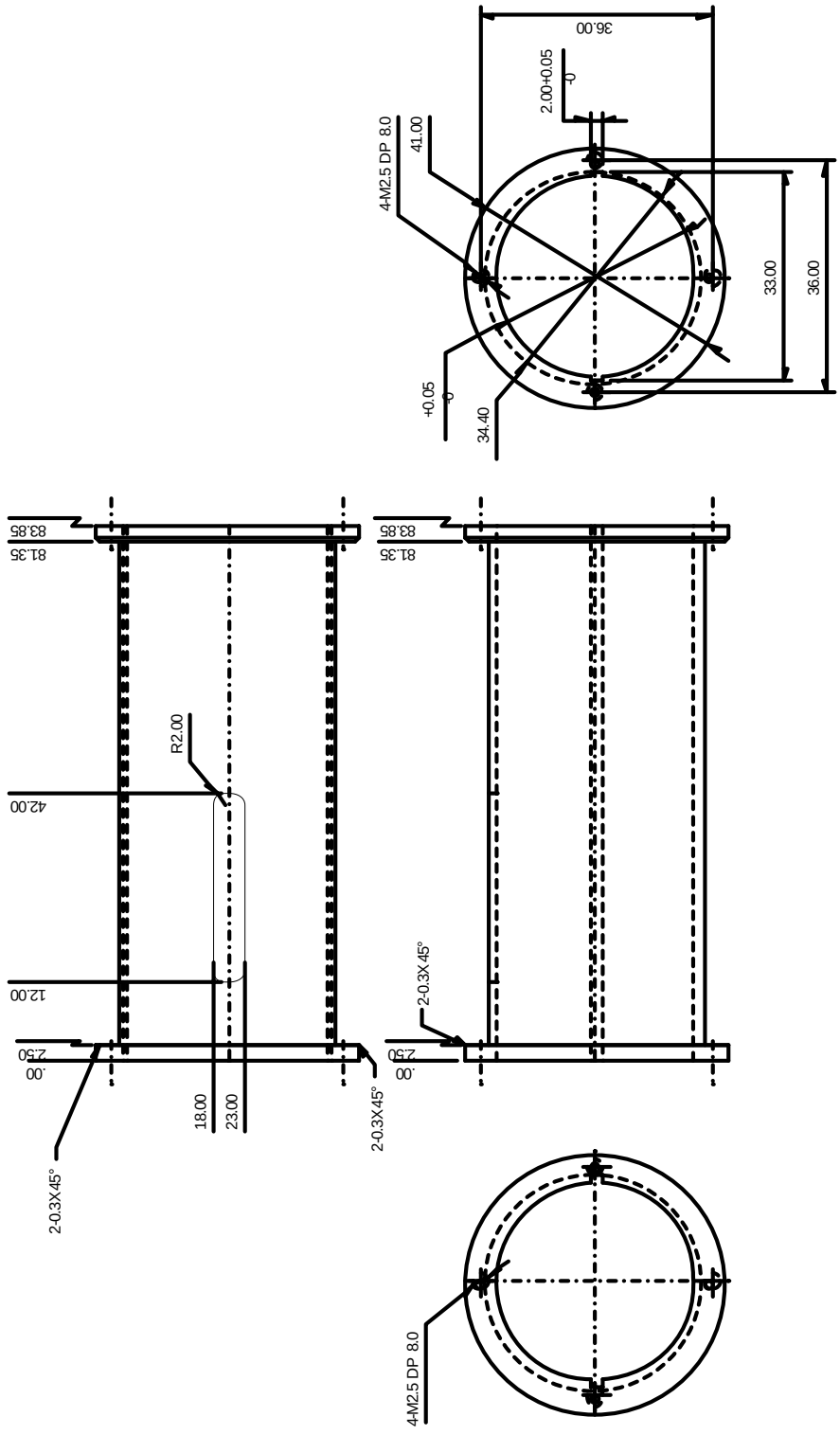
36.00
2.00+0.05
0
4-M2.5 DP 8.0
41.00
33.00
36.00
+0.05
0
34.40
81.35
83.85
R2.00
42.00
12.00
2.50
.00
18.00
23.00
2-0.3X45°
2-0.3X45°
2-0.3X45°
4-M2.5 DP 8.0

APPENDIX 3: Data for Indentor Calibration Tests

Static Loading Test

Data for Test 1

Weight of movable platform = 0.365 kg

Time (s)	Force measured by load cell (N)	Mass added each step (kg)	Cumulative mass on platform (kg)	Cumulative weight on platform (N)	Indentation distance (mm)
0	0	0	0	0	0.0
25	3.686	0	0.365	3.580	6.0
37	4.203	0.05	0.415	4.070	6.0
55	4.658	0.1	0.465	4.560	6.0
72	5.205	0.15	0.515	5.051	6.0
91.5	5.651	0.2	0.565	5.541	6.0
106.5	6.095	0.25	0.615	6.031	6.0
122	6.625	0.3	0.665	6.522	6.0
139.5	7.092	0.35	0.715	7.012	6.0
157.5	7.664	0.4	0.765	7.502	6.0
181.5	8.099	0.45	0.815	7.993	6.0
207.5	8.585	0.5	0.865	8.483	6.0
231	9.130	0.55	0.915	8.973	6.0
252.5	9.586	0.6	0.965	9.464	6.0
270	10.048	0.65	1.015	9.954	6.0
287.5	10.556	0.7	1.065	10.444	6.0
307.5	11.029	0.75	1.115	10.935	6.0
331	11.473	0.8	1.165	11.425	6.0
350.8	12.045	0.85	1.215	11.916	6.0
370.5	12.445	0.9	1.265	12.406	6.0
390.5	12.911	0.95	1.315	12.896	6.0
410	13.473	1	1.365	13.387	6.0

Data for Test 2

Weight of movable platform = 0.365 kg

Time (s)	Force measured by load cell (N)	Mass added each step (kg)	Cumulative mass on platform (kg)	Cumulative weight on platform (N)	Indentation distance (mm)
0	0	0	0	0	0
25	3.543	0	0.365	3.580	5.7
38	4.070	0.05	0.415	4.070	5.7
54	4.572	0.1	0.465	4.560	5.7
66.5	5.038	0.15	0.515	5.051	5.7
80	5.521	0.2	0.565	5.541	5.7
96.5	6.005	0.25	0.615	6.031	5.7
111	6.532	0.3	0.665	6.522	5.7
126	6.946	0.35	0.715	7.012	5.7
143.5	7.500	0.4	0.765	7.502	5.7
158	7.902	0.45	0.815	7.993	5.7
174.5	8.401	0.5	0.865	8.483	5.7
189	8.919	0.55	0.915	8.973	5.7
204	9.328	0.6	0.965	9.464	5.7
218	9.976	0.65	1.015	9.954	5.7
233	10.511	0.7	1.065	10.444	5.7
248	10.938	0.75	1.115	10.935	5.7
265.5	11.443	0.8	1.165	11.425	5.7
281.5	11.865	0.85	1.215	11.916	5.7
296	12.442	0.9	1.265	12.406	5.7
312.5	12.929	0.95	1.315	12.896	5.7
329.5	13.337	1	1.365	13.387	5.7

Data for Test 3

Weight of movable platform = 0.365 kg

Time (s)	Force measured by load cell (N)	Mass added each step (kg)	Cumulative mass on platform (kg)	Cumulative weight on platform (N)	Indentation distance (mm)
0	0	0	0	0	0
24.5	3.56	0	0.365	3.580	6.0
37	4.18	0.05	0.415	4.070	6.0
49	4.56	0.1	0.465	4.560	6.0
60.5	5.03	0.15	0.515	5.051	6.0
72.5	5.56	0.2	0.565	5.541	6.0
83.5	6.12	0.25	0.615	6.031	6.0
97.5	6.62	0.3	0.665	6.522	6.0
110	7.02	0.35	0.715	7.012	6.0
124.5	7.55	0.4	0.765	7.502	6.0
138.5	8.01	0.45	0.815	7.993	6.0
153.5	8.51	0.5	0.865	8.483	6.0
167.5	9.06	0.55	0.915	8.973	6.0
180.5	9.58	0.6	0.965	9.464	6.0
194	10.02	0.65	1.015	9.954	6.0
207.5	10.54	0.7	1.065	10.444	6.0
223	11.03	0.75	1.115	10.935	6.0
238.5	11.49	0.8	1.165	11.425	6.0
253.5	11.92	0.85	1.215	11.916	6.0
269	12.41	0.9	1.265	12.406	6.0
281.5	12.94	0.95	1.315	12.896	6.0
297	13.46	1	1.365	13.387	6.0

Graph for Test 1

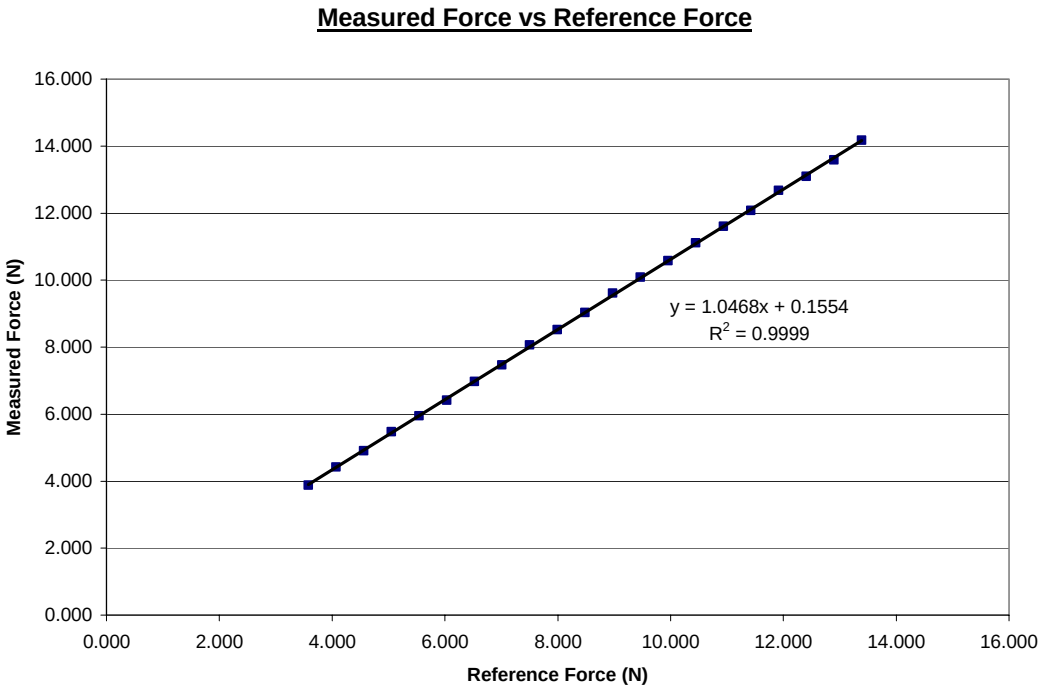

Graph for Test 2

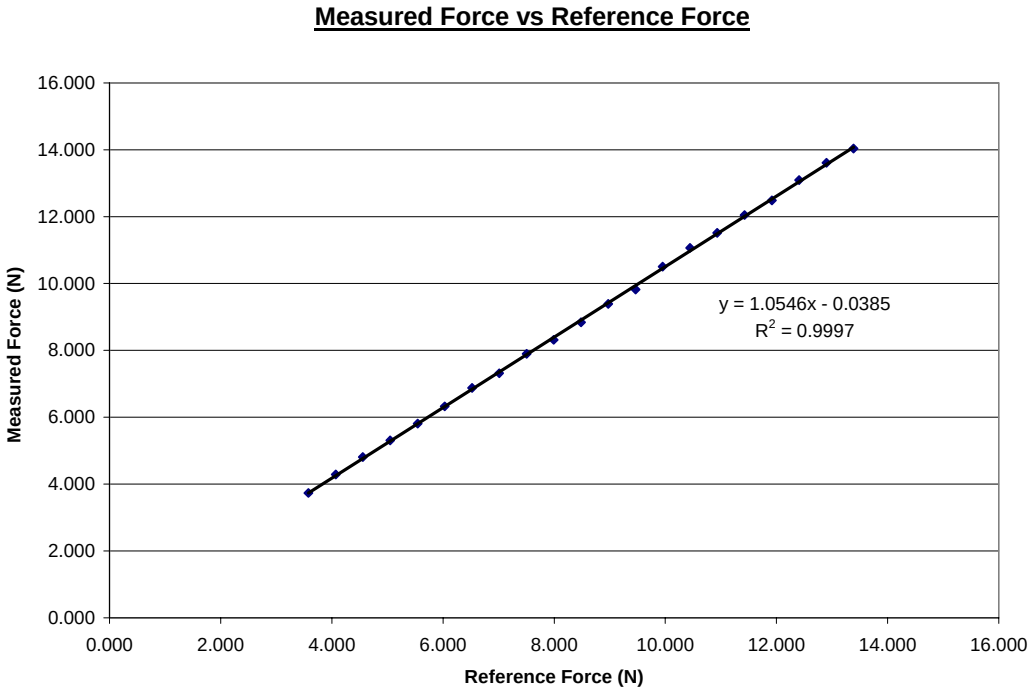

Graph for Test 3

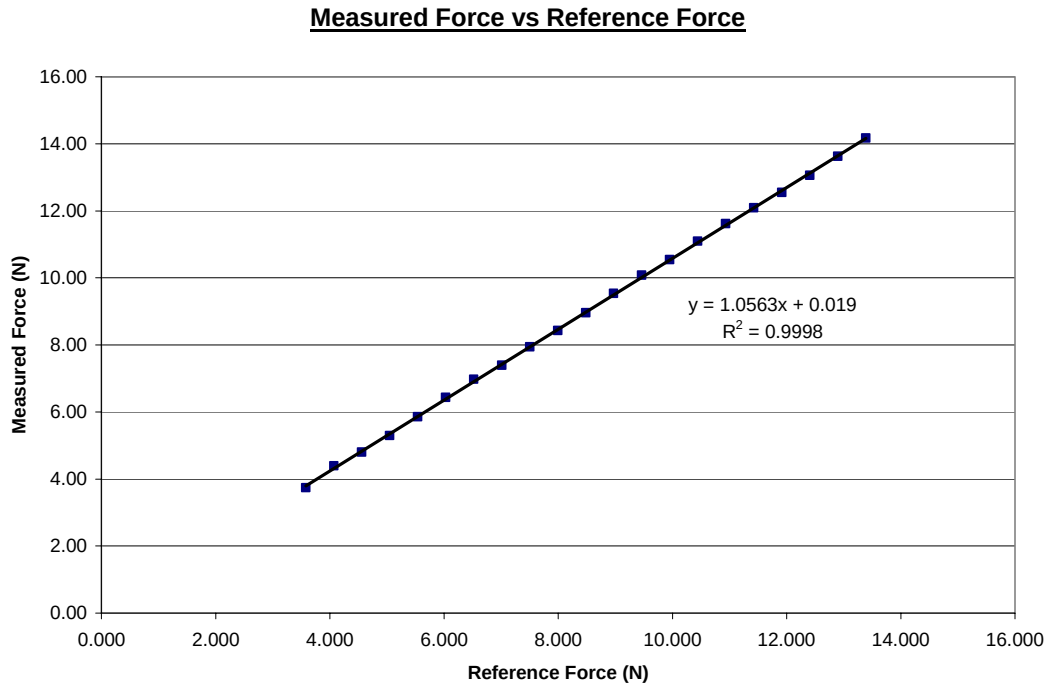

Static Displacement Test

Data for Test 1

Indentation speed = 0.5 mm/s

	Reading on dial gauge		Displacement measured by indentor	
	Displacement (mm)	Increment (mm)	Displacement (mm)	Increment (mm)
Start	1.38	-	1.3	-
1st Pause	5.37	3.99	5.4	4.1
2nd Pause	10.41	5.04	10.3	4.9
3rd Pause	15.38	4.97	15.3	5
4th Pause	20.41	5.03	20.2	4.9

Data for Test 2

Indentation speed = 0.5 mm/s

	Reading on dial gauge		Displacement measured by indentor	
	Displacement (mm)	Increment (mm)	Displacement (mm)	Increment (mm)
Start	1.33	-	1.6	-
1st Pause	5.35	4.02	5.7	4.1
2nd Pause	10.31	4.96	10.6	4.9
3rd Pause	15.33	5.02	15.6	5
4th Pause	20.36	5.03	20.4	4.8

Data for Test 3

Indentation speed = 1.0 mm/s

	Reading on dial gauge		Displacement measured by indentor	
	Displacement (mm)	Increment (mm)	Displacement (mm)	Increment (mm)
Start	1.47	-	1.8	-
1st Pause	4.65	3.18	5.3	3.5
2nd Pause	9.57	4.92	10.5	5.2
3rd Pause	14.68	5.11	15.7	5.2
4th Pause	20.43	5.75	21.2	5.5

Data for Test 4

Indentation speed = 1.0 mm/s

	Reading on dial gauge		Displacement measured by indentor	
	Displacement (mm)	Increment (mm)	Displacement (mm)	Increment (mm)
Start	1.36	-	1.6	-
1st Pause	5.38	4.02	5.8	4.2
2nd Pause	10.45	5.07	10.9	5.1
3rd Pause	15.3	4.85	15.9	5
4th Pause	20.57	5.27	21.4	5.5

Data for Test 5

Indentation speed = 1.5 mm/s

	Reading on dial gauge		Displacement measured by indentor	
	Displacement (mm)	Increment (mm)	Displacement (mm)	Increment (mm)
Start	1.43	-	1.8	-
1st Pause	4.82	3.39	5.7	3.9
2nd Pause	10.44	5.62	11.6	5.9
3rd Pause	14.77	4.33	16.4	4.8
4th Pause	20.35	5.58	22.2	5.8

Data for Test 6

Indentation speed = 1.5 mm/s

	Reading on dial gauge		Displacement measured by indentor	
	Displacement (mm)	Increment (mm)	Displacement (mm)	Increment (mm)
Start	1.7	-	2.1	-
1st Pause	5.41	3.71	5.9	3.8
2nd Pause	10.28	4.87	10.8	4.9
3rd Pause	15.52	5.24	16.5	5.7
4th Pause	20.48	4.96	21.5	5

Graph for Test 1

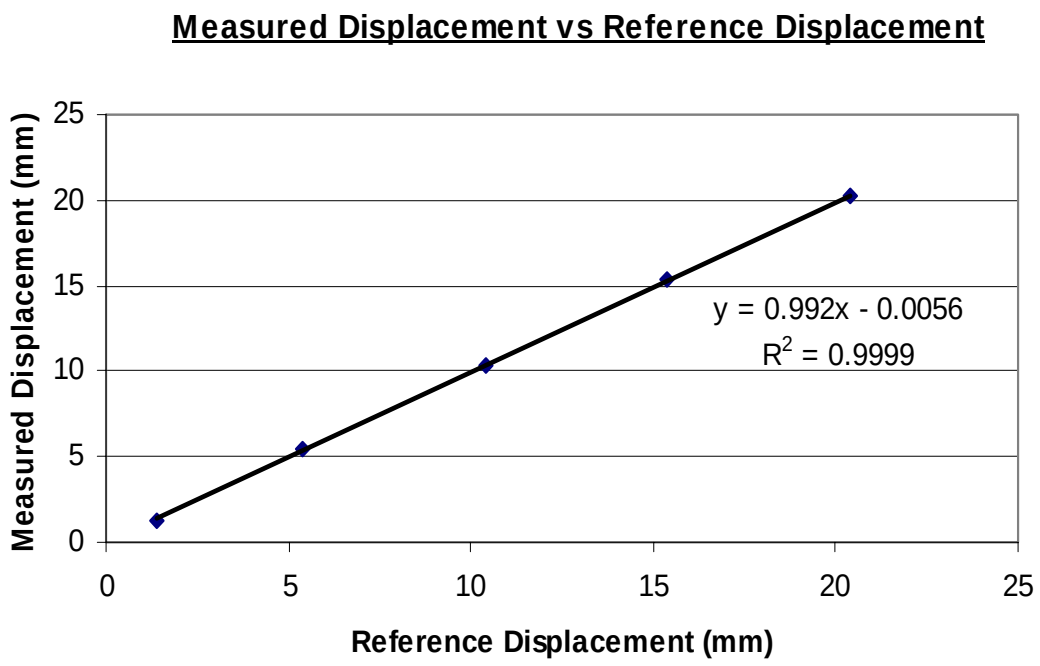

Graph for Test 2

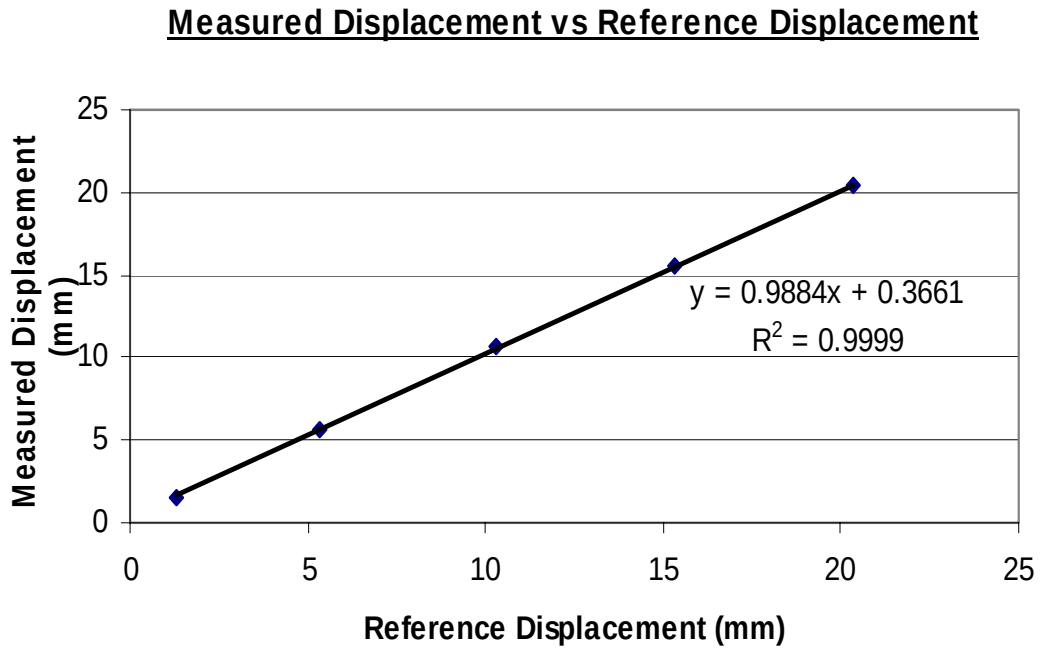

Graph for Test 3

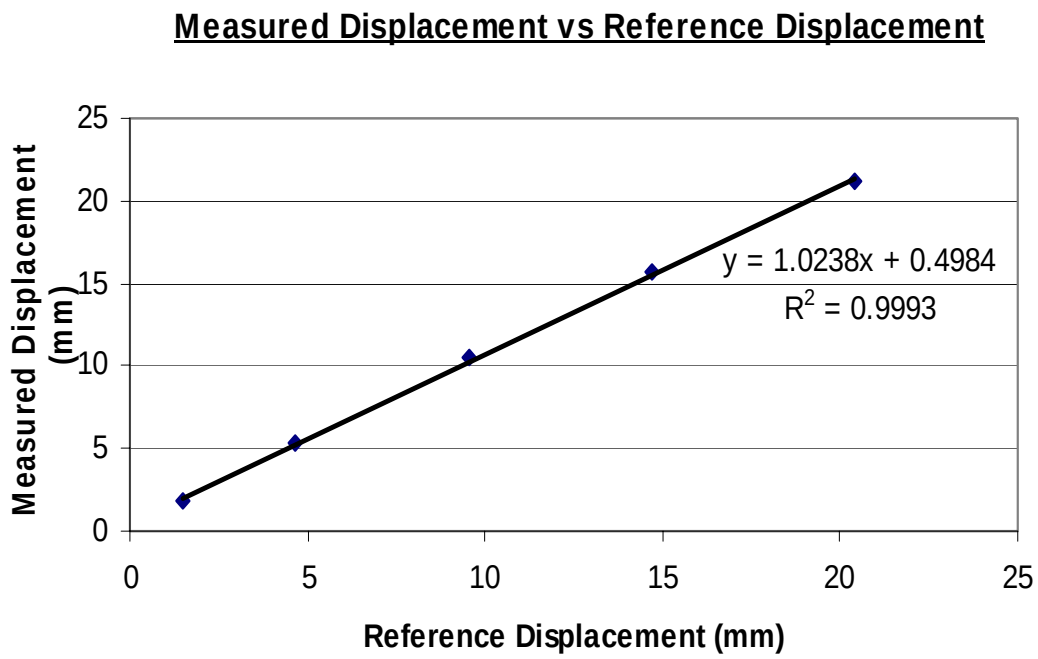

Graph for Test 4

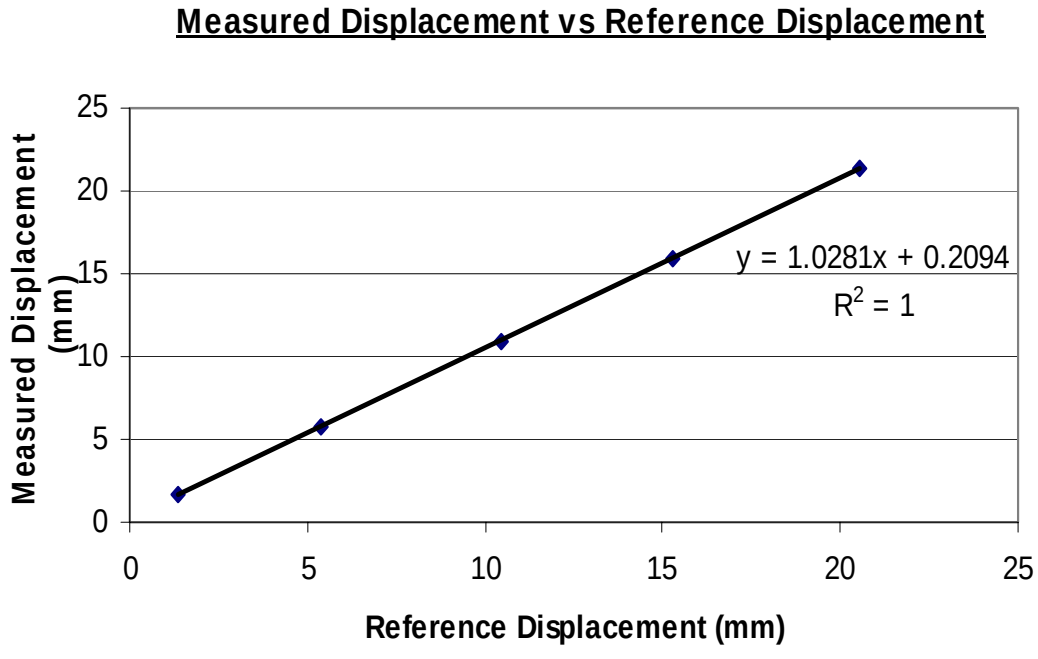

Graph for Test 5

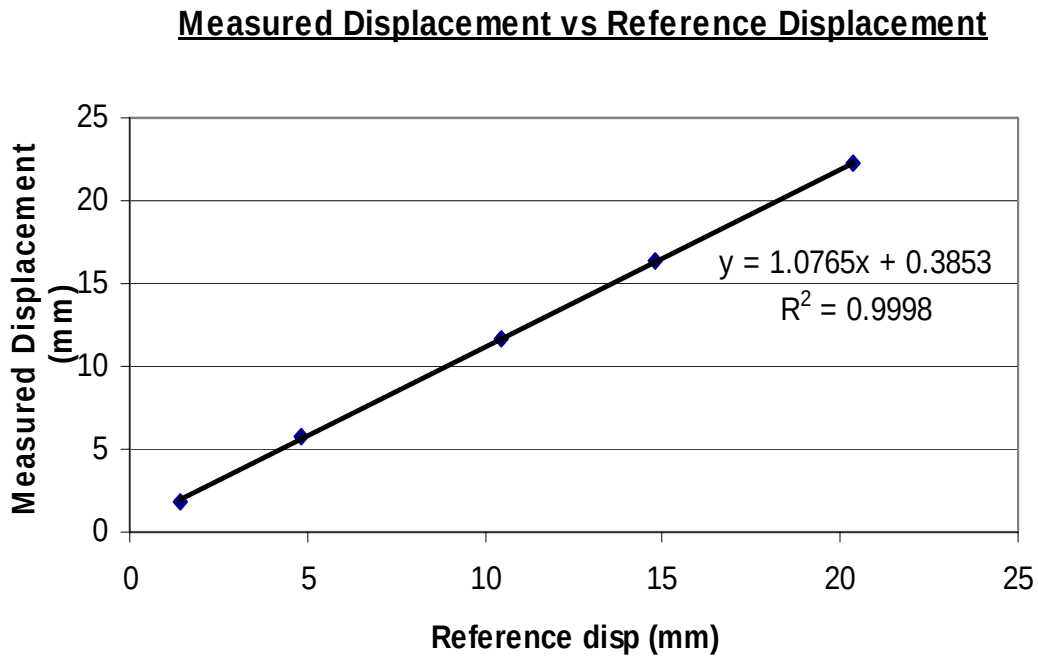

Graph for Test 6

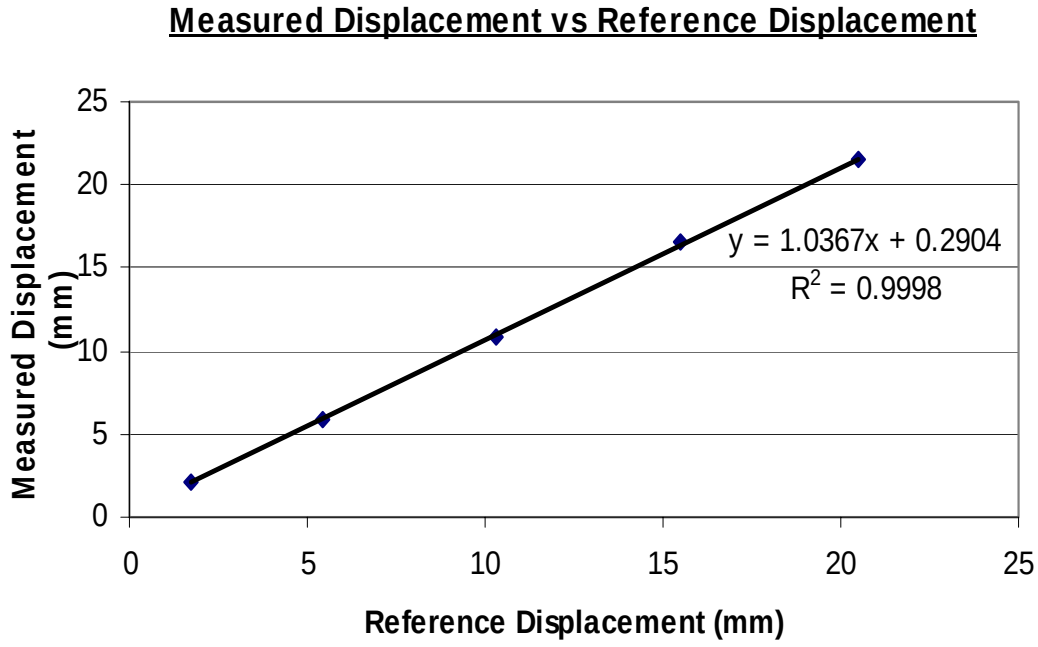

Cyclic Loading/Unloading Test

Indentation speed = 0.5 mm/s
Maximum displacement = 5.0 mm
Number of cycles = 3

Time (s)	Force (N)	Distance (mm)
0	0	0
0.1	0	0
0.2	0	0
0.3	-0.002	0
0.4	-0.004	0
0.5	-0.003	0
0.6	0.009	0
0.7	0.046	0
0.8	0.118	0
0.9	0.226	0
1	0.354	0.1
1.1	0.475	0.1
1.2	0.567	0.2
1.3	0.621	0.2
1.4	0.651	0.3
1.5	0.686	0.3
1.6	0.744	0.4
1.7	0.828	0.4
1.8	0.917	0.5
1.9	0.988	0.5
2	1.028	0.6
2.1	1.047	0.6
2.2	1.067	0.7
2.3	1.113	0.7
2.4	1.19	0.8
2.5	1.285	0.8
2.6	1.379	0.9
2.7	1.456	0.9
2.8	1.512	1
2.9	1.554	1
3	1.597	1.1
3.1	1.653	1.1
3.2	1.721	1.2
3.3	1.79	1.2
3.4	1.84	1.3
3.5	1.862	1.3
3.6	1.866	1.4
3.7	1.871	1.4
3.8	1.894	1.5
3.9	1.938	1.5
4	1.996	1.6
4.1	2.054	1.6
4.2	2.101	1.7

Time (s)	Force (N)	Distance (mm)
4.3	2.127	1.7
4.4	2.137	1.8
4.5	2.148	1.8
4.6	2.187	1.9
4.7	2.271	1.9
4.8	2.395	2
4.9	2.534	2
5	2.654	2.1
5.1	2.735	2.1
5.2	2.78	2.2
5.3	2.806	2.2
5.4	2.831	2.3
5.5	2.862	2.3
5.6	2.887	2.4
5.7	2.893	2.4
5.8	2.876	2.5
5.9	2.847	2.5
6	2.824	2.6
6.1	2.82	2.6
6.2	2.837	2.7
6.3	2.869	2.7
6.4	2.911	2.8
6.5	2.961	2.8
6.6	3.017	2.9
6.7	3.078	2.9
6.8	3.138	3
6.9	3.194	3
7	3.248	3.1
7.1	3.301	3.1
7.2	3.354	3.2
7.3	3.408	3.2
7.4	3.459	3.3
7.5	3.502	3.3
7.6	3.534	3.4
7.7	3.557	3.4
7.8	3.584	3.5
7.9	3.629	3.5
8	3.697	3.6
8.1	3.778	3.6
8.2	3.858	3.7
8.3	3.927	3.7
8.4	3.985	3.8
8.5	4.04	3.8

Time (s)	Force (N)	Distance (mm)
8.6	4.1	3.9
8.7	4.162	3.9
8.8	4.216	4
8.9	4.246	4
9	4.247	4.1
9.1	4.229	4.1
9.2	4.215	4.2
9.3	4.226	4.2
9.4	4.271	4.3
9.5	4.34	4.3
9.6	4.419	4.4
9.7	4.493	4.4
9.8	4.553	4.5
9.9	4.59	4.5
10	4.603	4.6
10.1	4.599	4.6
10.2	4.603	4.7
10.3	4.643	4.7
10.4	4.734	4.8
10.5	4.866	4.8
10.6	5.007	4.9
10.7	5.119	4.9
10.8	5.178	5
10.9	5.181	5
11	5.141	5
11.1	5.076	4.9
11.2	5.001	4.9
11.3	4.925	4.8
11.4	4.852	4.8
11.5	4.78	4.7
11.6	4.707	4.7
11.7	4.633	4.6
11.8	4.562	4.6
11.9	4.502	4.5
12	4.461	4.5
12.1	4.437	4.4
12.2	4.419	4.4
12.3	4.393	4.3
12.4	4.352	4.3
12.5	4.296	4.2
12.6	4.236	4.2
12.7	4.185	4.1
12.8	4.154	4.1
12.9	4.141	4
13	4.135	4
13.1	4.114	3.9
13.2	4.059	3.9
13.3	3.968	3.8
13.4	3.863	3.8
13.5	3.781	3.7
13.6	3.751	3.7

Time (s)	Force (N)	Distance (mm)
13.7	3.771	3.6
13.8	3.814	3.6
13.9	3.843	3.5
14	3.833	3.5
14.1	3.782	3.4
14.2	3.697	3.4
14.3	3.592	3.3
14.4	3.486	3.3
14.5	3.398	3.2
14.6	3.341	3.2
14.7	3.317	3.1
14.8	3.306	3.1
14.9	3.281	3
15	3.223	3
15.1	3.138	2.9
15.2	3.05	2.9
15.3	2.986	2.8
15.4	2.953	2.8
15.5	2.94	2.7
15.6	2.925	2.7
15.7	2.9	2.6
15.8	2.869	2.6
15.9	2.845	2.5
16	2.835	2.5
16.1	2.828	2.4
16.2	2.806	2.4
16.3	2.752	2.3
16.4	2.668	2.3
16.5	2.571	2.2
16.6	2.488	2.2
16.7	2.432	2.1
16.8	2.401	2.1
16.9	2.378	2
17	2.344	2
17.1	2.291	1.9
17.2	2.221	1.9
17.3	2.137	1.8
17.4	2.043	1.8
17.5	1.944	1.7
17.6	1.852	1.7
17.7	1.779	1.6
17.8	1.734	1.6
17.9	1.717	1.5
18	1.716	1.5
18.1	1.713	1.4
18.2	1.696	1.4
18.3	1.66	1.3
18.4	1.615	1.3
18.5	1.574	1.2
18.6	1.553	1.2
18.7	1.552	1.1

Time (s)	Force (N)	Distance (mm)
18.8	1.561	1.1
18.9	1.563	1
19	1.545	1
19.1	1.503	0.9
19.2	1.446	0.9
19.3	1.386	0.8
19.4	1.336	0.8
19.5	1.298	0.7
19.6	1.265	0.7
19.7	1.225	0.6
19.8	1.171	0.6
19.9	1.104	0.5
20	1.028	0.5
20.1	0.952	0.4
20.2	0.885	0.4
20.3	0.841	0.3
20.4	0.834	0.3
20.5	0.858	0.2
20.6	0.88	0.2
20.7	0.857	0.1
20.8	0.759	0.1
20.9	0.593	0
21	0.406	0
21.1	0.26	0
21.2	0.203	0
21.3	0.239	0
21.4	0.332	0
21.5	0.432	0
21.6	0.504	0.1
21.7	0.551	0.1
21.8	0.6	0.2
21.9	0.679	0.2
22	0.791	0.3
22.1	0.911	0.3
22.2	1.012	0.4
22.3	1.082	0.4
22.4	1.132	0.5
22.5	1.18	0.5
22.6	1.225	0.6
22.7	1.256	0.6
22.8	1.261	0.7
22.9	1.251	0.7
23	1.248	0.8
23.1	1.272	0.8
23.2	1.325	0.9
23.3	1.392	0.9
23.4	1.457	1
23.5	1.509	1
23.6	1.543	1.1
23.7	1.565	1.1
23.8	1.579	1.2

Time (s)	Force (N)	Distance (mm)
23.9	1.597	1.2
24	1.633	1.3
24.1	1.695	1.3
24.2	1.786	1.4
24.3	1.895	1.4
24.4	2.009	1.5
24.5	2.114	1.5
24.6	2.2	1.6
24.7	2.261	1.6
24.8	2.293	1.7
24.9	2.304	1.7
25	2.309	1.8
25.1	2.33	1.8
25.2	2.378	1.9
25.3	2.449	1.9
25.4	2.518	2
25.5	2.563	2
25.6	2.573	2.1
25.7	2.561	2.1
25.8	2.555	2.2
25.9	2.579	2.2
26	2.638	2.3
26.1	2.71	2.3
26.2	2.768	2.4
26.3	2.794	2.4
26.4	2.799	2.5
26.5	2.81	2.5
26.6	2.855	2.6
26.7	2.938	2.6
26.8	3.042	2.7
26.9	3.132	2.7
27	3.182	2.8
27.1	3.186	2.8
27.2	3.163	2.9
27.3	3.142	2.9
27.4	3.145	3
27.5	3.186	3
27.6	3.258	3.1
27.7	3.352	3.1
27.8	3.452	3.2
27.9	3.546	3.2
28	3.621	3.3
28.1	3.669	3.3
28.2	3.687	3.4
28.3	3.683	3.4
28.4	3.678	3.5
28.5	3.689	3.5
28.6	3.721	3.6
28.7	3.759	3.6
28.8	3.784	3.7
28.9	3.796	3.7

Time (s)	Force (N)	Distance (mm)
29	3.814	3.8
29.1	3.867	3.8
29.2	3.958	3.9
29.3	4.067	3.9
29.4	4.16	4
29.5	4.221	4
29.6	4.254	4.1
29.7	4.276	4.1
29.8	4.295	4.2
29.9	4.309	4.2
30	4.312	4.3
30.1	4.306	4.3
30.2	4.3	4.4
30.3	4.309	4.4
30.4	4.347	4.5
30.5	4.419	4.5
30.6	4.522	4.6
30.7	4.639	4.6
30.8	4.747	4.7
30.9	4.826	4.7
31	4.87	4.8
31.1	4.897	4.8
31.2	4.932	4.9
31.3	4.986	4.9
31.4	5.045	5
31.5	5.075	5
31.6	5.051	5
31.7	4.975	4.9
31.8	4.873	4.9
31.9	4.776	4.8
32	4.701	4.8
32.1	4.651	4.7
32.2	4.616	4.7
32.3	4.592	4.6
32.4	4.575	4.6
32.5	4.561	4.5
32.6	4.541	4.5
32.7	4.508	4.4
32.8	4.461	4.4
32.9	4.411	4.3
33	4.37	4.3
33.1	4.342	4.2
33.2	4.317	4.2
33.3	4.284	4.1
33.4	4.229	4.1
33.5	4.149	4
33.6	4.054	4
33.7	3.963	3.9
33.8	3.899	3.9
33.9	3.871	3.8
34	3.871	3.8

Time (s)	Force (N)	Distance (mm)
34.1	3.874	3.7
34.2	3.863	3.7
34.3	3.838	3.6
34.4	3.81	3.6
34.5	3.785	3.5
34.6	3.758	3.5
34.7	3.717	3.4
34.8	3.653	3.4
34.9	3.568	3.3
35	3.474	3.3
35.1	3.379	3.2
35.2	3.288	3.2
35.3	3.206	3.1
35.4	3.135	3.1
35.5	3.082	3
35.6	3.052	3
35.7	3.041	2.9
35.8	3.039	2.9
35.9	3.033	2.8
36	3.015	2.8
36.1	2.986	2.7
36.2	2.957	2.7
36.3	2.937	2.6
36.4	2.923	2.6
36.5	2.908	2.5
36.6	2.878	2.5
36.7	2.828	2.4
36.8	2.759	2.4
36.9	2.683	2.3
37	2.61	2.3
37.1	2.546	2.2
37.2	2.487	2.2
37.3	2.428	2.1
37.4	2.368	2.1
37.5	2.309	2
37.6	2.253	2
37.7	2.199	1.9
37.8	2.143	1.9
37.9	2.086	1.8
38	2.031	1.8
38.1	1.983	1.7
38.2	1.943	1.7
38.3	1.909	1.6
38.4	1.873	1.6
38.5	1.83	1.5
38.6	1.778	1.5
38.7	1.717	1.4
38.8	1.658	1.4
38.9	1.609	1.3
39	1.58	1.3
39.1	1.569	1.2

Time (s)	Force (N)	Distance (mm)
39.2	1.566	1.2
39.3	1.554	1.1
39.4	1.52	1.1
39.5	1.46	1
39.6	1.383	1
39.7	1.302	0.9
39.8	1.233	0.9
39.9	1.183	0.8
40	1.154	0.8
40.1	1.137	0.7
40.2	1.124	0.7
40.3	1.105	0.6
40.4	1.071	0.6
40.5	1.013	0.5
40.6	0.928	0.5
40.7	0.828	0.4
40.8	0.738	0.4
40.9	0.678	0.3
41	0.65	0.3
41.1	0.625	0.2
41.2	0.57	0.2
41.3	0.467	0.1
41.4	0.341	0.1
41.5	0.239	0
41.6	0.207	0
41.7	0.254	0
41.8	0.352	0.1
41.9	0.457	0.1
42	0.541	0.2
42.1	0.607	0.2
42.2	0.679	0.3
42.3	0.775	0.3
42.4	0.889	0.4
42.5	1	0.4
42.6	1.085	0.5
42.7	1.14	0.5
42.8	1.174	0.6
42.9	1.199	0.6
43	1.215	0.7
43.1	1.221	0.7
43.2	1.226	0.8
43.3	1.247	0.8
43.4	1.3	0.9
43.5	1.378	0.9
43.6	1.455	1
43.7	1.507	1
43.8	1.529	1.1
43.9	1.535	1.1
44	1.547	1.2
44.1	1.574	1.2
44.2	1.609	1.3

Time (s)	Force (N)	Distance (mm)
44.3	1.644	1.3
44.4	1.674	1.4
44.5	1.705	1.4
44.6	1.744	1.5
44.7	1.796	1.5
44.8	1.864	1.6
44.9	1.943	1.6
45	2.027	1.7
45.1	2.109	1.7
45.2	2.181	1.8
45.3	2.235	1.8
45.4	2.268	1.9
45.5	2.285	1.9
45.6	2.293	2
45.7	2.298	2
45.8	2.308	2.1
45.9	2.329	2.1
46	2.369	2.2
46.1	2.427	2.2
46.2	2.496	2.3
46.3	2.561	2.3
46.4	2.613	2.4
46.5	2.656	2.4
46.6	2.705	2.5
46.7	2.778	2.5
46.8	2.876	2.6
46.9	2.983	2.6
47	3.078	2.7
47.1	3.147	2.7
47.2	3.189	2.8
47.3	3.207	2.8
47.4	3.207	2.9
47.5	3.198	2.9
47.6	3.193	3
47.7	3.209	3
47.8	3.253	3.1
47.9	3.315	3.1
48	3.38	3.2
48.1	3.435	3.2
48.2	3.475	3.3
48.3	3.502	3.3
48.4	3.518	3.4
48.5	3.524	3.4
48.6	3.532	3.5
48.7	3.556	3.5
48.8	3.608	3.6
48.9	3.69	3.6
49	3.788	3.7
49.1	3.881	3.7
49.2	3.947	3.8
49.3	3.979	3.8

Time (s)	Force (N)	Distance (mm)
49.4	3.991	3.9
49.5	4.004	3.9
49.6	4.034	4
49.7	4.081	4
49.8	4.133	4.1
49.9	4.174	4.1
50	4.198	4.2
50.1	4.211	4.2
50.2	4.232	4.3
50.3	4.276	4.3
50.4	4.347	4.4
50.5	4.434	4.4
50.6	4.518	4.5
50.7	4.586	4.5
50.8	4.644	4.6
50.9	4.708	4.6
51	4.785	4.7
51.1	4.867	4.7
51.2	4.935	4.8
51.3	4.982	4.8
51.4	5.016	4.9
51.5	5.048	4.9
51.6	5.075	5
51.7	5.076	5
51.8	5.036	5
51.9	4.957	4.9
52	4.865	4.9
52.1	4.785	4.8
52.2	4.731	4.8
52.3	4.698	4.7
52.4	4.666	4.7
52.5	4.614	4.6
52.6	4.527	4.6
52.7	4.409	4.5
52.8	4.285	4.5
52.9	4.187	4.4
53	4.141	4.4
53.1	4.15	4.3
53.2	4.191	4.3
53.3	4.228	4.2
53.4	4.227	4.2
53.5	4.174	4.1
53.6	4.08	4.1
53.7	3.97	4
53.8	3.871	4
53.9	3.802	3.9
54	3.769	3.9
54.1	3.773	3.8
54.2	3.8	3.8
54.3	3.827	3.7
54.4	3.824	3.7

Time (s)	Force (N)	Distance (mm)
54.5	3.773	3.6
54.6	3.68	3.6
54.7	3.571	3.5
54.8	3.478	3.5
54.9	3.415	3.4
55	3.375	3.4
55.1	3.342	3.3
55.2	3.3	3.3
55.3	3.248	3.2
55.4	3.193	3.2
55.5	3.14	3.1
55.6	3.094	3.1
55.7	3.058	3
55.8	3.039	3
55.9	3.046	2.9
56	3.074	2.9
56.1	3.104	2.8
56.2	3.109	2.8
56.3	3.07	2.7
56.4	2.987	2.7
56.5	2.878	2.6
56.6	2.765	2.6
56.7	2.664	2.5
56.8	2.581	2.5
56.9	2.514	2.4
57	2.46	2.4
57.1	2.418	2.3
57.2	2.393	2.3
57.3	2.386	2.2
57.4	2.389	2.2
57.5	2.386	2.1
57.6	2.362	2.1
57.7	2.312	2
57.8	2.248	2
57.9	2.187	1.9
58	2.134	1.9
58.1	2.081	1.8
58.2	2.02	1.8
58.3	1.956	1.7
58.4	1.908	1.7
58.5	1.892	1.6
58.6	1.905	1.6
58.7	1.921	1.5
58.8	1.909	1.5
58.9	1.853	1.4
59	1.762	1.4
59.1	1.657	1.3
59.2	1.563	1.3
59.3	1.494	1.2
59.4	1.454	1.2
59.5	1.438	1.1

Time (s)	Force (N)	Distance (mm)
59.6	1.435	1.1
59.7	1.428	1
59.8	1.402	1
59.9	1.35	0.9
60	1.271	0.9
60.1	1.178	0.8
60.2	1.088	0.8
60.3	1.013	0.7
60.4	0.955	0.7
60.5	0.906	0.6
60.6	0.859	0.6
60.7	0.813	0.5
60.8	0.774	0.5
60.9	0.746	0.4
61	0.724	0.4
61.1	0.695	0.3
61.2	0.651	0.3
61.3	0.595	0.2
61.4	0.536	0.2
61.5	0.483	0.1
61.6	0.432	0

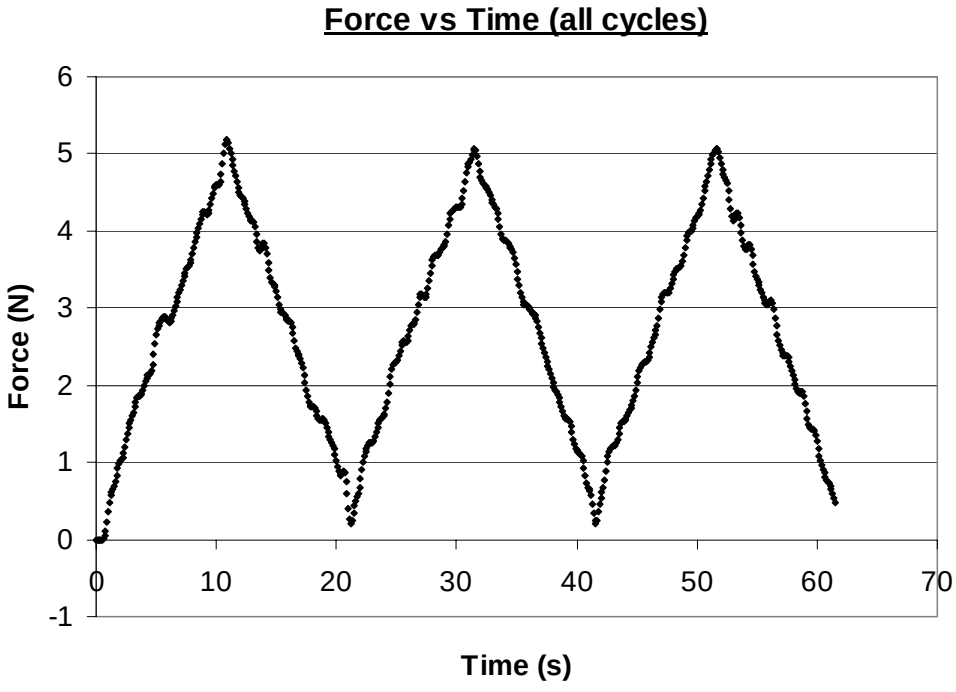

Force vs Displacement (Cycle 1 Loading)

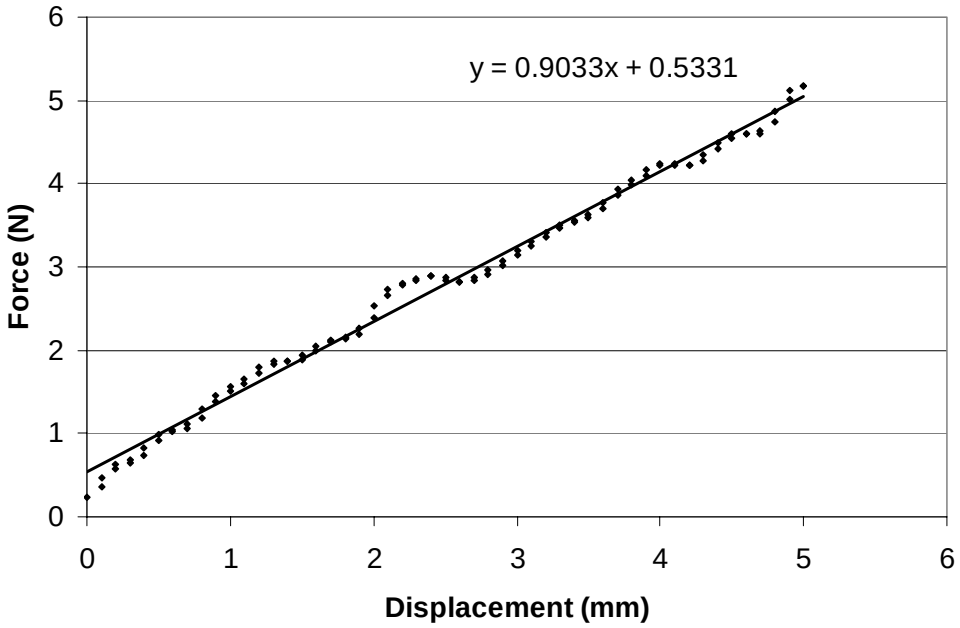

Force vs Displacement (Cycle 1 Unloading)

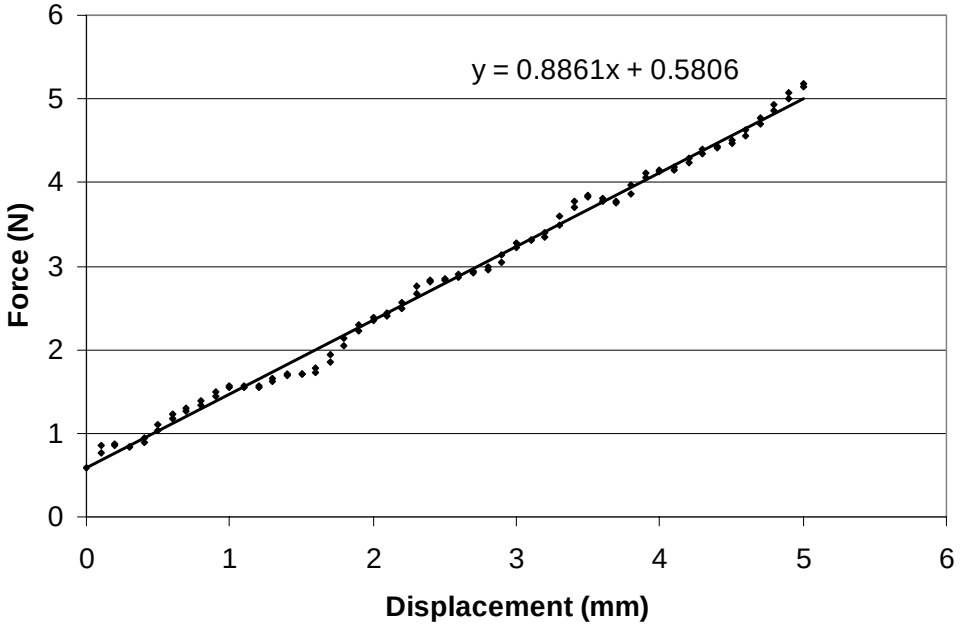

Force vs Displacement (Cycle 2 Loading)

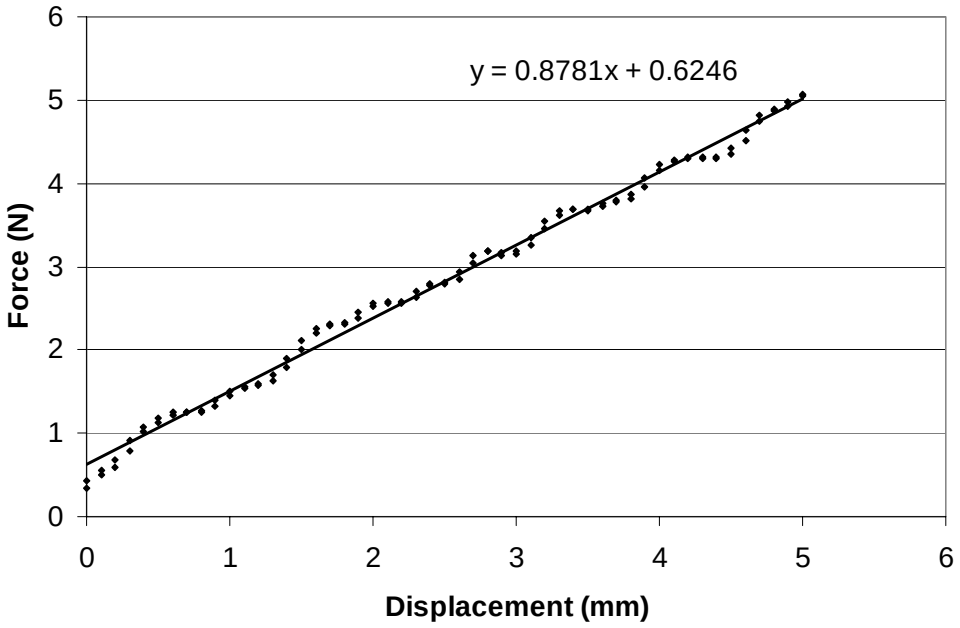

Force vs Displacement (Cycle 2 Unloading)

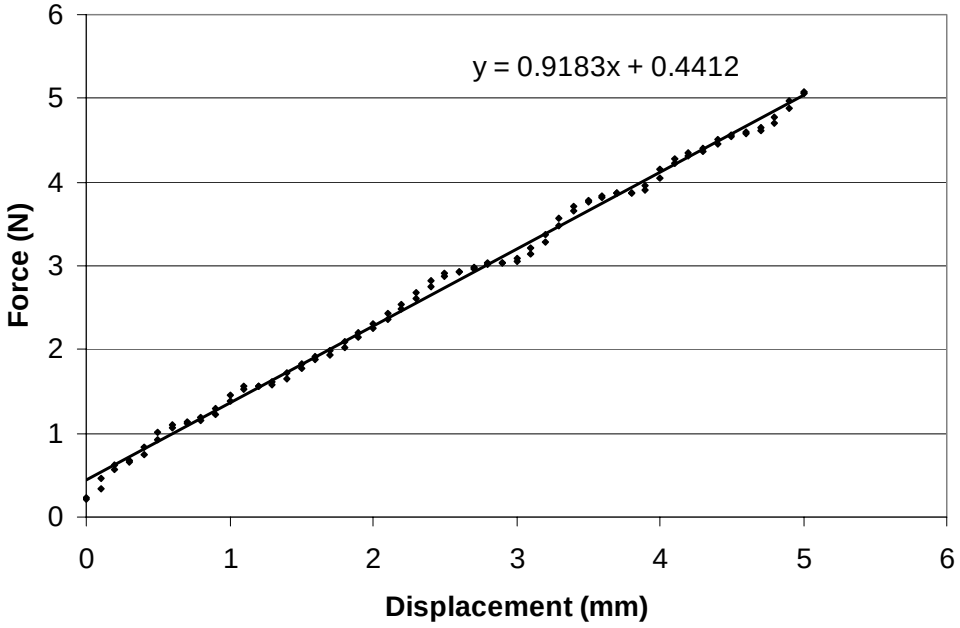

Force vs Displacement (Cycle 3 Loading)

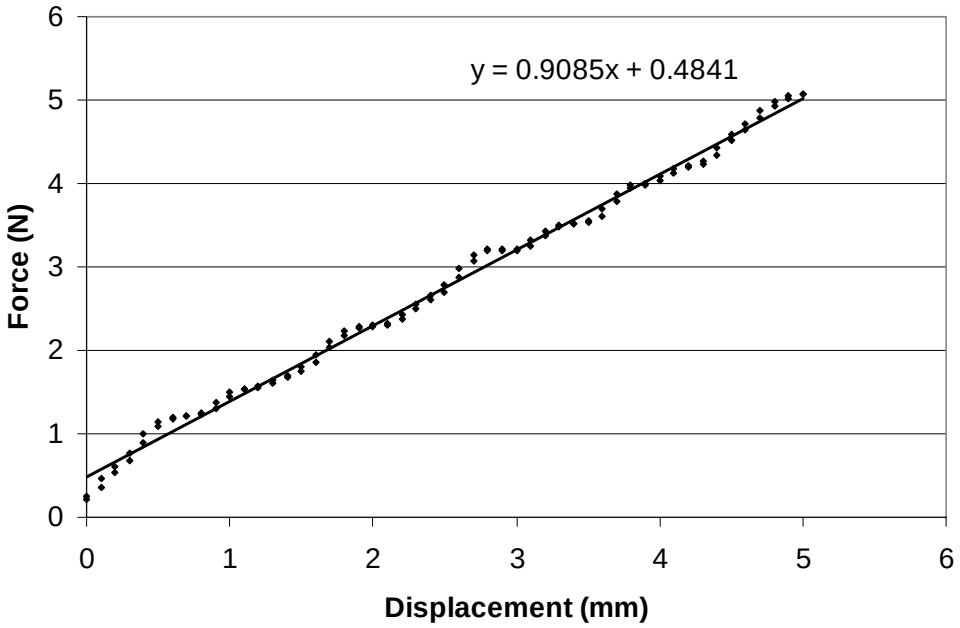

Force vs Displacement (Cycle 3 Unloading)

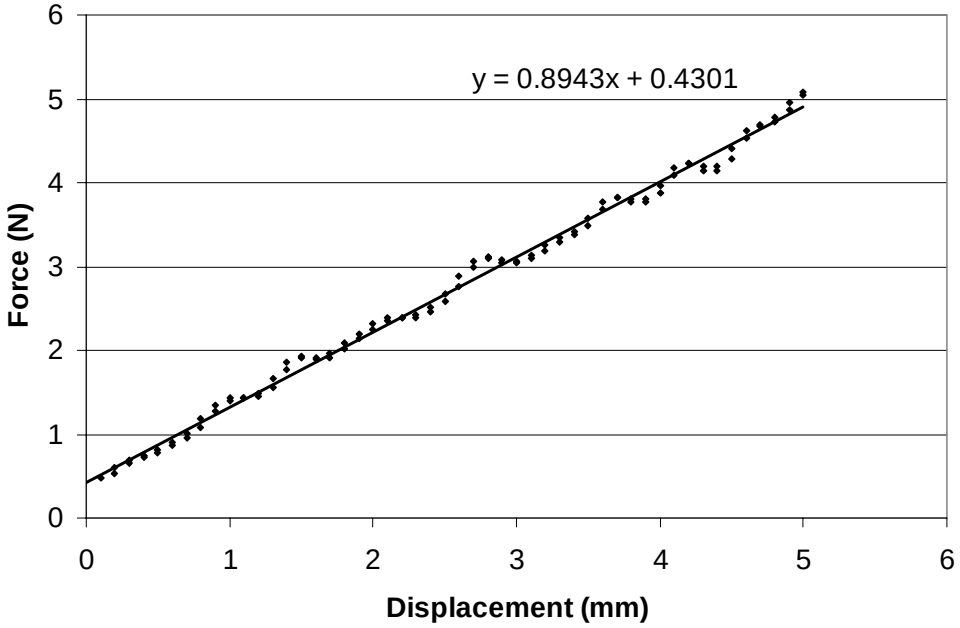

APPENDIX 4: Indentation Data for all Subjects

SUBJECT 1				
Location	Tissue Thickness (mm) *	Indentation Depth (mm)	*a/h* Ratio	*k* Value **
1,1	9.99	12.5	0.25	0.815
1,2	13.54	7.5	0.18	0.772
1,3	25.66	8.0	0.10	0.721
1,4	37.78	13.5	0.07	0.705
1,5	37.78	16.0	0.07	0.705
1,6	37.78	15.5	0.07	0.705
1,7	16.23	10.5	0.15	0.753
1,8	16.58	6.5	0.15	0.751
2,1	16.23	5.0	0.15	0.753
2,2	13.54	10.0	0.18	0.772
2,3	25.66	11.5	0.10	0.721
2,4	37.78	13.5	0.07	0.705
2,5	37.78	24.0	0.07	0.705
2,6	37.78	13.5	0.07	0.705
2,7	16.23	13.5	0.15	0.753
2,8	16.58	5.5	0.15	0.751
3,1	16.23	6.5	0.15	0.753
3,2	24.76	14.0	0.10	0.723
3,3	38.43	20.0	0.07	0.705
3,4	52.09	24.2	0.05	0.697
3,5	52.09	23.1	0.05	0.697
3,6	52.09	18.0	0.05	0.697
3,7	32.06	13.0	0.08	0.711
3,8	25.46	7.6	0.10	0.722
4,1	16.23	12.2	0.15	0.753
4,2	24.76	14.3	0.10	0.723
4,3	38.43	14.0	0.07	0.705
4,4	52.09	19.4	0.05	0.697
4,5	52.09	24.0	0.05	0.697
4,6	52.09	17.0	0.05	0.697
4,7	32.06	14.5	0.08	0.711
4,8	25.46	11.7	0.10	0.722

* Values obtained from Tönük and Silver-Thorn [215]

** Values obtained from Hayes *et al*. [51]

SUBJECT 1				
Location	Tissue Modulus (kPa)	Discomfort Threshold (kPa)	Pain Threshold (kPa)	Tissue Type
1,1	344.26	265.52	442.14	tendon
1,2	594.80	188.18	450.44	bony
1,3	297.29	86.44	241.10	bony
1,4	248.96	149.41	339.33	tendon
1,5	208.31	145.71	316.48	soft
1,6	216.58	144.36	343.07	tendon
1,7	333.71	62.39	309.26	bony
1,8	174.97	38.37	356.66	bony
2,1	129.55	17.97	264.36	bony
2,2	268.44	47.95	404.65	soft
2,3	386.08	79.54	422.66	bony
2,4	151.27	108.65	210.12	soft
2,5	117.86	114.11	222.65	soft
2,6	89.78	61.26	147.23	soft
2,7	113.77	67.49	167.11	bony
2,8	90.06	14.25	97.20	bony
3,1	187.87	5.90	461.81	bony
3,2	159.65	32.07	385.88	soft
3,3	148.98	141.24	321.31	soft
3,4	100.13	74.28	178.36	soft
3,5	118.40	112.05	202.32	soft
3,6	81.59	68.67	160.04	soft
3,7	95.04	43.73	112.57	soft
3,8	139.06	31.39	167.28	soft
4,1	168.71	142.41	287.50	bony
4,2	224.48	112.96	286.77	soft
4,3	141.49	68.59	296.28	soft
4,4	102.83	60.95	165.21	soft
4,5	107.66	77.15	229.00	soft
4,6	105.22	102.16	154.99	soft
4,7	78.34	42.08	189.60	soft
4,8	244.75	87.35	320.80	soft

SUBJECT 2				
Location	Tissue Thickness (mm) *	Indentation Depth (mm)	*a/h* Ratio	*k* Value **
1,1	9.99	20.0	0.25	0.815
1,2	13.54	5.0	0.18	0.772
1,3	25.66	18.0	0.10	0.721
1,4	37.78	24.0	0.07	0.705
1,5	37.78	20.0	0.07	0.705
1,6	37.78	15.3	0.07	0.705
1,7	16.23	9.5	0.15	0.753
1,8	16.58	7.0	0.15	0.751
2,1	16.23	2.5	0.15	0.753
2,2	13.54	12.0	0.18	0.772
2,3	25.66	20.0	0.10	0.721
2,4	37.78	24.0	0.07	0.705
2,5	37.78	23.0	0.07	0.705
2,6	37.78	15.2	0.07	0.705
2,7	16.23	13.5	0.15	0.753
2,8	16.58	14.0	0.15	0.751
3,1	16.23	4.0	0.15	0.753
3,2	24.76	18.0	0.10	0.723
3,3	38.43	24.0	0.07	0.705
3,4	52.09	24.0	0.05	0.697
3,5	52.09	24.0	0.05	0.697
3,6	52.09	20.0	0.05	0.697
3,7	32.06	17.0	0.08	0.711
3,8	25.46	13.3	0.10	0.722
4,1	16.23	10.3	0.15	0.753
4,2	24.76	24.0	0.10	0.723
4,3	38.43	24.0	0.07	0.705
4,4	52.09	24.0	0.05	0.697
4,5	52.09	23.0	0.05	0.697
4,6	52.09	23.2	0.05	0.697
4,7	32.06	24.0	0.08	0.711
4,8	25.46	18.0	0.10	0.722

* Values obtained from Tönük and Silver-Thorn [215]
** Values obtained from Hayes *et al*. [51]

SUBJECT 2				
Location	Tissue Modulus (kPa)	Discomfort Threshold (kPa)	Pain Threshold (kPa)	Tissue Type
1,1	733.11	282.90	1,004.74	tendon
1,2	559.97	46.03	501.52	bony
1,3	367.73	118.46	545.09	bony
1,4	257.28	110.75	406.35	tendon
1,5	163.41	129.01	330.08	soft
1,6	307.56	186.43	349.60	tendon
1,7	722.17	301.02	524.23	bony
1,8	861.47	204.05	525.40	bony
2,1	1,319.62	48.42	448.76	bony
2,2	341.51	65.81	453.13	bony
2,3	334.45	140.68	424.64	bony
2,4	177.54	117.51	275.87	soft
2,5	253.80	243.06	297.74	soft
2,6	387.68	217.47	430.29	soft
2,7	362.23	195.84	461.77	bony
2,8	511.79	381.63	827.06	soft
3,1	1,718.87	115.36	481.77	bony
3,2	509.39	283.77	485.08	soft
3,3	338.10	284.52	347.78	soft
3,4	499.73	311.49	481.26	soft
3,5	266.79	285.17	375.76	soft
3,6	282.35	293.02	469.78	soft
3,7	647.46	315.23	633.96	bony
3,8	366.10	228.23	451.38	soft
4,1	486.67	216.73	483.84	bony
4,2	398.34	301.98	536.86	soft
4,3	259.60	232.77	352.59	soft
4,4	226.83	277.31	399.02	soft
4,5	337.55	321.90	416.88	soft
4,6	448.27	366.49	525.18	soft
4,7	564.19	453.53	654.47	bony
4,8	467.63	298.30	511.12	soft

SUBJECT 3				
Location	Tissue Thickness (mm) *	Indentation Depth (mm)	*a/h* Ratio	*k* Value **
1,1	9.99	11.8	0.25	0.815
1,2	13.54	4.0	0.18	0.772
1,3	25.66	6.5	0.10	0.721
1,4	37.78	9.1	0.07	0.705
1,5	37.78	17.7	0.07	0.705
1,6	37.78	18.8	0.07	0.705
1,7	16.23	5.8	0.15	0.753
1,8	16.58	6.0	0.15	0.751
2,1	16.23	3.6	0.15	0.753
2,2	13.54	4.6	0.18	0.772
2,3	25.66	11.5	0.10	0.721
2,4	37.78	15.2	0.07	0.705
2,5	37.78	19.0	0.07	0.705
2,6	37.78	19.8	0.07	0.705
2,7	16.23	14.0	0.15	0.753
2,8	16.58	11.8	0.15	0.751
3,1	16.23	11.0	0.15	0.753
3,2	24.76	4.8	0.10	0.723
3,3	38.43	18.0	0.07	0.705
3,4	52.09	17.4	0.05	0.697
3,5	52.09	15.5	0.05	0.697
3,6	52.09	24.0	0.05	0.697
3,7	32.06	24.0	0.08	0.711
3,8	25.46	16.2	0.10	0.722
4,1	16.23	11.0	0.15	0.753
4,2	24.76	5.0	0.10	0.723
4,3	38.43	19.5	0.07	0.705
4,4	52.09	19.0	0.05	0.697
4,5	52.09	15.0	0.05	0.697
4,6	52.09	19.8	0.05	0.697
4,7	32.06	20.2	0.08	0.711
4,8	25.46	17.8	0.10	0.722

* Values obtained from Tönük and Silver-Thorn [215]
** Values obtained from Hayes *et al*. [51]

SUBJECT 3				
Location	Tissue Modulus (kPa)	Discomfort Threshold (kPa)	Pain Threshold (kPa)	Tissue Type
1,1	695.34	238.88	629.98	tendon
1,2	1441.80	176.58	477.63	bony
1,3	1108.42	198.20	572.40	bony
1,4	792.36	267.06	540.78	tendon
1,5	263.04	221.70	429.70	soft
1,6	358.47	285.27	581.43	tendon
1,7	1462.62	431.57	767.08	bony
1,8	1180.90	376.84	635.45	bony
2,1	2103.34	273.97	419.96	bony
2,2	1840.79	455.61	771.07	bony
2,3	314.24	138.97	317.34	bony
2,4	317.17	265.52	390.26	soft
2,5	249.77	233.97	345.26	soft
2,6	282.23	277.11	494.92	soft
2,7	327.02	184.82	362.86	bony
2,8	660.45	417.86	695.29	soft
3,1	418.70	189.87	329.52	bony
3,2	1065.57	205.26	390.67	bony
3,3	241.96	161.17	290.02	soft
3,4	218.35	207.74	272.65	soft
3,5	334.17	211.13	362.67	soft
3,6	257.12	276.26	450.78	soft
3,7	271.33	243.22	479.53	soft
3,8	298.06	209.73	384.65	soft
4,1	322.55	150.96	368.54	bony
4,2	809.56	119.51	308.62	bony
4,3	166.84	128.97	246.19	soft
4,4	241.87	273.97	419.96	soft
4,5	134.44	146.82	219.19	soft
4,6	270.55	301.59	481.61	soft
4,7	252.79	202.26	445.69	soft
4,8	415.28	358.77	554.70	soft

SUBJECT 4				
Location	Tissue Thickness (mm) *	Indentation Depth (mm)	*a/h* Ratio	*k* Value **
1,1	9.99	13.6	0.25	0.815
1,2	16.58	5.6	0.15	0.751
1,3	16.23	12.0	0.15	0.753
1,4	37.78	-	0.07	0.705
1,5	37.78	-	0.07	0.705
1,6	37.78	-	0.07	0.705
1,7	25.66	15.0	0.10	0.721
1,8	13.54	7.5	0.18	0.772
2,1	16.23	3.7	0.15	0.753
2,2	16.58	18.0	0.15	0.751
2,3	16.23	18.0	0.15	0.753
2,4	37.78	23.5	0.07	0.705
2,5	37.78	21.0	0.07	0.705
2,6	37.78	14.5	0.07	0.705
2,7	25.66	20.0	0.10	0.721
2,8	13.54	9.5	0.18	0.772
3,1	16.23	14.0	0.15	0.753
3,2	25.46	24.0	0.10	0.722
3,3	32.06	19.1	0.08	0.711
3,4	52.09	24.0	0.05	0.697
3,5	52.09	23.1	0.05	0.697
3,6	52.09	24.0	0.05	0.697
3,7	38.43	20.0	0.07	0.705
3,8	24.76	13.9	0.10	0.723

* Values obtained from Tönük and Silver-Thorn [215]

** Values obtained from Hayes *et al*. [51]

SUBJECT 4				
Location	Tissue Modulus (kPa)	Discomfort Threshold (kPa)	Pain Threshold (kPa)	Tissue Type
1,1	339.57	380.48	-	tendon
1,2	1239.19	560.79	-	bony
1,3	1942.84	426.98	-	bony
1,4	-	-	-	tendon
1,5	-	-	-	soft
1,6	-	-	-	tendon
1,7	1029.99	394.70	-	bony
1,8	1344.82	431.43	-	bony
2,1	1878.53	482.91	-	bony
2,2	344.72	164.60	-	soft
2,3	818.20	372.28	-	bony
2,4	306.01	254.93	-	soft
2,5	245.57	214.84	-	soft
2,6	312.47	246.33	-	soft
2,7	797.07	314.38	-	bony
2,8	1120.25	655.02	-	bony
3,1	900.22	809.30	-	bony
3,2	615.62	469.90	-	soft
3,3	269.67	286.98	-	soft
3,4	197.37	133.28	-	soft
3,5	171.19	136.39	-	soft
3,6	209.16	134.51	-	soft
3,7	279.59	279.20	-	soft
3,8	1065.43	542.65	-	bony

SUBJECT 5				
Location	Tissue Thickness (mm) *	Indentation Depth (mm)	*a/h* Ratio	*k* Value **
1,1	9.99	8.6	0.25	0.815
1,2	16.58	8.0	0.15	0.751
1,3	16.23	7.9	0.15	0.753
1,4	37.78	15.3	0.07	0.705
1,5	37.78	13.0	0.07	0.705
1,6	37.78	7.6	0.07	0.705
1,7	25.66	5.4	0.10	0.721
1,8	13.54	6.0	0.18	0.772
2,1	16.23	6.5	0.15	0.753
2,2	16.58	10.0	0.15	0.751
2,3	16.23	13.5	0.15	0.753
2,4	37.78	10.8	0.07	0.705
2,5	37.78	12.4	0.07	0.705
2,6	37.78	13.0	0.07	0.705
2,7	25.66	22.0	0.10	0.721
2,8	13.54	4.5	0.18	0.772
3,1	16.23	8.5	0.15	0.753
3,2	25.46	10.2	0.10	0.722
3,3	32.06	18.0	0.08	0.711
3,4	52.09	22.0	0.05	0.697
3,5	52.09	12.6	0.05	0.697
3,6	52.09	12.6	0.05	0.697
3,7	38.43	22.0	0.07	0.705
3,8	24.76	12.0	0.10	0.723

* Values obtained from Tönük and Silver-Thorn [215]

** Values obtained from Hayes *et al*. [51]

SUBJECT 5				
Location	Tissue Modulus (kPa)	Discomfort Threshold (kPa)	Pain Threshold (kPa)	Tissue Type
1,1	1774.10	852.88	-	tendon
1,2	869.90	730.56	-	bony
1,3	2093.14	684.14	-	bony
1,4	730.26	538.43	-	tendon
1,5	623.60	249.89	-	soft
1,6	321.48	116.65	-	tendon
1,7	2139.00	541.86	-	bony
1,8	2066.33	523.77	-	bony
2,1	1344.82	554.98	-	bony
2,2	851.04	388.25	-	soft
2,3	1100.61	743.77	-	bony
2,4	1314.15	581.51	-	bony
2,5	241.47	131.18	-	soft
2,6	291.82	179.70	-	soft
2,7	310.80	191.53	-	soft
2,8	1099.45	118.27	-	bony
3,1	1372.55	487.08	-	bony
3,2	1087.03	436.14	-	bony
3,3	548.18	522.70	-	soft
3,4	714.15	285.22	-	soft
3,5	570.11	219.75	-	soft
3,6	363.24	117.29	-	soft
3,7	305.30	281.77	-	soft
3,8	489.99	318.63	-	soft

APPENDIX 5: Finite Element Simulation Data

Data for indentation location 1,1 (patellar tendon)

Indentation Depth (mm)	Experimental Indentation Force (N)	Soft Tissue Modulus calculated from Hayes' equation (kPa)	Uniaxial Stress (MPa)	Strain
0	0	0	0	0
1.0	0.27	49.590	4.96E-03	0.1001
2.0	0.51	68.513	1.37E-02	0.2002
3.0	1.20	74.820	2.25E-02	0.3003
4.0	1.70	321.516	1.29E-01	0.4005
5.0	3.75	442.770	2.22E-01	0.5006
6.0	6.45	564.023	3.39E-01	0.6007

		Mooney-Rivlin		Neo Hookean	
Indentation Depth (mm)	Experimental Indentation Force (N)	FE-Predicted Force (N)	% Difference	FE-Predicted Force (N)	% Difference
0	0	0	0	0	0
1.0	0.27	0.42	59.42	0.18	-32.05
2.0	0.51	0.94	85.58	0.46	-8.61
3.0	1.20	1.69	40.36	0.84	-30.17
4.0	1.70	2.05	21.14	1.13	-33.15
5.0	3.75	2.80	-25.16	1.58	-57.94
6.0	6.45	2.79	-56.67	1.71	-73.46

		Ogden		Reduced Polynomial	
Indentation Depth (mm)	Experimental Indentation Force (N)	FE-Predicted Force (N)	% Difference	FE-Predicted Force (N)	% Difference
0	0	0	0	0	0
1.0	0.27	0.15	-42.02	0.18	-34.11
2.0	0.51	0.58	14.21	0.48	-5.18
3.0	1.20	0.94	-21.81	0.84	-30.17
4.0	1.70	1.27	-24.99	1.12	-34.20
5.0	3.75	1.25	-66.49	1.58	-57.94
6.0	6.45	1.45	-77.48	1.76	-72.64

		Yeoh	
Indentation Depth (mm)	Experimental Indentation Force (N)	FE-Predicted Force (N)	% Difference
0	0	0	0
1.0	0.27	0.11	-58.56
2.0	0.51	0.48	-5.95
3.0	1.20	0.90	-25.35
4.0	1.70	1.68	-0.69
5.0	3.75	2.32	-38.13
6.0	6.45	3.05	-52.66

Data for indentation location 3,2 (distal tibial edge)

Indentation Depth (mm)	Experimental Indentation Force (N)	Soft Tissue Modulus calculated from Hayes' equation (kPa)	Uniaxial Stress (MPa)	Strain
0	0	0	0	0
1.0	1.29	417.190	1.64E-02	0.0393
2.0	3.97	709.862	5.58E-02	0.0785
3.0	8.04	1002.534	1.18E-01	0.1178
4.0	13.51	1295.205	2.03E-01	0.1571

		Marlow		Neo Hookean	
Indentation Depth (mm)	Experimental Indentation Force (N)	FE-Predicted Force (N)	% Difference	FE-Predicted Force (N)	% Difference
0	0	0	0	0	0
0.8	0.92	1.79	94.85	0.89	-3.48
1.6	2.73	6.78	148.39	2.76	0.91
2.4	5.43	14.68	170.20	3.46	-36.24
3.2	9.02	18.35	103.29	5.51	-38.96
4.0	13.51	17.24	27.59	6.49	-51.93

		Ogden		Reduced Polynomial	
Indentation Depth (mm)	Experimental Indentation Force (N)	FE-Predicted Force (N)	% Difference	FE-Predicted Force (N)	% Difference
0	0	0	0	0	0
0.8	0.92	1.03	11.63	0.89	-3.48
1.6	2.73	3.55	30.21	2.76	0.91
2.4	5.43	8.62	58.76	3.46	-36.24
3.2	9.02	14.32	58.65	5.51	-38.96
4.0	13.51	27.33	102.33	6.49	-51.93

		Yeoh	
Indentation Depth (mm)	Experimental Indentation Force (N)	FE-Predicted Force (N)	% Difference
0	0	0	0
1.0	1.29	0.24	-81.61
2.0	3.97	0.99	-75.07
3.0	8.04	2.18	-72.93
4.0	13.51	2.61	-80.68

Data for indentation location 3,5 (distal popliteal region)

Indentation Depth (mm)	Experimental Indentation Force (N)	Soft Tissue Modulus calculated from Hayes' equation (kPa)	Uniaxial Stress (MPa)	Strain
0	0	0	0	0
2.0	0.46	73.400	2.82E-03	0.0384
4.0	1.35	120.094	9.22E-03	0.0768
6.0	2.66	166.788	1.92E-02	0.1152
8.0	4.40	213.481	3.28E-02	0.1536
10.0	6.57	260.175	4.99E-02	0.1920

		Marlow		Neo Hookean	
Indentation Depth (mm)	Experimental Indentation Force (N)	FE-Predicted Force (N)	% Difference	FE-Predicted Force (N)	% Difference
0	0	0	0	0	0
2.0	0.46	0.67	46.47	0.47	2.96
4.0	1.35	2.43	80.68	1.17	-12.74
6.0	2.66	4.84	81.82	2.01	-24.28
8.0	4.40	7.06	60.37	2.71	-38.51
10.0	6.57	8.87	34.96	3.62	-44.87

		Ogden		Reduced Polynomial	
Indentation Depth (mm)	Experimental Indentation Force (N)	FE-Predicted Force (N)	% Difference	FE-Predicted Force (N)	% Difference
0	0	0	0	0	0
2.0	0.46	0.69	50.63	0.71	55.17
4.0	1.35	2.47	83.28	2.55	89.30
6.0	2.66	5.64	111.99	5.54	108.16
8.0	4.40	9.90	124.85	10.15	130.62
10.0	6.57	16.99	158.44	17.22	161.90

APPENDIX 6: Derivation of Hayes' Solution for Soft Tissue Modulus

In 1972, Hayes *et al*. [51] derived a rigorous elasticity solution to the problem of an infinitesimal indentation by a frictionless, rigid, axisymmetric indentor on a thin elastic layer bonded to a rigid foundation. The following is an extract from their paper describing its derivation.

Their investigation considered the indentation mechanics of an infinite elastic layer bonded to a rigid half-space as a model for the layered geometry of cartilage and subchondral bone. The analysis is formulated as a mixed boundary value problem of the theory of elasticity based on the Lebedev and Ufliand [186] solution for the case of a bonded layer indented by the plane end of a rigid cylinder or by a rigid sphere.

The elastic layer deformed under the action of a rigid axisymmetric punch pressed normal to the surface by an axial force P. Shear tractions between punch and layer are assumed negligible and the layer is assumed to adhere to the half-space at the surface $z = h$. Under these assumptions the problem is represented mathematically by a mixed boundary value problem satisfying the field equations of the linear theory of elasticity for homogeneous, isotropic materials. The displacement equation is written as

$$(1-2\nu)\nabla^2\mathbf{u} + \nabla(\nabla.\mathbf{u}) = 0 \qquad \text{-----} \quad (3)$$

in which body forces and inertial effects are neglected, $\mathbf{u}$ is the displacement vector, ν is the Poisson's ratio, and ∇ is the gradient operator.

The boundary conditions at the surface ($z = 0$) are mixed with respect to normal traction and displacement, the shear stress being zero over the entire surface. At $z = h$, the adhesion condition requires the displacements to be prescribed as zero. In cylindrical coordinates, (r,θ,z), the boundary conditions are

$$u_z = \omega_0 - \psi(r) \qquad 0 \leq r \leq a\ ,\ z = 0 \qquad \text{-----} \quad (4)$$

$$\sigma_{zz} = 0 \qquad a < r < \infty\ ,\ z = 0 \qquad \text{-----} \quad (5)$$

$$\sigma_{rz} = 0 \qquad 0 \leq r < \infty\ ,\ z = 0 \qquad \text{-----} \quad (6)$$

$$u_z = u_r = 0 \qquad 0 \leq r < \infty\ ,\ z = h \qquad \text{-----} \quad (7)$$

in which $(u_r, 0, u_z)$ are the components of the displacement vector, and σ_{zz} and σ_{rz} are the normal and tangential stress components, respectively. The prescribed elastic displacement of the centre of the punch ($r = 0$) in the z direction is given by ω_0, and $\psi(r)$ expresses the axisymmetric shape of the indentor and the radius of the contact region is a.

Subsequent solution of partial differential equations following from equation (3), given the boundary conditions in equations (4) – (7), led to the expression of Young's modulus presented on page 21.

Values of the dimensionless factor k were numerically obtained by Hayes *et al*. [51] and were provided in their paper. These are reproduced on the following page.

Table of values of k for a plane-ended cylindrical indentor from Hayes *et al*. [51]

a/h	$\nu = 0.30$	$\nu = 0.35$	$\nu = 0.40$	$\nu = 0.45$	$\nu = 0.50$
0.2	1.207	1.218	1.232	1.252	1.281
0.4	1.472	1.502	1.542	1.599	1.683
0.6	1.784	1.839	1.917	2.031	2.211
0.8	2.124	2.211	2.337	2.532	2.855
1.0	2.480	2.603	2.789	3.085	3.609
1.5	3.400	3.629	3.996	4.638	5.970
2.0	4.335	4.685	5.271	6.380	9.069
3.0	6.218	6.829	7.923	10.26	17.86
3.5	7.160	7.906	9.274	12.32	23.74
4.0	8.100	8.983	10.63	14.45	30.75
5.0	9.976	11.13	13.35	18.80	48.47
6.0	11.84	13.27	16.07	23.23	71.75
7.0	13.70	15.41	18.79	27.69	101.27
8.0	15.55	17.53	21.49	32.15	137.7

Table of values of k for a spherical indentor from Hayes *et al*. [51]

a/h	$\nu = 0.30$	$\nu = 0.35$	$\nu = 0.40$	$\nu = 0.45$	$\nu = 0.50$
0.04	0.6809	0.6816	0.6826	0.6838	0.6855
0.06	0.6891	0.6902	0.6917	0.6936	0.6963
0.08	0.6975	0.6990	0.7010	0.7037	0.7073
0.1	0.7061	0.7080	0.7106	0.7140	0.7187
0.2	0.7520	0.7564	0.7622	0.7701	0.7810
0.3	0.8031	0.8105	0.8204	0.8339	0.8530
0.4	0.8594	0.8705	0.8854	0.9060	0.9355
0.5	0.9209	0.9363	0.9572	0.9866	1.029
0.6	0.9872	1.008	1.036	1.076	1.135
0.7	1.058	1.084	1.121	1.173	1.252
0.8	1.133	1.165	1.211	1.278	1.381
0.9	1.210	1.250	1.307	1.390	1.522
1.0	1.291	1.339	1.407	1.509	1.674
1.25	1.503	1.571	1.673	1.831	2.102
1.50	1.723	1.816	1.957	2.184	2.597
1.75	1.949	2.069	2.254	2.564	3.161
2.00	2.179	2.327	2.561	2.967	3.797
2.25	2.412	2.589	2.877	3.391	4.507
2.50	2.647	2.855	3.199	3.834	5.296
2.75	2.883	3.124	3.527	4.294	6.169
3.00	3.121	3.394	3.860	4.770	7.130

APPENDIX 7: Forms of Strain Energy Models Used

The forms of each strain energy model used are as follows:

Arruda-Boyce

$$U = \mu\left\{\frac{1}{2}\left(\overline{I}_1 - 3\right) + \frac{1}{20\lambda_m^2}\left(\overline{I}_1^2 - 9\right) + \frac{11}{1050\lambda_m^4}\left(\overline{I}_1^3 - 27\right) + \frac{19}{7000\lambda_m^6}\left(\overline{I}_1^4 - 81\right) + \ldots\right\} + \frac{1}{D}\left(\frac{J_{el}^2 - 1}{2} - \ln J_{el}\right)$$

where U is the strain energy per unit of reference volume; μ, λ_m and D are temperature-dependent material parameters; $\overline{I}_1$ is the first deviatoric strain invariant defined as $\overline{I}_1 = \overline{\lambda_1}^2 + \overline{\lambda_2}^2 + \overline{\lambda_3}^2$, where the deviatoric stretches $\overline{\lambda_i} = J^{-\frac{1}{3}}\lambda_i$; J is the total volume ratio; J^{el} is the elastic volume ratio and λ_i are the principal stretches.

Marlow

$$U = U_{dev}\left(\overline{I}_1\right) + U_{vol}\left(J_{el}\right),$$

where U is the strain energy per unit of reference volume, with U_{dev} as its deviatoric part and U_{vol} as its volumetric part; $\overline{I}_1$ is the first deviatoric strain invariant defined as $\overline{I}_1 = \overline{\lambda_1}^2 + \overline{\lambda_2}^2 + \overline{\lambda_3}^2$, where the deviatoric stretches $\overline{\lambda_i} = J^{-\frac{1}{3}}\lambda_i$; J is the total volume ratio; J^{el} is the elastic volume ratio and λ_i are the principal stretches.

Mooney-Rivlin

$$U = C_{10}\left(\overline{I}_1 - 3\right) + C_{01}\left(\overline{I}_2 - 3\right) + \frac{1}{D_1}\left(J^{el} - 1\right)^2,$$

where U is the strain energy per unit of reference volume; C_{10}, C_{01} and D_1 are temperature-dependent material parameters; $\overline{I}_1$ and $\overline{I}_2$ are the first and second deviatoric strain invariants defined as $\overline{I}_1 = \overline{\lambda}_1^2 + \overline{\lambda}_2^2 + \overline{\lambda}_3^2$ and $\overline{I}_2 = \overline{\lambda}_1^{(-2)} + \overline{\lambda}_2^{(-2)} + \overline{\lambda}_3^{(-2)}$, where the deviatoric stretches $\overline{\lambda}_i = J^{-\frac{1}{3}}\lambda_i$; J is the total volume ratio; J^{el} is the elastic volume ratio and λ_i are the principal stretches.

Neo-Hookean

$$U = C_{10}\left(\overline{I}_1 - 3\right) + \frac{1}{D_1}\left(J^{el} - 1\right)^2 ,$$

where U is the strain energy per unit of reference volume; C_{10} and D_1 are temperature-dependent material parameters; $\overline{I}_1$ is the first deviatoric strain invariant defined as $\overline{I}_1 = \overline{\lambda}_1^2 + \overline{\lambda}_2^2 + \overline{\lambda}_3^2$, where the deviatoric stretches $\overline{\lambda}_i = J^{-\frac{1}{3}}\lambda_i$; J is the total volume ratio; J^{el} is the elastic volume ratio and λ_i are the principal stretches.

Ogden

$$U = \sum_{i=1}^{N} \frac{2\mu_i}{\alpha_i^2}\left(\overline{\lambda}_1^{\alpha_i} + \overline{\lambda}_2^{\alpha_i} + \overline{\lambda}_3^{\alpha_i} - 3\right) + \sum_{i=1}^{N} \frac{1}{D_1}\left(J^{el} - 1\right)^{2i} ,$$

where $\overline{\lambda}_i$ are the deviatoric principal stretches $\overline{\lambda}_i = J^{-\frac{1}{3}}\lambda_i$; λ_i are the principal stretches; N is a material parameter; and μ_i, α_i and D_i are temperature-dependent material parameters.

The Mooney-Rivlin and neo-Hookean forms can also be obtained from the general Ogden strain energy potential for special choices of μ_i and α_i.

Reduced Polynomial

$$U = \sum_{i=1}^{N} C_{i0} \left(\overline{I}_1 - 3 \right)^i + \sum_{i=1}^{N} \frac{1}{D_i} \left(J^{el} - 1 \right)^{2i} ,$$

where U is the strain energy per unit of reference volume; N is a material parameter; C_{i0} and D_i are temperature-dependent material parameters; $\overline{I}_1$ is the first deviatoric strain invariant defined as $\overline{I}_1 = \overline{\lambda_1}^2 + \overline{\lambda_2}^2 + \overline{\lambda_3}^2$, where the deviatoric stretches $\overline{\lambda_i} = J^{-\frac{1}{3}} \lambda_i$; J is the total volume ratio; J^{el} is the elastic volume ratio and λ_i are the principal stretches.

Yeoh

$$U = C_{10} \left(\overline{I}_1 - 3 \right) + C_{20} \left(\overline{I}_1 - 3 \right)^2 + C_{30} \left(\overline{I}_1 - 3 \right)^3 + \frac{1}{D_1} \left(J^{el} - 1 \right)^2 + \frac{1}{D_2} \left(J^{el} - 1 \right)^4 + \frac{1}{D_3} \left(J^{el} - 1 \right)^6 ,$$

where U is the strain energy per unit of reference volume; C_{i0} and D_i are temperature-dependent material parameters; $\overline{I}_1$ is the first deviatoric strain invariant defined as $\overline{I}_1 = \overline{\lambda_1}^2 + \overline{\lambda_2}^2 + \overline{\lambda_3}^2$, where the deviatoric stretches $\overline{\lambda_i} = J^{-\frac{1}{3}} \lambda_i$; J is the total volume ratio; J^{el} is the elastic volume ratio and λ_i are the principal stretches.